MAGNETIC FIELD MEASUREMENTS

IN QUADRUPOLE MAGNETS

by

ROBERT DAVID FYVIE

B.Sc., University of Victoria, 1968

A THESIS SUBMITTED IN PARTIAL FULFILLMENT OF

THE REQUIREMENTS FOR THE DEGREE OF

MASTER OF SCIENCE

in the Department

of

Physics

ACCEPTED

FACULTY OF GRADUATE STUDIES

[redacted]

DEAN

DATE 26 Apr 73

We accept this thesis as conforming
to the required standard

[redacted]

UNIVERSITY OF VICTORIA

April 1973

ABSTRACT

Supervisor: Dr. D.E. Lobb

Magnetic field measurements have been made on a 4" diameter aperture beam-line quadrupole magnet. One method of measurement uses a rotating coil with a narrow bandwidth wave analyzer and the other a Hall plate survey system interfaced to an on-line mini-computer. The measurements are analyzed to yield the pole tip field as a function of the excitation current, the harmonic content of the field both as a function of axial position and of the entire magnet and the effective length of the field.

Quadrupole field measurements using a short rotating coil are analyzed to determine the fringe field configuration. Errors in the two methods are considered in detail, including the effect of misalignment of the rotating coil and cross-coupling in the Hall plate.

[redacted]

ACKNOWLEDGEMENTS

The author wishes to thank Dr. D.E. Lobb for his help and guidance with the production of this work.

For reading the manuscript and suggesting many valuable comments, the author is indebted to Dr. H.W. Dosso, Dr. G.A. Beer, Dr. W.J. Balfour and Mr. P.A. Reeve. The author wishes to thank Mr. P.A. Reeve, Mr. T.R. Gathright and Mrs. L.M. Williams for supplying the Hall plate data required for this work. The author also wishes to thank Mrs. E.M. James for the typing of the final manuscript.

The author gratefully acknowledges financial support from TRIUMF.

TABLE OF CONTENTS

		Page
ABSTRACT		ii
ACKNOWLEDGEMENTS		iii
LIST OF TABLES		vii
LIST OF FIGURES		viii
CHAPTER 1	INTRODUCTION	1
CHAPTER 2	THEORY OF THE QUADRUPOLE MAGNETIC FIELD	3
CHAPTER 3	ROTATING COIL	12
	3.1 Theory	12
	3.2 Equipment	17
	3.3 Tests Performed on the Apparatus	30
	3.4 Measurements of Quadrupole 4Q19/8	34
	3.4.1 Measurements of Harmonic Content, Effective Length and Linearity	34
	3.4.2 Measurement of B_z and Contribution to the Total emf. due to B_z	43
	3.5 Errors	58
	3.5.1 Systematic Errors	58
	3.5.2 Random Errors	62
CHAPTER 4	THE HALL PLATE	64
	4.1 Theory	64
	4.2 Equipment and Computer Software	80

		Page
	4.3 Calibration of the Hall Plate	86
	4.4 Measurements of 4Q19/8	87
	4.5 Errors	100
	4.5.1 Systematic Errors	100
	4.5.2 Random Errors	105
CHAPTER 5	ANALYSIS OF THE TWO METHODS AND THE RESULTS OBTAINED	108
	5.1 Harmonic Content	108
	5.2 Effective Length	111
	5.3 Linearity of Magnetic Field With Field Excitation Current	112
CHAPTER 6	SUGGESTED IMPROVEMENTS IN THE TWO METHODS	113
	6.1 Rotating Coil	113
	6.2 Hall Plate	117
CHAPTER 7	SUMMARY AND CONCLUSIONS	119
REFERENCES		121
APPENDIX A	GENERATION OF "FALSE" HARMONICS DUE TO MISALIGNMENT	124
APPENDIX B	CONTRIBUTION TO THE EMF. DUE TO B_z ..	130
	B.1 General Theory	130
	B.2 Short Coil	136
	B.3 Long Coil	141
APPENDIX C	GENERATION OF "FALSE" HARMONICS DUE TO CROSS-COUPLING IN THE HALL PLATE	144
APPENDIX D	SOFTWARE FOR THE HALL PLATE SURVEYS AND ANALYSIS	149

		Page
D.1	Supernova Programs	149
D.2	FORIT Subroutine	149

LIST OF TABLES

Table		Page
3.1	Results of r_o^h test (all induced emf.'s in mV.)	31
3.2	Results of off-axis test (all emf.'s in mV.)	32
3.3	Integrated harmonic content of 4Q19/8 as measured by rotating coil	34
3.4	The gradient coefficients in terms of the induced emf. coefficients	48
3.5	The field coefficients in terms of the gradient coefficients	54
4.1	Integrated harmonic content of 4Q19/8 as measured by Hall plate	97
4.2	Harmonics generated due to cross-coupling	102
A.1	Theoretical values of harmonics generated due to misalignment	129
B.1	The field coefficient in terms of the gradient coefficients	135
C.1	Harmonics generated due to cross-coupling	148

LIST OF FIGURES

		Page
2.1	The two-dimensional co-ordinate system in the aperture of a quadrupole	3
2.2	The equipotentials in an ideal quadrupole	6
2.3	A practical quadrupole magnet	7
2.4	The harmonics in a quadrupole as a function of the ratio of pole face radius to aperture radius (Bellendir and Lari 1965)	9
2.5	The quadrupole (4Q19/8) used for measurement. (The pole face length perpendicular to the figure is 19".)	10
3.1.1	The rectangular coil	12
3.2.1	The rotating coil apparatus showing the friction wheel, flywheel and synchronous motor. (The actual coil can be seen in the upper right hand corner.)	18
3.2.2	The low noise rings and multiple brushes	19
3.2.3	The rotating coil apparatus clamped to the head of the lathe. (The wheels to the left are for the x and z adjustments. The y adjustment is in the upper left hand corner.) ..	20
3.2.4	A block diagram of the apparatus	22
3.2.5	An oscilloscope trace: the bottom signal is the total signal from the rotating coil, the top signal is the restored output of the analyzer tuned to the n = 3 harmonic. The phase difference between the two signals is measured directly from these traces.	24
3.2.6	The frequency spectrum of the induced emf. (0 - 130 Hz)	25
3.2.7	The frequency spectrum of the induced emf. (40 - 120 Hz)	26

3.2.8	The frequency spectrum of the induced emf. (100 - 180 Hz)	27
3.3.1	The phototransistor trigger circuit	30
3.4.1	The harmonics of the induced emf. as a function of z (n = 2,3 and 4)	36
3.4.2	The harmonics of the induced emf. as a function of z (n = 6 and 10)	37
3.4.3a	The position of the sextupole in the magnet aperture	38
3.4.3b	The position of the octupole in the magnet aperture	38
3.4.3c	The position of the decapole in the magnet aperture	39
3.4.3d	The position of the 12-pole in the magnet aperture	39
3.4.3e	The position of the 14-pole in the magnet aperture	40
3.4.3f	The position of the 20-pole in the magnet aperture	40
3.4.4	The pole tip field vs. field excitation current as measured by the rotating coil. (the non-linearity is due to iron saturation and decreasing rotational speed as the field increases	42
3.4.5	The quadrupole harmonic of the induced emf. as a function of z as measured by the short coil	45
3.4.6	B_z/B_r as a function of z in the polynomial and exponential regions of the fringe field	49
3.4.7	The long coil in the fringe field	52
4.1.1	The Hall plate measuring system	64
4.1.2	Hall plate rotated about its own axis with a fixed integral relationship to its angular position	69
4.1.3	The Hall plate orientation when m = 0	72
4.1.4	The Hall plate orientation when m = 1	72

4.1.5	The Hall plate orientation when m = 2	73
4.1.6	The directions of B_z in the fringe fields of a magnet	77
4.2.1	The Hall plate is on the end of the probe shown here mounted on the head of the lathe	81
4.2.2	A block diagram of the Hall plate survey equipment (Gathright and Reeve 1972)	83
4.4.1	Magnet harmonics as a function of z (n = 2)	88
4.4.2	Magnet harmonics as a function of z (n = 3)	89
4.4.3	Magnet harmonics as a function of z (n = 4)	90
4.4.4	Magnet harmonics as a function of z (n = 5)	91
4.4.5	Magnet harmonics as a function of z (n = 6)	92
4.4.6	Magnet harmonics as a function of z (n = 7)	93
4.4.7	Magnet harmonics as a function of z (n = 8)	94
4.4.8	Magnet harmonics as a function of z (n = 9)	95
4.4.9	Magnet harmonics as a function of z (n = 10)	96
4.4.10	The pole tip field vs. field excitation current as measured by the Hall plate	99
4.5.1	The Hall plate orientation for m = 2 with a bent probe arm (Hall plate flipped)	104
4.5.2	The Hall plate orientation for m = 2 with a bent probe arm (Hall plate not flipped)	104
6.1	Twin "T" notch filter	115
A.1	The rotational axis displaced from the magnetic axis by a distance R	125
B.1	Coil rotating in the fringe field of a magnet where $z_1 < z_2$. (Main field is to the left in the diagram.)	130
B.2	The long coil in the fringe field	142

C.1 The Hall plate in a magnetic field $\vec{B}$ 144

C.2 Hall plate rotated about its own axis with a fixed integral relationship to its angular position 145

D.1 Flow diagram of RAP 1 (Gathright and Reeve 1972) 151

D.2 Flow diagram of RAP 2 (Gathright and Reeve 1972) 152

D.3 Flow diagram of ERR 2 (Gathright and Reeve 1972) 153

CHAPTER 1

INTRODUCTION

There are many different methods available to measure magnetic fields. The method to use depends on the properties of the field such as source, strength and homogeneity as well as the sensitivity and accuracy required. As an example, nuclear magnetic resonance is one of the most precise methods of measuring a homogeneous magnetic field over a wide range of values. However, this method cannot be used to measure the magnetic field of an extra-terrestrial body, since the sample must be placed directly in the field, or the field in a quadrupole magnet since this field is quite inhomogeneous.

Advances in semiconductor technology and the development of new materials has made the Hall generator and magnetoresistor attractive methods to measure both homogeneous and inhomogeneous fields in the laboratory (Turin 1970; Turck 1971; Jung 1972a; Jung 1972b; Turck 1972).

The use of coils has been and still is a common method for measuring all types of magnetic fields including those which are time varying or pulsed (Kobayashi and Yamashita 1972a; Kobayashi and Yamashita 1972b). If constant fields are to be measured, the coils must be rotated, vibrated, flipped or moved along the axis of the field. The coils can be stationary if the field is time

varying or pulsed. The induced emf. in the coil can be analyzed to obtain harmonic content, effective length and position of the multipoles in the field (Cobb and Muray 1965; Cobb and Cole 1965; Lamb and Lari 1965; Kats and Khasanov 1969; Kobayashi et al. 1971; Kobayashi and Yamashita 1972b).

The principles of these methods and others such as peaking strips, fluxmeters, current balances, floating wires, magnetrons, methods involving the Zeeman and Faraday effect and superconducting devices can be found in bibliographical reviews on the measurement of magnetic fields (Germain 1963; Verma et al. 1972).

Of interest in this paper are the rotating coil and Hall plate measurements of a beam-line quadrupole magnet. In Chapter 2, the theory of a quadrupole field is discussed. In Chapters 3 and 4, the rotating coil and Hall plate methods for measuring harmonic content, effective length and linearity of the field with applied excitation current are discussed along with the measured results from a beam-line quadrupole magnet. Also discussed are errors inherent in each system. An analysis of the two methods, their measured results and suggestions for possible improvements are the topics of Chapters 5 and 6 with the summary and conclusions in Chapter 7.

CHAPTER 2

THEORY OF THE QUADRUPOLE MAGNETIC FIELD

The magnetic field over the central region in a quadrupole magnet can be found by solving the two dimensional Laplace equation for the scalar potential in cylindrical co-ordinates. The magnet is assumed to be of infinite length so that the scalar potential has no z dependence. The origin of the co-ordinate system is taken to be the magnetic centre of the magnet (see Fig. 2.1). This centre is defined as the intersection of the planes of magnetic antisymmetry.

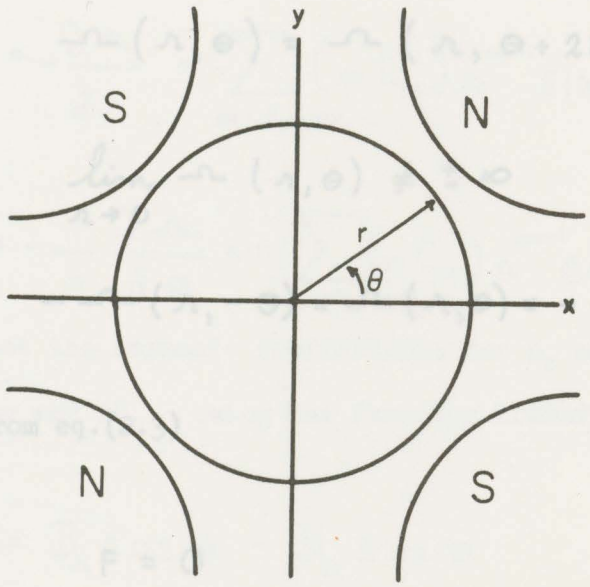

Fig. 2.1 The two-dimensional co-ordinate system in the aperture of a quadrupole

Assuming the scalar potential has a solution of the form

$$\Omega(r,\theta) = R(r)\,\Theta(\theta) \tag{2.1}$$

Laplace's equation yields the following expression for the scalar potential (Steffen 1965; Cobb and Muray 1965).

$$\Omega(r,\theta) = \sum_{m=1}^{\infty}\left[A_m \sin(m\theta) + B_m \cos(m\theta)\right]\left(C_m r^m + D_m r^{-m}\right) + \left(E + F\theta\right)\left(G + H \log r\right) \tag{2.2}$$

Using the following boundary conditions for quadrupole symmetry,

$$\Omega(r,\theta) = \Omega(r,\theta + 2\pi) \tag{2.3}$$

$$\lim_{r\to 0} \Omega(r,\theta) \neq \pm\infty \tag{2.4}$$

$$-\Omega(r,-\theta) = \Omega(r,\theta) = -\Omega(r,\theta+\pi/2) \tag{2.5}$$

we have from eq.(2.3)

$$F = 0 \tag{2.6}$$

AND $$n = 1, 2, 3, \ldots \tag{2.7}$$

from eq.(2.4)

$$H = D = 0 \tag{2.8}$$

and from eq.(2.5)

$$EG = B = 0 \tag{2.9}$$

AND $n = 2 + 4m$ WHERE $m = 1, 2, 3 \ldots$ (2.10)

Therefore the scalar potential for quadrupole symmetry is

$$\Omega(r, \theta) = \sum_{n=2,6,10\ldots} C_n r^n \sin(n\theta + \phi_n) \tag{2.11}$$

where ϕ_n is the phase angle.

The magnetic field components in a quadrupole of infinite length are therefore,

$$B_r = -\frac{\partial \Omega}{\partial r} = -\sum_{n=2,6,10\ldots} (nC_n) r^{n-1} \sin(n\theta + \phi_n) \tag{2.12}$$

$$B_\theta = -\frac{1}{r}\frac{\partial \Omega}{\partial \theta} = -\sum_{n=2,6,10\ldots} (nC_n) r^{n-1} \cos(n\theta + \phi_n) \tag{2.13}$$

Note that the harmonic coefficients for B_r and B_θ in this notation are nC_n. Using the familiar transformations

$$B_x = B_r \cos\theta - B_\theta \sin\theta \tag{2.14}$$

$$B_y = B_r \sin\theta + B_\theta \cos\theta \tag{2.15}$$

the magnetic field components in cartesian co-ordinates are

$$B_x = -\sum_{n=2,6,10\ldots} (n C_n) r^{n-1} \sin\left[(n-1)\theta + \phi_n\right] \qquad (2.16)$$

$$B_y = -\sum_{n=2,6,10\ldots} (n C_n) r^{n-1} \cos\left[(n-1)\theta + \phi_n\right] \qquad (2.17)$$

For an ideal quadrupole the scalar potential has only one term with all harmonics coefficients vanishing except C_2. From eq.(2.2) the equipotential lines for any z position in an ideal quadrupole are hyperbolae (see Fig. 2.2).

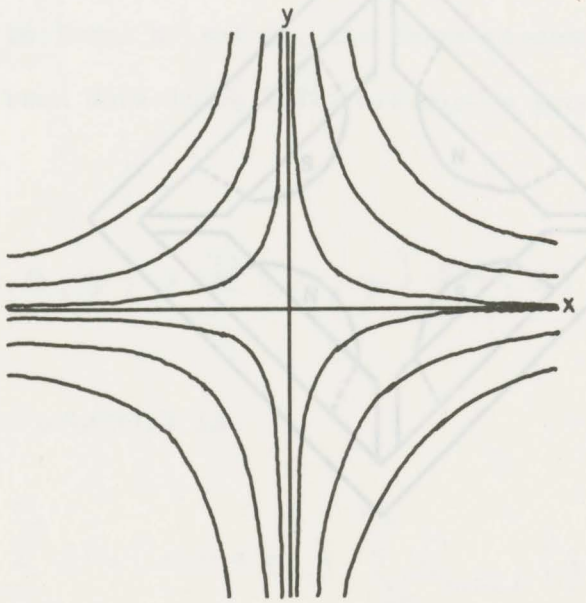

Fig. 2.2 The equipotentials in an ideal quadrupole

In a practical quadrupole the ideal hyperbolic pole face is replaced by a circular profile and the pole face must be truncated to allow room for excitation windings (see Fig. 2.3). The circular approximation to the hyperbolic surface and the truncation of the pole faces are a major cause of higher harmonic content in the quadrupole field. Other harmonics due to mechanical asymmetries and saturation are discussed by Cobb and Cole (1965).

The harmonic content in quadrupoles with circular pole faces has been extensively treated (Bellendir and Lari 1965; Lee-Whiting and Yamazaki 1971; Kobayashi 1972). It has been found

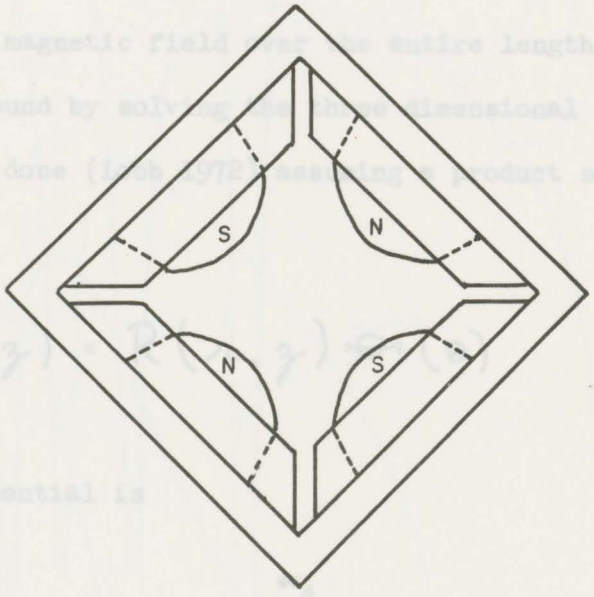

Fig. 2.3 A practical quadrupole magnet

that if the ratio of the radius of curvature of the pole face to the aperture radius is between 1.14 and 1.15, the higher harmonics, notably the duodecapole (12-pole), are minimized. In Fig. 2.4 the harmonics are plotted as a function of this ratio (Bellendir and Lari 1965). The beam-line quadrupole, designated 4Q19/8, used for the measurements in this paper has circular pole faces whose radius of curvature are 2.34 inches and an aperture radius of 2.03 inches (see Fig. 2.5). The ratio of pole face radius to aperture radius for this quadrupole is therefore 1.143. The alpha-numeric designation of the quadrupole refers to the type of magnet (Q), the aperture diameter (4"), the pole length (19") and the maximum pole tip field (8 kG).

The magnetic field over the entire length of the quadrupole can be found by solving the three dimensional Laplace equation. This has been done (Lobb 1972) assuming a product solution of the form

$$\Omega(r,\theta,z) = R(r,z)\,\Theta(\theta) \qquad (2.18)$$

The scalar potential is

$$\Omega = \sum_{n=1}^{\infty} \mathrm{SIN}(n\theta + \phi_n) \sum_{i=0}^{\infty} {}_{m}C_{n+2i}(z)\, r^{n+2i} \qquad (2.19)$$

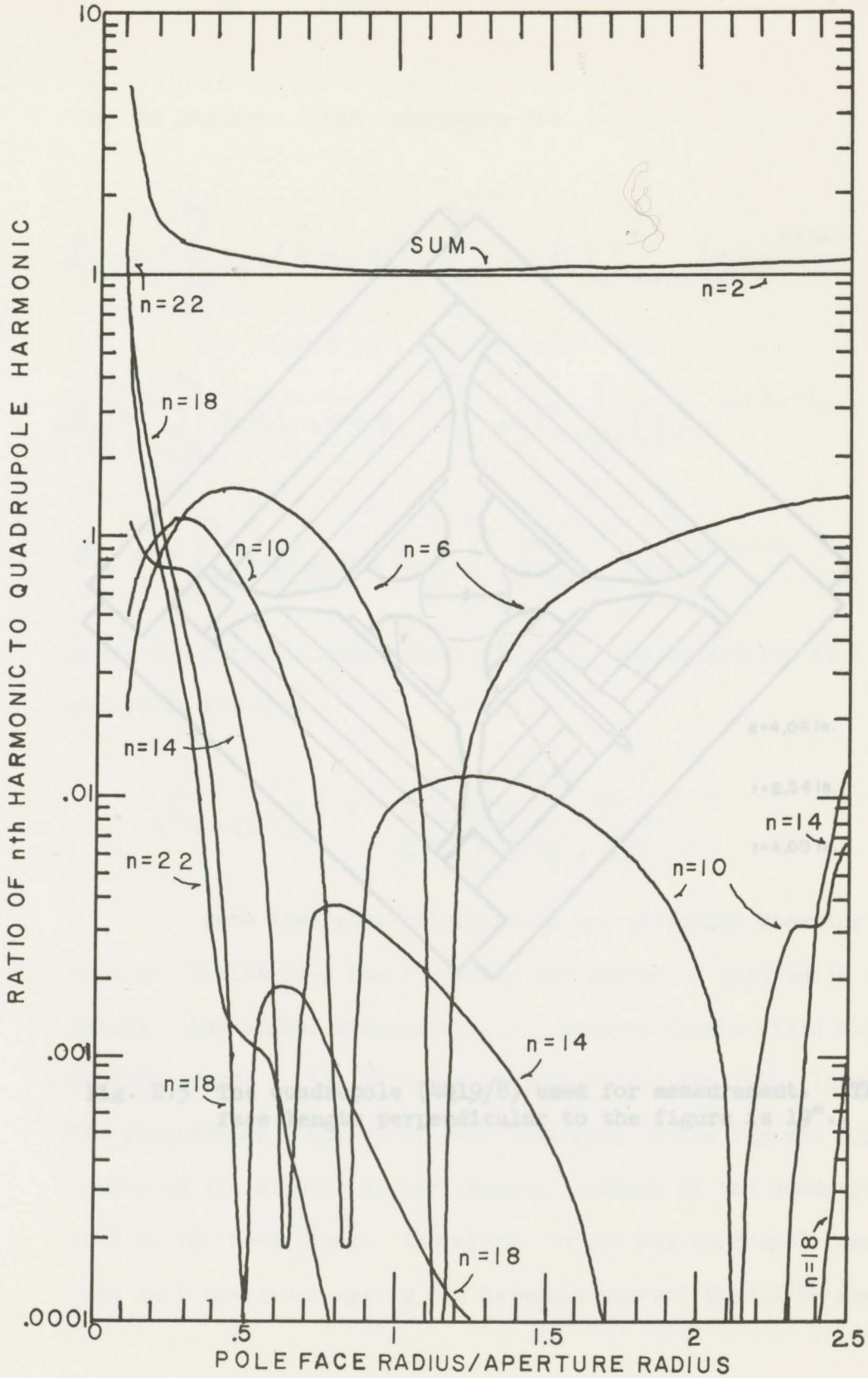

Fig. 2.4 The harmonics in a quadrupole as a function of the ratio of pole face radius to aperture radius (Bellendir and Lari 1965)

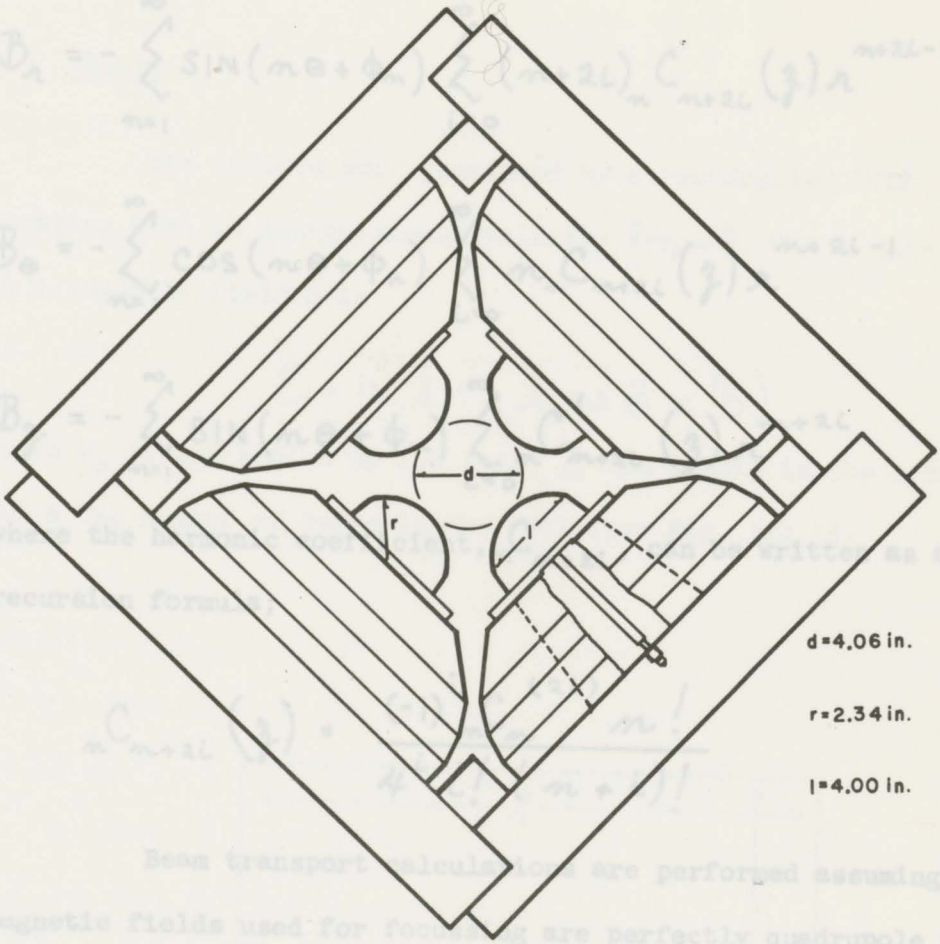

Fig. 2.5 The quadrupole (4Q19/8) used for measurement. (The pole face length perpendicular to the figure is 19".)

and the magnetic field components are

$$B_r = -\sum_{n=1}^{\infty} \mathrm{SIN}(n\theta+\phi_n) \sum_{i=0}^{\infty} (n+2i)_n C_{n+2i}(z)\, r^{n+2i-1} \qquad (2.20)$$

$$B_\theta = -\sum_{n=1}^{\infty} \cos(n\theta+\phi_n) \sum_{i=0}^{\infty} {}_n C_{n+2i}(z)\, r^{n+2i-1} \qquad (2.21)$$

$$B_z = -\sum_{n=1}^{\infty} \mathrm{SIN}(n\theta+\phi_n) \sum_{i=0}^{\infty} {}_n C'_{n+2i}(z)\, r^{n+2i} \qquad (2.22)$$

where the harmonic coefficient, ${}_n C_{n+2i}$, can be written as a recursion formula;

$${}_n C_{n+2i}(z) = \frac{(-1)^i {}_n C_n^{(2i)}\, n!}{4^i\, i!\, (n+i)!} \qquad (2.23)$$

Beam transport calculations are performed assuming the magnetic fields used for focussing are perfectly quadrupole in nature. Any higher harmonics ($n>2$) present in the field will produce errors in the particle trajectories (Lobb 1970, 1972). The performance required of each transport system imposes upper limits on the allowed higher harmonic content of the quadrupoles used in the beam lines. Therefore before any quadrupole can be used in a transport system the harmonic content should be measured.

CHAPTER 3

ROTATING COIL

3.1 Theory

The induced emf. generated by a rectangular coil rotating with an instantaneous velocity $\vec{V}=r_o\omega\hat{\theta}$, where $\omega = \frac{d\theta}{dt}$, in a magnetic field $\vec{B}$ is

$$\mathcal{E} = N\vec{l}\cdot\left(r_o\omega\hat{\theta}\times\vec{B}\right) \qquad (3.1)$$

where r_o is the radius of the coil, l the length in the z direction and N the number of turns in the coil (see Fig. 3.1.1).

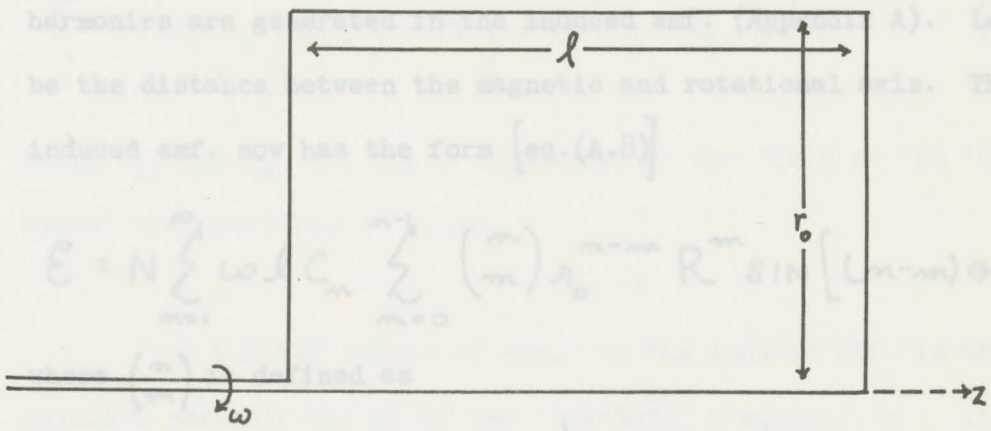

Fig. 3.1.1 The rectangular coil.

Reversing the order of the dot and cross products in eq. (3.1), we have

$$\mathcal{E} = N\vec{B} \cdot (\vec{l} \times r_0 \omega \hat{\theta}) \tag{3.2}$$

The cross-product yields only one term if B_z can be assumed to be zero and eq. (3.2) becomes

$$\mathcal{E} = - N r_0 \omega l B_r \tag{3.3}$$

From eq. (2.12), the induced emf. is

$$\mathcal{E} = N r_0 \omega l \sum_{n=1}^{\infty} (n C_n) r^{n-1} \sin(n\theta + \phi_n) \tag{3.4}$$

If the coil is rotated about the centre of the co-ordinate system so that $r_0 = r$ eq.(3.4) becomes

$$\mathcal{E} = N \sum_{n=1}^{\infty} n \omega l C_n r_0^n \sin(n\theta + \phi_n) \tag{3.5}$$

Therefore the induced emf. has a discrete frequency spectrum.

If the rotating axis and the magnetic axis are misaligned, "false" harmonics are generated in the induced emf. (Appendix A). Let R be the distance between the magnetic and rotational axis. The induced emf. now has the form [eq.(A.8)]

$$\mathcal{E} = N \sum_{n=1}^{\infty} \omega l C_n \sum_{m=0}^{n-1} \binom{n}{m} r_0^{n-m} R^m \sin[(n-m)\theta + \phi_n] \tag{3.6}$$

where $\binom{n}{m}$ is defined as

$$\binom{n}{m} = \frac{n!}{m!(n-m)!} \tag{3.7}$$

The secondary harmonics generated by misalignment will always be of lower order than the magnetic field harmonic which produced them. That is, the quadrupole harmonic will only produce a dipole

term. This is caused by the large quadrupole harmonic coefficient, C_2. Therefore by adjusting the rotating coil apparatus so that the dipole harmonic is minimized in the induced emf., R is also made small with respect to r_o. In practice the dipole term was minimized so that R < .002". Therefore by dipole minimization, $r_o \approx r$ and eq.(3.5) can be used for the induced emf.

If the rotating coil is used in the fringe field of a quadrupole, the assumption that B_z is zero is no longer valid and a contribution to the induced emf. due to the radial arms cutting the B_z flux lines must be considered (Appendix B). From eq.(B.1), the induced emf. for a coil being rotated in the fringe field has the form

$$\mathcal{E} = -N\omega r_o \int_{z_1}^{z_2} B_r \, dz - N \int_0^{r_o} r\omega \left[B_{z_1} - B_{z_2} \right] dr \qquad (3.8)$$

where B_{z1} and B_{z2} are the z components of the field at the two radial arm positions z_1 and z_2.

A further source of error in the induced emf. is the possible periodic nature of the rotational frequency, ω. It has been shown (Cobb 1970) that angular speed variations which are periodic can produce "false" harmonics in the induced emf. The rotational frequency has been monitored over a period of time and the results are discussed in Sec. 3.3.

Assuming that the dipole harmonic has been minimized and the coil is rotating inside the quadrupole where B_z is zero, the harmonic coefficients, normalized with respect to the quadrupole can be calculated from eq.(3.5). Let e_n be the amplitude of the n^{th} harmonic of the induced emf., then

$$\left(\frac{n C_n}{2 C_2}\right)_{r_0} = \left(\frac{e_n}{e_2}\right)_{r_0} \tag{3.9}$$

The subscript, r_0, denotes the radius at which the harmonics are calculated. If the harmonic content is required at a different radius, r_0', then the normalized coefficients are

$$\left(\frac{n C_n}{2 C_2}\right)_{r_0'} = \left(\frac{r_0'}{r_0}\right)^{n-2} \left(\frac{n C_n}{2 C_2}\right)_{r_0} \tag{3.10}$$

The integrated harmonic content can be found by stepping the coil and recording the emf. harmonics, after the dipole is minimized, at each z position.

The effective length of the quadrupole can be calculated from the quadrupole harmonic of the induced emf. The coil is again stepped through the field along z. The effective length at some chosen radius is defined as (Banford 1966)

$$\ell_{EFF.} = \frac{\int_{-\infty}^{\infty} B_{r2}\Big]_{MAX} dz}{B_{r2}\Big]_{MAIN\ FIELD}} \tag{3.11}$$

Note that if the field is pure quadrupole, $\ell_{EFF.}$, is not a function of r (Lobb 1972).

From eq.(3.3) this can be written in terms of the quadrupole harmonic of the emf

$$\ell_{EFF.} = \frac{\Sigma e_2}{e_2 \text{ PER UNIT LENGTH IN MAIN FIELD}} \qquad (3.12)$$

The errors introduced by B_z in these calculations are discussed in Sec. 3.5.

The linearity of magnetic field vs. field excitation current can be found by again using the quadrupole harmonic of the induced emf. From eq.(3.3) the radial magnetic field can be calculated from the induced emf. and the known dimensions, number of turns and angular velocity of the coil used. However, the current in the windings reacts with the magnetic field to produce a torque which opposes the angular motion of the coil. Therefore, the angular velocity depends on B_r . The error introduced by assuming a constant angular velocity is discussed in Sec. 3.5.

The rotating coil can therefore be used to measure harmonic content both as a function of z and for the whole magnet (integrated). From the same data the effective length can also be calculated. The linearity of the field with excitation current can be measured and the amount of B_z in the fringe field can be calculated.

3.2 Equipment

The apparatus consists of a rotating coil driven through a friction wheel by a synchronous motor. The ratio of the motor shaft to the flywheel on the coil shaft is such that possible harmonics from the motor and the AC line are displaced in frequency from those of the coil emf. The coil shaft itself is supported by two bearings. A large flywheel is used to minimize rotational frequency fluctuations (see Fig. 3.2.1). The induced emf. from the coil is obtained from low noise rings and multiple brushes to minimize contact noise (see Fig. 3.2.2).

The support structure for the rotating coil is clamped to a Versa-mill on the head of a lathe. The lathe is positioned so that the lathe bed and magnetic axis of the magnet are as near to being parallel as possible. The head can then be moved in the z direction along the magnetic axis with x and y adjustments available on the Versa-mill (see Fig. 3.2.3).

To monitor the rotational frequency of the coil a light beam is reflected off one face of a hexagon nut on the shaft to a battery driven phototransistor. The time between pulses is measured, using a period counter.

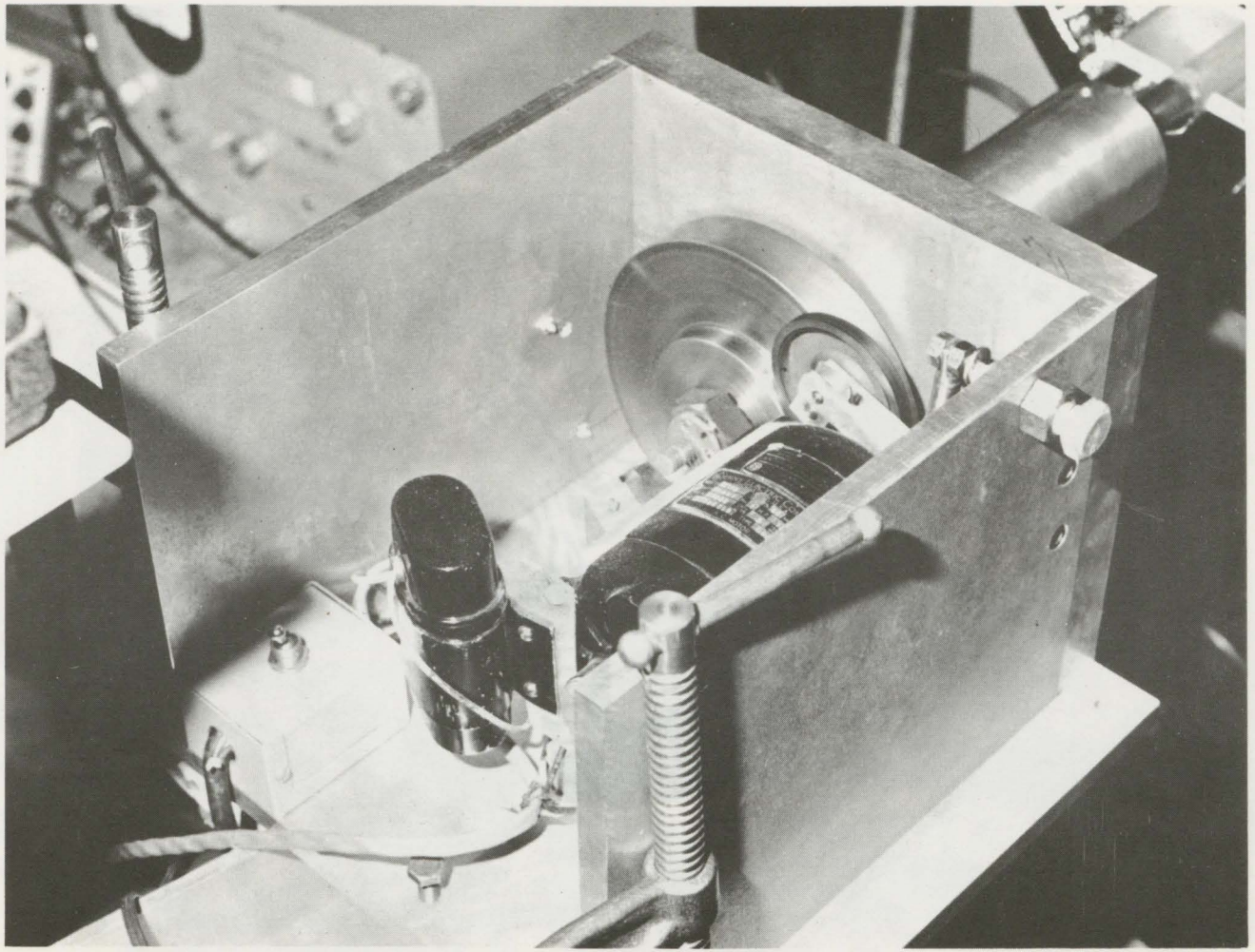

Fig. 3.2.1 The rotating coil apparatus showing the friction wheel, flywheel and synchronous motor. (The actual coil can be seen in the upper right hand corner.)

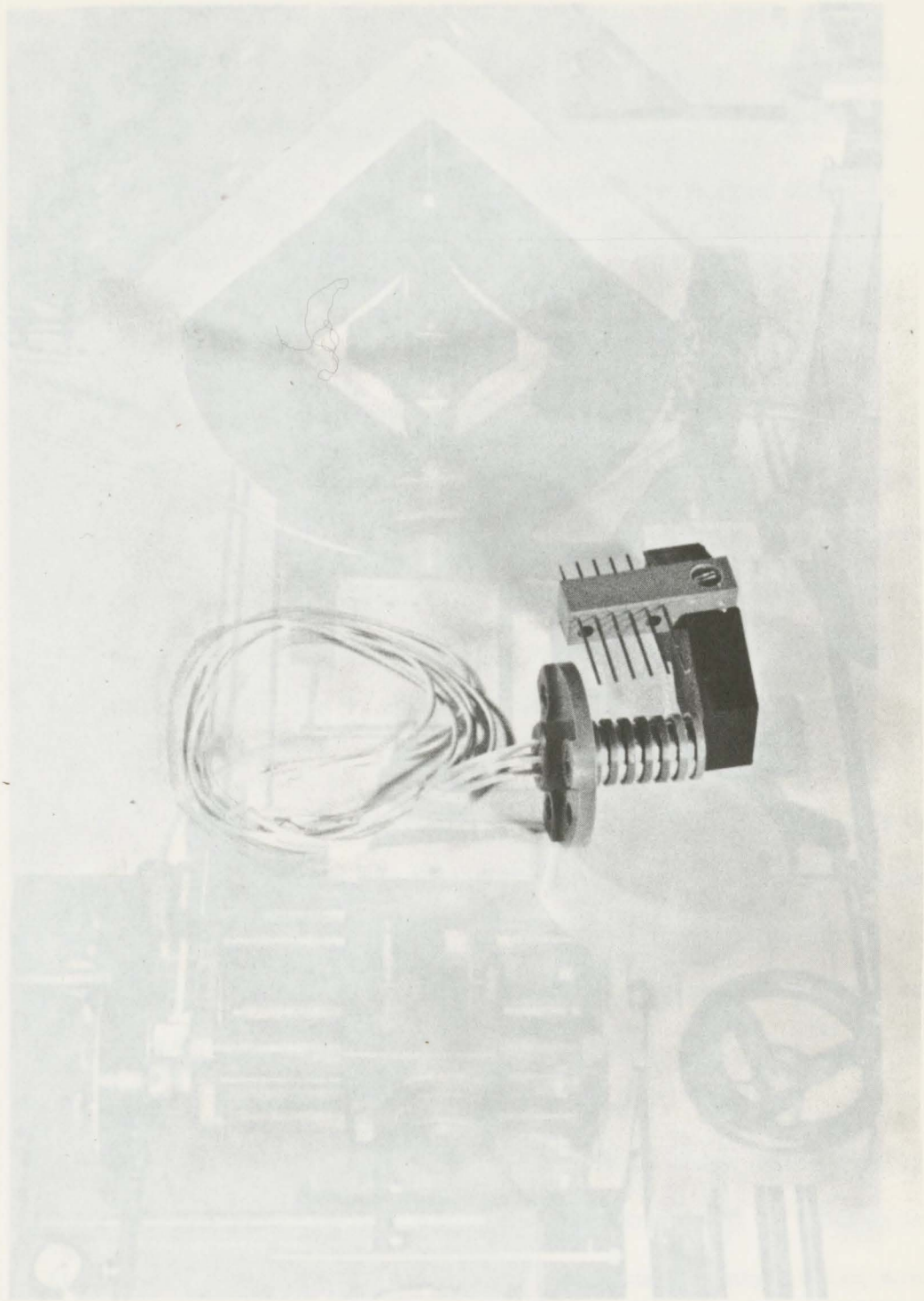

Fig. 3.2.2 The low noise rings and multiple brushes

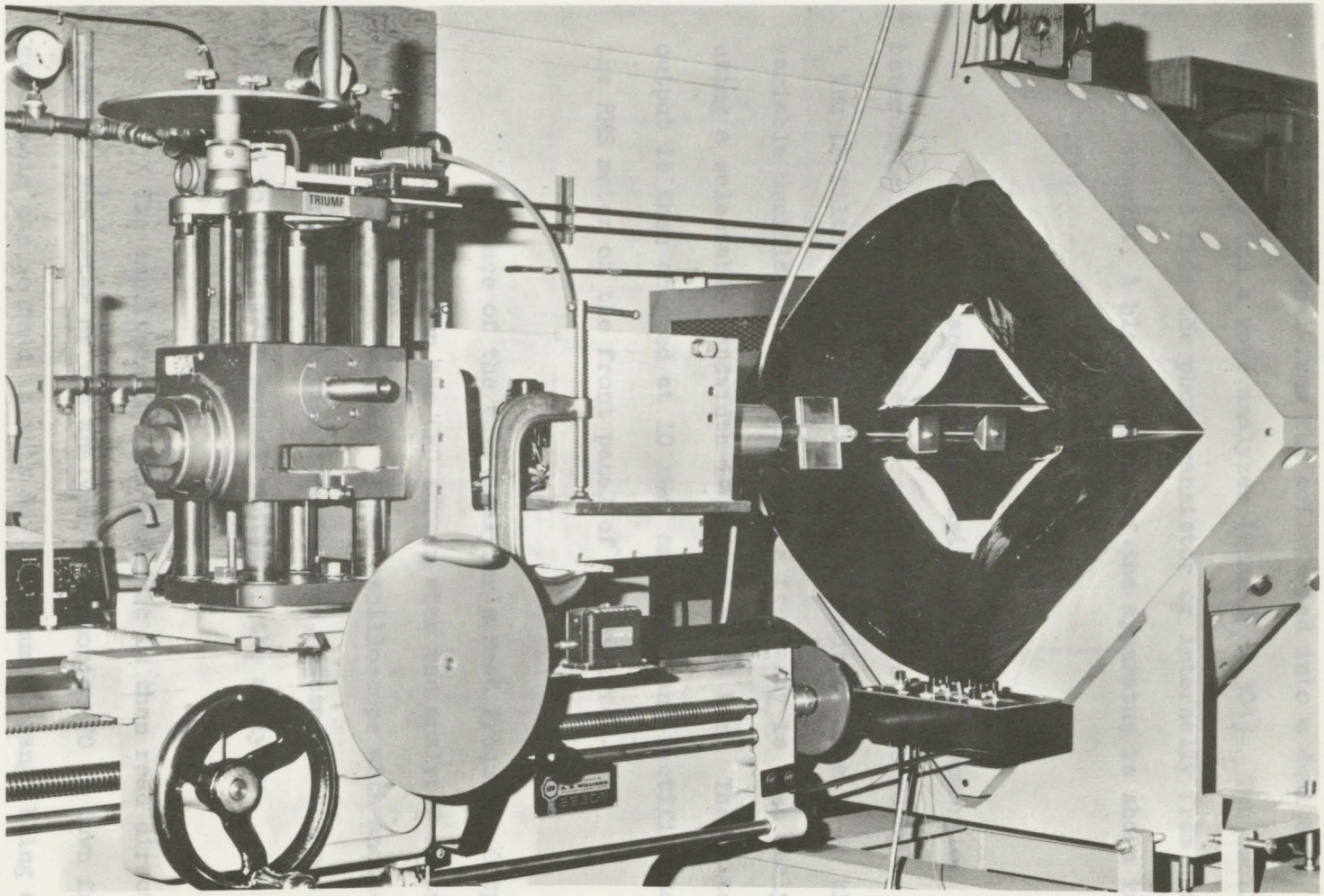

Fig. 3.2.3 The rotating coil apparatus clamped to the head of the lathe. (The wheels to the left are for the x and z adjustments. The y adjustment is in the upper left hand corner.)

The signal from the coil is fed into a dual beam oscilloscope and a wave analyzer (Quan-Tech 304). The oscilloscope is triggered from the phototransistor or internally from the coil signal itself. A block diagram of the apparatus is shown in Fig. 3.2.4.

The wave analyzer is basically a dual conversion heterodyne receiver. The incoming signal is filtered by a 5 kHz LP filter and then mixed with the output of a 10-15 kHz variable oscillator. The difference frequency is then analyzed using a selectable bandwidth LP filter at 10 kHz. The filter output is then chopped at 10 kHz, amplified and rectified to drive the RMS meter on the front panel of the analyzer.

A trace of the wave analyzer's Beat Frequency Output remains stationary on the CRO screen when the analyzer is tuned to a harmonic of the signal. If an oscilloscope with another amplifier instead of a time base is used, Lissajous figures can be obtained to facilitate manual tuning of the analyzer.

The amplitude of each harmonic is then read directly from the RMS meter of the analyzer. Harmonics 70 db down from the quadrupole can be read in this way, maximum db range being available by using the variable input attenuation of the analyzer.

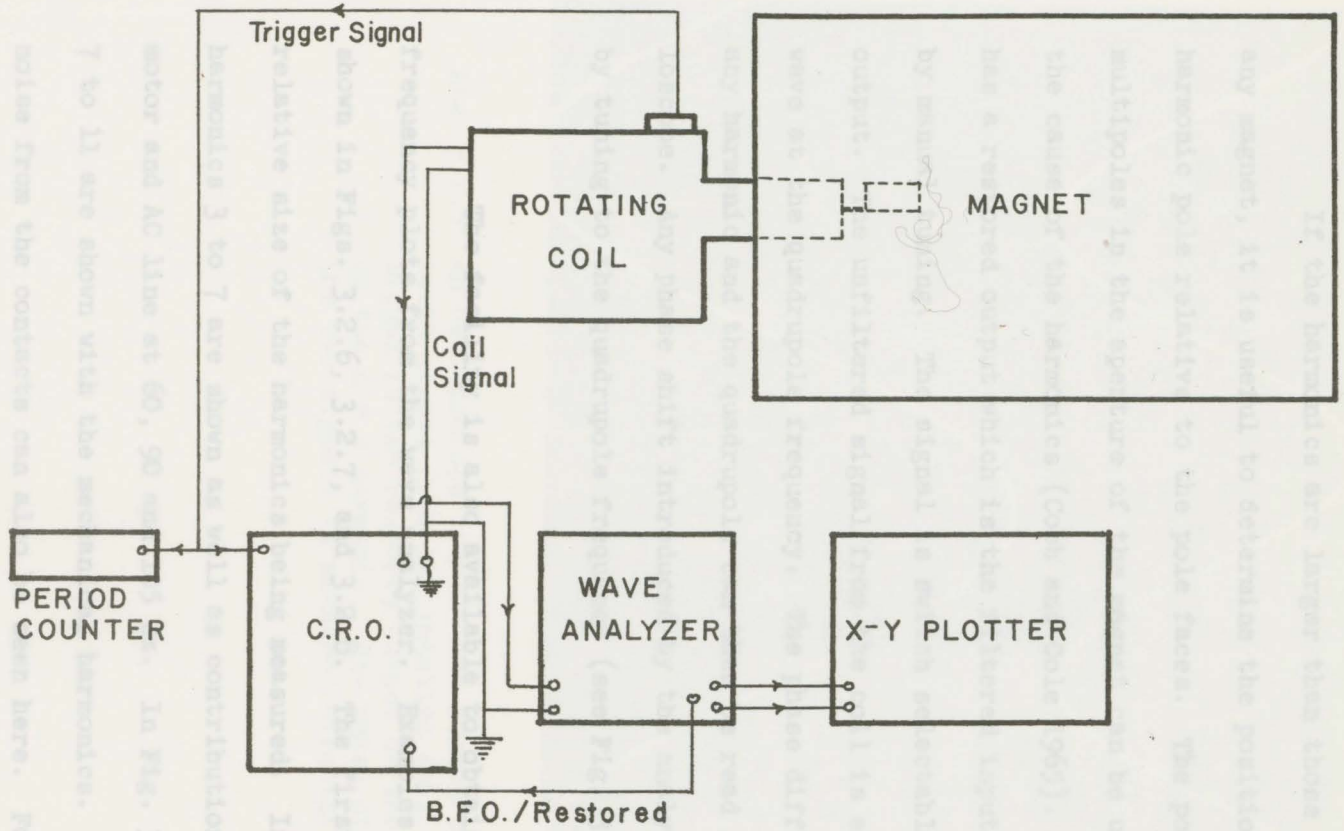

Fig. 3.2.4 A block diagram of the apparatus

If the harmonics are larger than those specified for any magnet, it is useful to determine the position of any harmonic pole relative to the pole faces. The position of the multipoles in the aperture of the magnet can be used to determine the cause of the harmonics (Cobb and Cole 1965). The wave analyzer has a restored output which is the filtered input signal as determined by manual tuning. The signal is switch selectable with the BFO output. The unfiltered signal from the coil is essentially a sine wave at the quadrupole frequency. The phase difference between any harmonic and the quadrupole can then be read from the oscilloscope. Any phase shift introduced by the analyzer can be checked by tuning to the quadrupole frequency (see Fig. 3.2.5).

The facility is also available to obtain amplitude vs. frequency plots from the wave analyzer. Examples of this are shown in Figs. 3.2.6, 3.2.7, and 3.2.8. The first figure shows the relative size of the harmonics being measured. In Fig. 3.2.7, harmonics 3 to 7 are shown as well as contributions due to the motor and AC line at 60, 90 and 105 Hz. In Fig. 3.2.8, harmonics 7 to 11 are shown with the mechanical harmonics. The level of the noise from the contacts can also be seen here. For maximum accuracy in the amplitude vs. frequency plots the bandwidth, sweepwidth and sweeptime controls are not interlocked. Care must be taken not to sweep the selected frequency range too fast

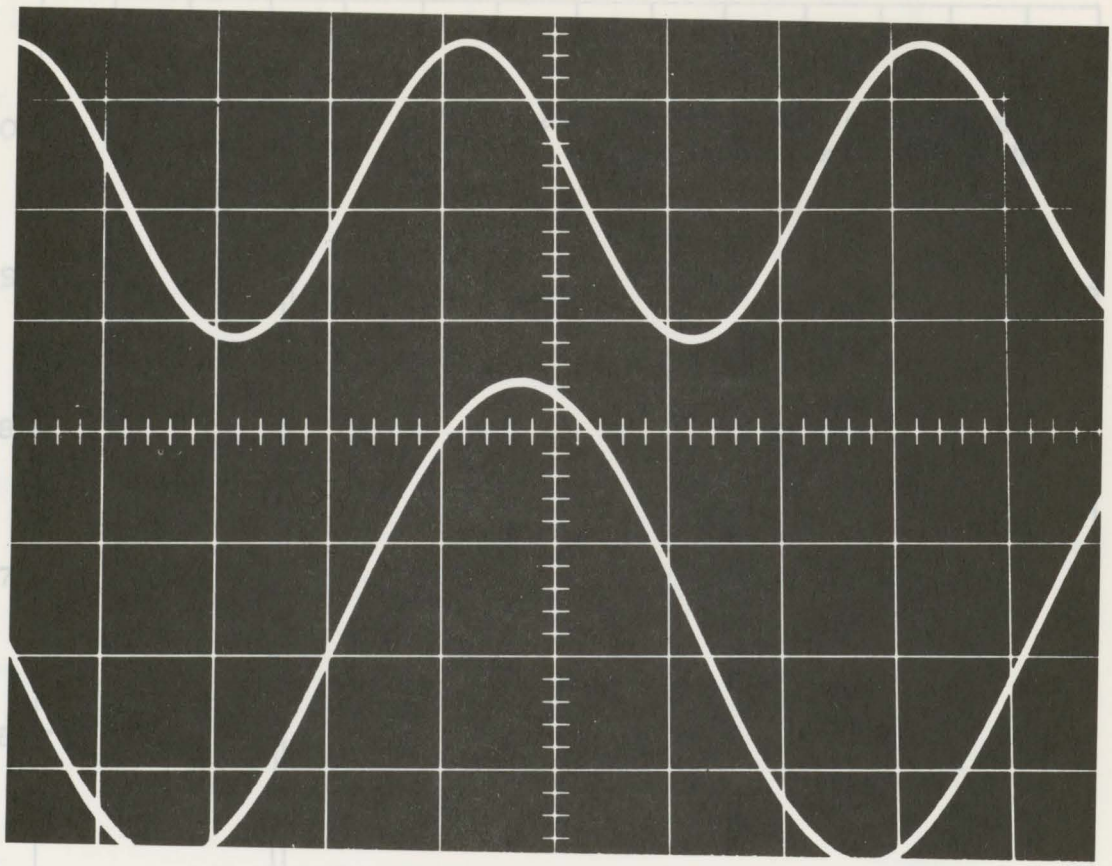

Fig. 3.2.5 An oscilloscope trace: the bottom signal is the total signal from the rotating coil, the top signal is the restored output of the analyzer tuned to the n = 3 harmonic. The phase difference between the two signals is measured directly from these traces.

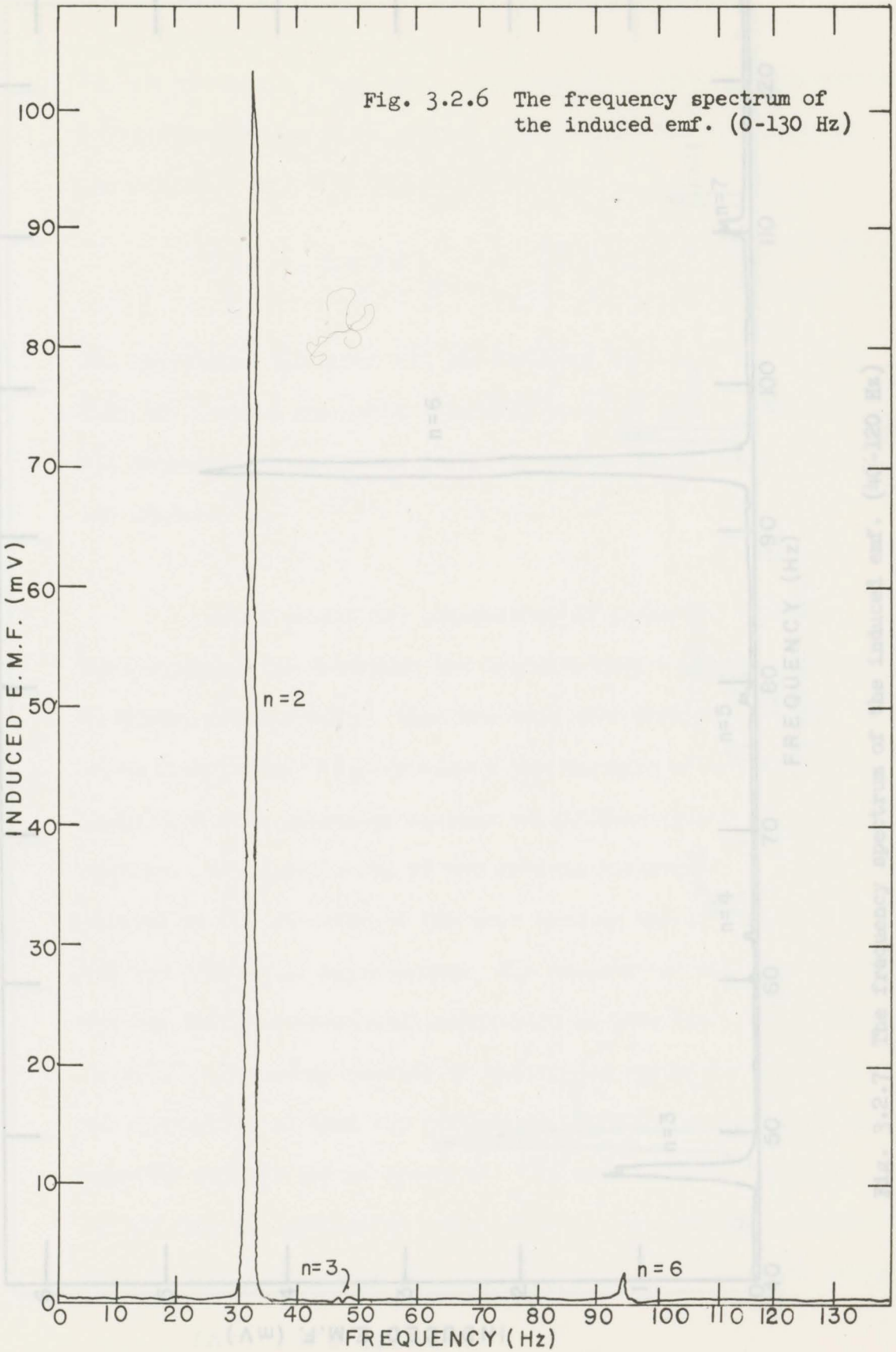

Fig. 3.2.6 The frequency spectrum of the induced emf. (0-130 Hz)

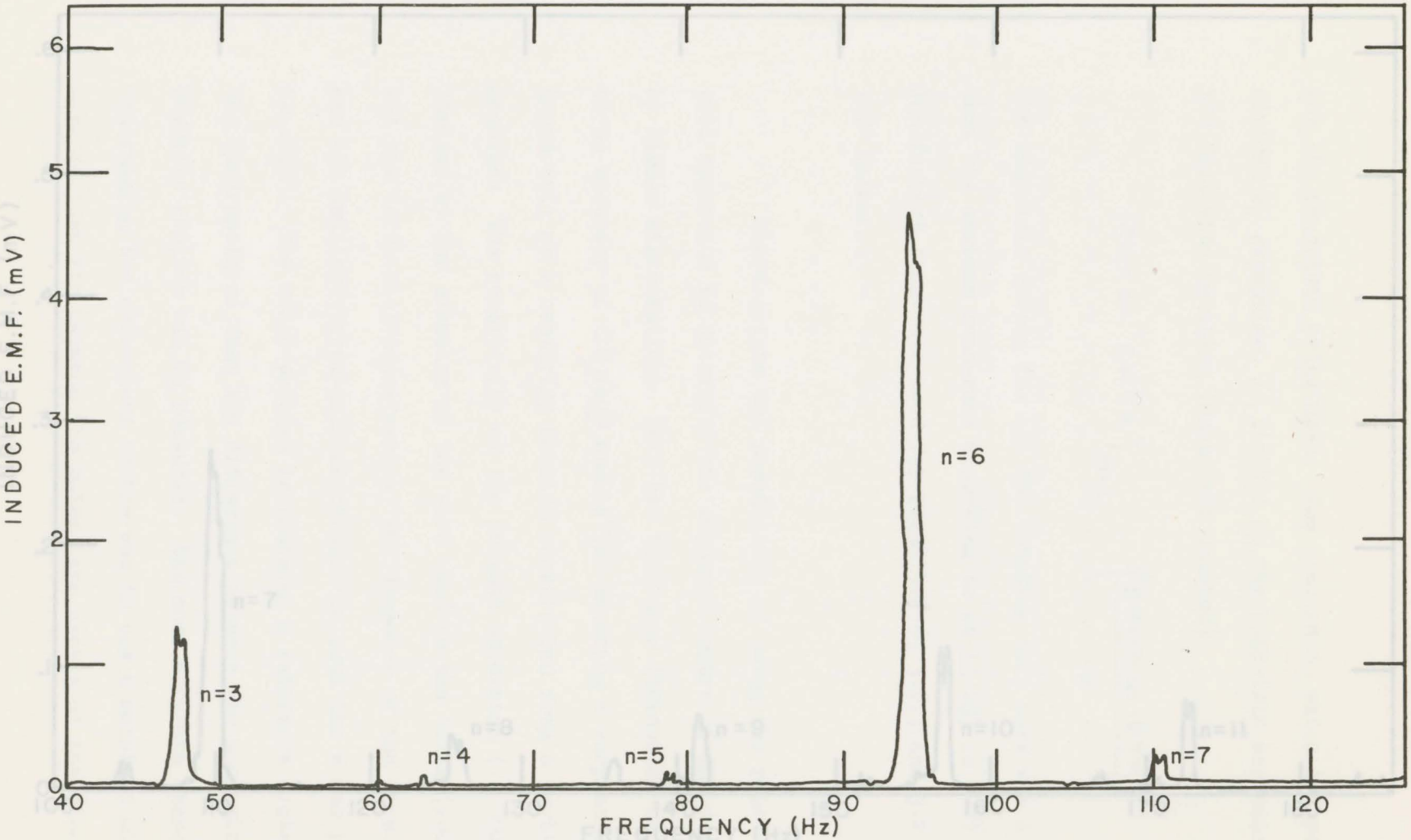

Fig. 3.2.7 The frequency spectrum of the induced emf. (40-120 Hz)

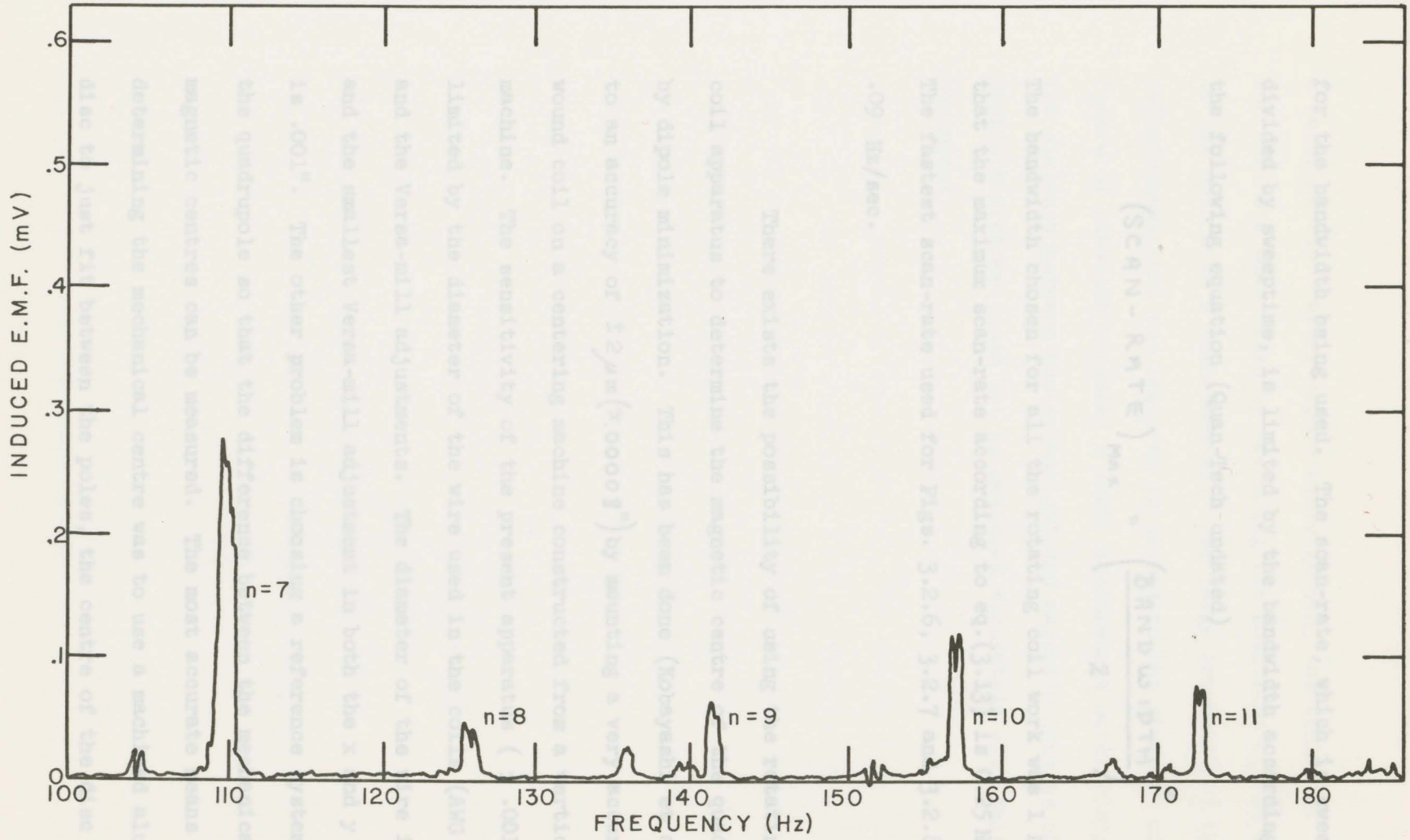

Fig. 3.2.8 The frequency spectrum of the induced emf. (100-180 Hz)

for the bandwidth being used. The scan-rate, which is sweepwidth divided by sweeptime, is limited by the bandwidth according to the following equation (Quan-Tech undated)

$$(\text{SCAN-RATE})_{MAX} = \left(\frac{\text{BANDWIDTH}}{2}\right)^2 \qquad (3.13)$$

The bandwidth chosen for all the rotating coil work was 1 Hz so that the maximum scan-rate according to eq.(3.13) is 0.25 Hz/sec. The fastest scan-rate used for Figs. 3.2.6, 3.2.7 and 3.2.8 was .09 Hz/sec.

There exists the possibility of using the rotating coil apparatus to determine the magnetic centre of the quadrupole, by dipole minimization. This has been done (Kobayashi et al. 1971) to an accuracy of $\pm 2\mu m$ ($\simeq .00008"$) by mounting a very accurately wound coil on a centering machine constructed from a vertical milling machine. The sensitivity of the present apparatus ($\pm$ .001") is limited by the diameter of the wire used in the coils (AWG 43) and the Versa-mill adjustments. The diameter of the wire is .0023" and the smallest Versa-mill adjustment in both the x and y directions is .001". The other problem is choosing a reference system using the quadrupole so that the difference between the mechanical and magnetic centres can be measured. The most accurate means of determining the mechanical centre was to use a machined aluminum disc to just fit between the poles, the centre of the disc being

a machined tip. After dipole minimization, the centre of the coil was determined by measuring the positions of the edges of the coil with a cathetometer. The large traversal of the cathetometer that was required to determine the position of the centre of rotation produced a large measurement uncertainty ($\pm .005"$). The distance between the mechanical and magnetic centres of the magnet therefore could not be measured accurately with this equipment.

3.3 Tests Performed on the Apparatus

To test for the possible periodicity in the rotational frequency of the coil, a trigger circuit was built using a FPT 100 phototransistor. The light was reflected off one face of a hexagon nut on the rotating coil shaft and collimated by a small hole in the support wall of the coil apparatus.

The period was recorded over a 15 minute period with a period counter and chart recorder. The average frequency was 15.5 Hz. The largest fluctuation in the rotational frequency was .08 Hz with typical random changes of .03 Hz. Since the driving motor is of synchronous type, the changes are due only to line frequency fluctuations. Of primary importance, however, is that the changes are not periodic but random.

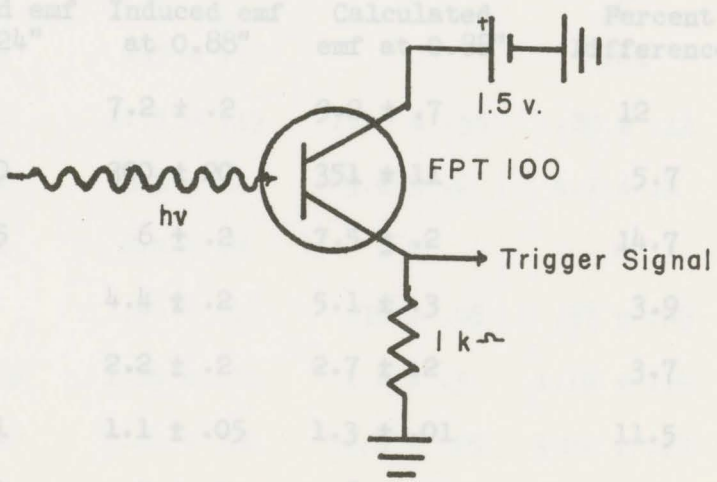

Fig. 3.3.1 The phototransistor trigger circuit

According to the equation for the induced emf. eq.(3.5), the coil signal is proportional to r^n where n is the harmonic index. To test this relationship, two coils of the same length and number of turns were wound, one at an average radius of 1.24" and the other at 0.88". To increase the harmonic content, an iron bar was placed on one pole face of a test quadrupole (Alpha model 3000 test magnet) and no attempt to minimize the dipole term was made. Table 3.1 shows the induced emf. measured at both radii and the value calculated at 0.88" for each harmonic. The harmonics at 0.88" were calculated from the harmonics at 1.24" and eq.(3.5). The uncertainties are from the wave analyzer meter. The differences between the harmonics measured and calculated can be accounted for and will be discussed later (Sec. 3.5).

TABLE 3.1

Results of r_o^n Test (All Induced emf.'s in mV)

n	Induced emf at 1.24"	Induced emf at 0.88"	Calculated emf at 0.88"	Percent Difference
1	13 ± 1	7.2 ± .2	9.2 ± .7	12
2	700 ± 20	300 ± 20	351 ± 11	5.7
3	21 ± .5	6 ± .2	7.5 ± .2	14.7
4	20 ± 1	4.4 ± .2	5.1 ± .3	3.9
5	15 ± 1	2.2 ± .2	2.7 ± .2	3.7
6	10 ± .1	1.1 ± .05	1.3 ± .01	11.5
7	6.8 ± .2	.5 ± .2	.6 ± .02	0
8	4.0 ± .2	.2 ± .1	.3 ± .02	0

To test the possibility of recording false harmonics due to misalignment of the rotating coil and magnetic axis, the apparatus was used in the test quadrupole with the dipole term first minimized. The apparatus was then displaced, the distance being measured by a cathetometer, and the harmonics again measured. In Table 3.2 the changes in each harmonic are measured and calculated. The change in e_n for R = .122" were calculated from the theoretical values listed in Table A.1. Again, the uncertainties are from the wave analyzer meter and the differences between the measured and calculated results will be discussed in Sec. 3.5.

T A B L E 3.2

Results of Off-Axis Test (All emf.'s in mV)

n	Induced emf R ≤ .53x10-3in	Induced emf R=.122in.	Δe_n	Calculated Δe_n	Percent Difference
1	.4	115 ± 2	115 ± 2	92.5 ± 6	16.8
2	940 ± 10	940 ± 10	0	0	0
3	1.0 ± .2	.95 ± .15	0	.01	-
4	.4 ± .2	1.75 ± .15	1.35 ± .35	.82 ± .11	8.5
5	.3 ± .1	5.5 ± .1	5.2 ± .2	4.1 ± .1	19.5
6	8.4 ± .1	8.4 ± .2	0	0	0
7	.1	.45 ± .05	.35 ± .05	.27 ± .06	0
8	.15 ± .05	1.85 ± .15	1.6 ± .3	1.19 ± .14	0
9	.10 ± .05	3.80 ± .20	3.70 ± .25	3.02 ± .23	6.6
10	3.4 ±	3.4 ± .1	0	0	0

To ensure that the equipment measured harmonics that actually existed in a magnetic field, the rotating coil was placed in a large dipole field. Over the area where the coil was rotated, the field was measured with a high precision NMR gaussmeter. The inhomogeneity in the dipole field over the area the coil swept was measured as a gradient of .0296 ± .0071% of the dipole field. The gradient measured with the rotating coil as a quadrupole component was .0476 ± .0247% of the dipole field. All other harmonics measured were less than .01%. The cause of the large uncertainty in the rotating coil measurement will be discussed later in Sec. 3.5.

The conclusions of the tests on the equipment are as follows. The induced emf. from the coil does scale as r^n and false harmonics will be generated if the rotational axis and magnetic axis are not aligned. The rotational frequency is not periodic but does contain small fluctuations. The equipment does measure the harmonic content in a magnetic field.

3.4 Measurements of Quadrupole 4Q19/8

3.4.1 Measurements of Harmonic Content, Effective Length and Linearity

Harmonic content of quadrupole 4Q19/8 was calculated from data obtained using a 25 turn coil of radius 1.8125" and length 2.625". The results are listed in Table 3.3 for two field excitation currents; 250 and 500 amps.

TABLE 3.3

Integrated Harmonic Content of 4Q19/8 as Measured by Rotating Coil

Harmonic	$nC_n/2C_2$	$nC_n/2C_2$
n	I_Q = 250 Amps	I_Q = 500 Amps
1	$< 3.37 \times 10^{-4}$	$< 3.9 \times 10^{-4}$
2	1	1
3	$2.8 \pm .21 \times 10^{-3}$	$2.74 \pm .21 \times 10^{-3}$
4	$< 4.52 \times 10^{-4}$	$< 4.66 \times 10^{-4}$
5	$< 1.68 \times 10^{-4}$	$< 2.46 \times 10^{-4}$
6	$4.32 \pm .21 \times 10^{-3}$	$4.55 \pm .27 \times 10^{-3}$
7	$< 1.75 \times 10^{-4}$	$< 3.03 \times 10^{-4}$
8	$< 1.35 \times 10^{-4}$	$< 2.08 \times 10^{-4}$
9	$< 1.68 \times 10^{-4}$	$< 2.08 \times 10^{-4}$
10	$5.00 \pm .20 \times 10^{-3}$	$4.50 \pm .25 \times 10^{-3}$
14	$6.45 \pm 1.68 \times 10^{-4}$	$6.45 \pm .70 \times 10^{-4}$

Measurements of induced emf.'s for harmonic indices n=2,3,4,6 and 10 along the magnetic axis are shown in Figs. 3.4.1 and 3.4.2. The coil apparatus was stepped along the z direction a distance equal to the length of the coil used. For the large coil measurements, the dipole term was minimized at each z position. The coil radius was chosen to be at least 90% of the 2" aperture radius. The total harmonic content that was measured could be compared with the specifications without scaling according to eq.(3.10).

The present rotating coil apparatus was capable of measuring the harmonic content over only half of the length of 4Q19/8 (see Figs. 3.4.1 and 3.4.2). The integrated harmonic content was calculated using eq.(3.9) assuming the magnet was perfectly symmetric. That is, the harmonic content was assumed to be the same in both fringe fields. From Figs. 3.4.1 and 3.4.2 and Table 3.3, most of the harmonic content namely n=3 and n=6 is in the fringe field of the magnet. To check that the harmonics were symmetric, the magnet was turned around. The induced emf. harmonics at either end of the magnet were well within experimental uncertainties of each other so that the original assumption of symmetry was valid.

The position of the multipoles in the fringe field were plotted from phase measurements using the restored output of the wave analyzer. The results are shown in Figs. 3.4.3a to 3.4.3f. The north poles in the figures indicate the maximum signal for that

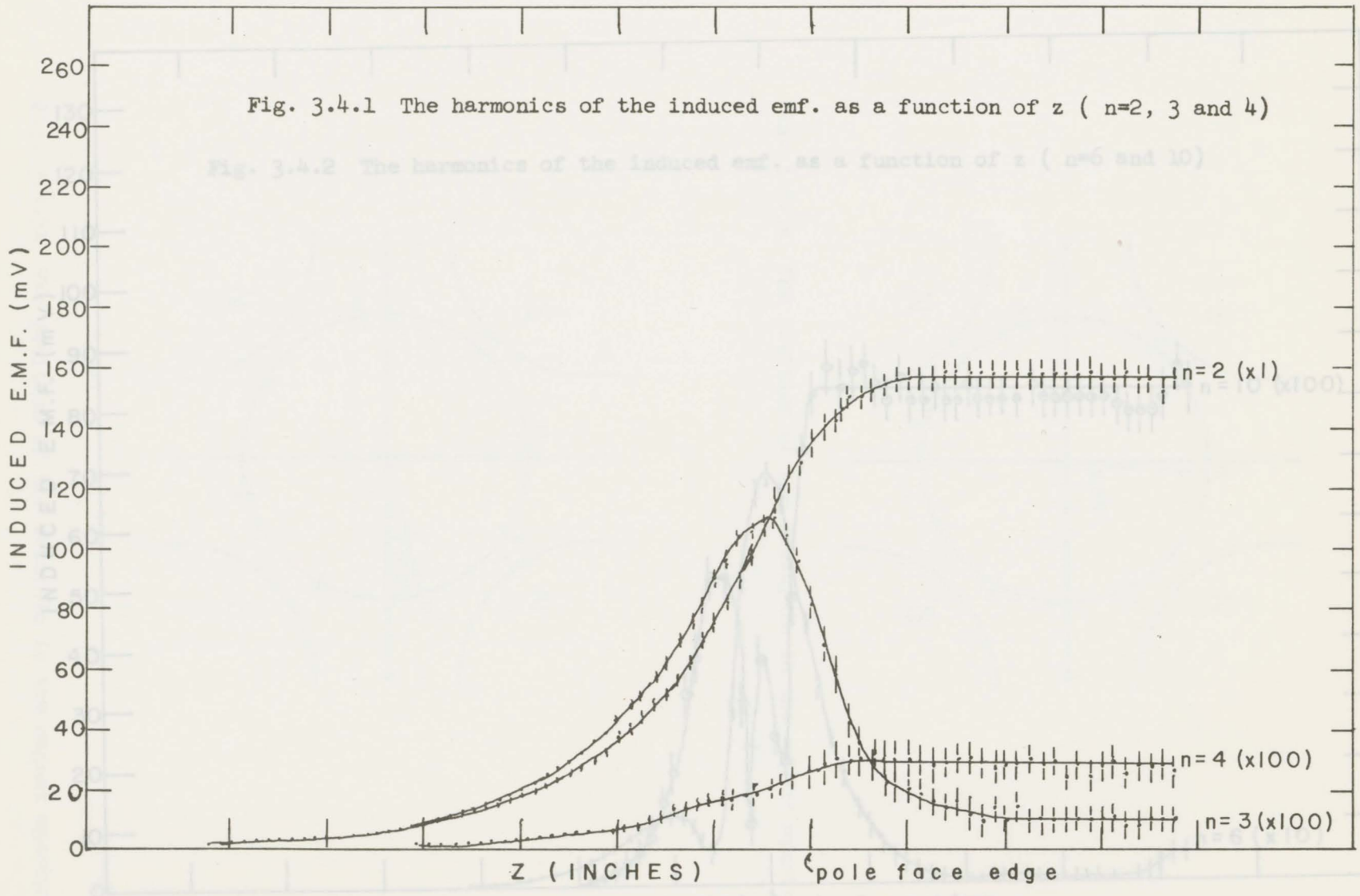

Fig. 3.4.1 The harmonics of the induced emf. as a function of z (n=2, 3 and 4)

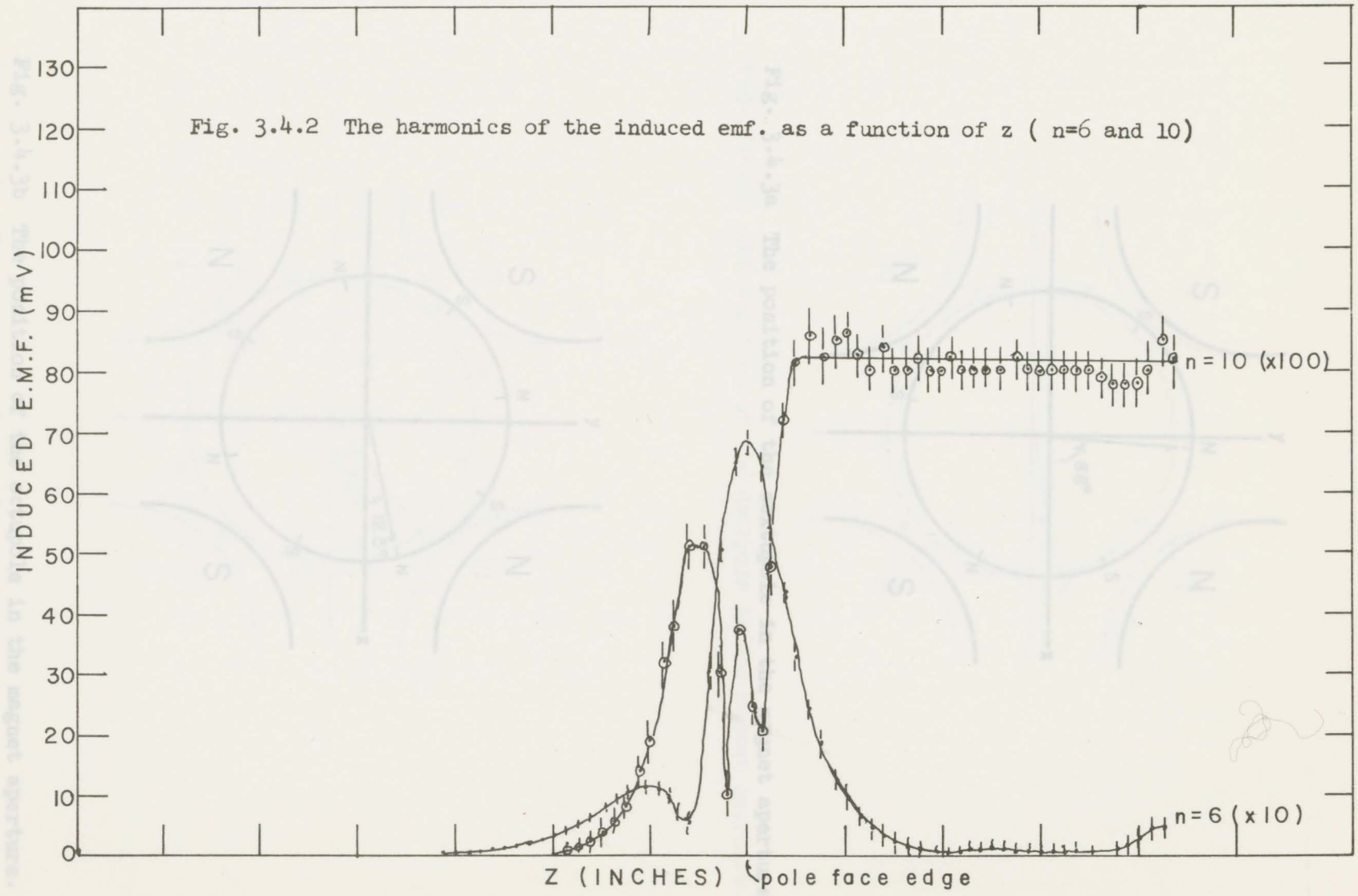

Fig. 3.4.2 The harmonics of the induced emf. as a function of z (n=6 and 10)

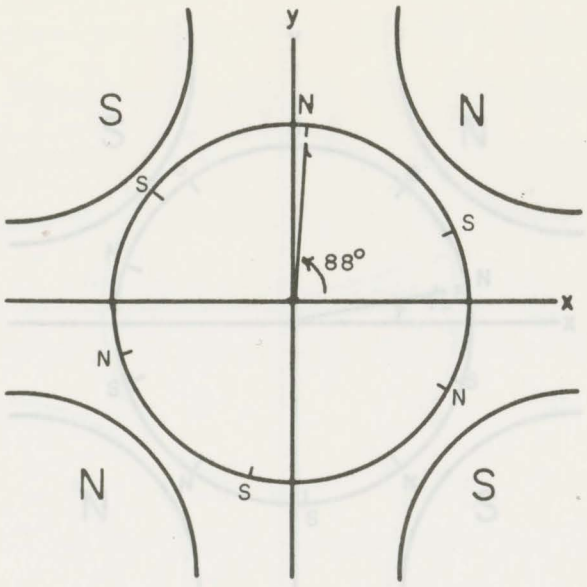

Fig. 3.4.3a The position of the sextupole in the magnet aperture.

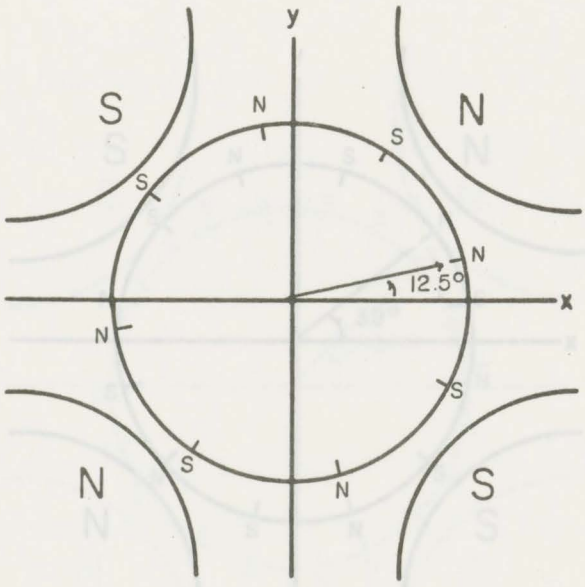

Fig. 3.4.3b The position of the octupole in the magnet aperture.

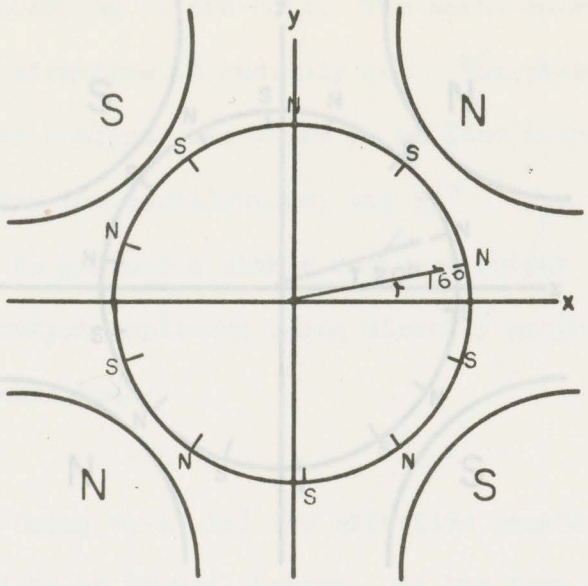

Fig. 3.4.3c The position of the decapole in the magnet aperture.

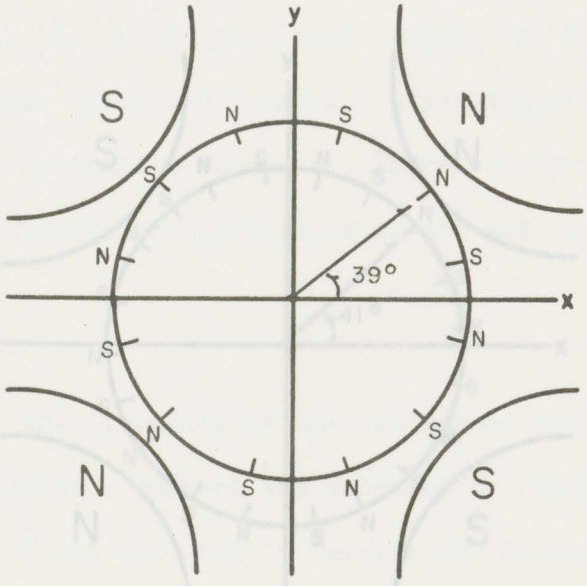

Fig. 3.4.3d The position of the 12-pole in the magnet aperture.

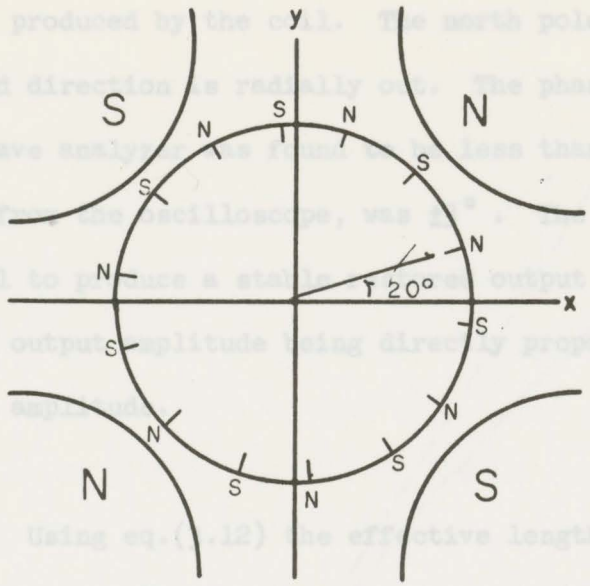

Fig. 3.4.3e The position of the 14-pole in the magnet aperture.

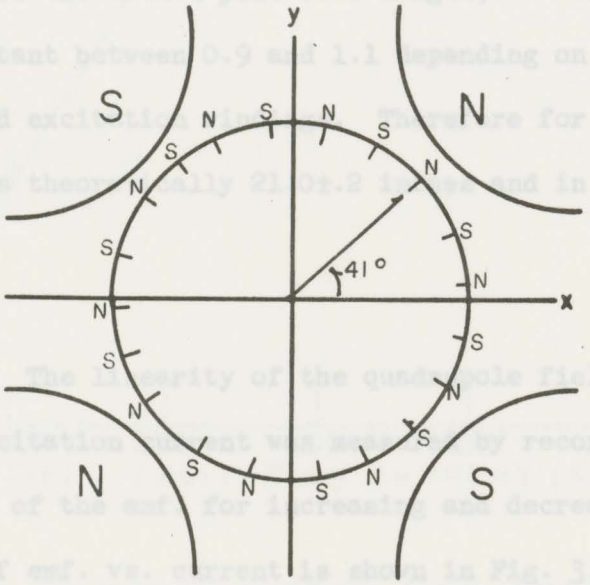

Fig. 3.4.3f The position of the 20-pole in the magnet aperture

harmonic produced by the coil. The north poles then indicate where the field direction is radially out. The phase shift introduced by the wave analyzer was found to be less than 1° and the accuracy, reading from the oscilloscope, was $\pm 3^{\circ}$. The other harmonics were too small to produce a stable restored output signal on the CRO, the restored output amplitude being directly proportional to the input harmonic amplitude.

Using eq.(3.12) the effective length of the quadrupole was calculated to be 20.9±.1 inches. It has been found (Banford 1966) that the effective length of a quadrupole lens can be put in the form

$$\ell_{EFF.} = \ell + ka \qquad (3.14)$$

where ℓ is the actual pole face length, 'a' the aperture radius and k a constant between 0.9 and 1.1 depending on the end shape of the poles and excitation windings. Therefore for 4Q19/8, the effective length is theoretically 21.0±.2 inches and in fact was specified to be 21".

The linearity of the quadrupole field as a function of field excitation current was measured by recording the quadrupole harmonic of the emf. for increasing and decreasing excitation current. A plot of emf. vs. current is shown in Fig. 3.4.4. The theoretical pole tip field on the right hand axis was calculated from the known

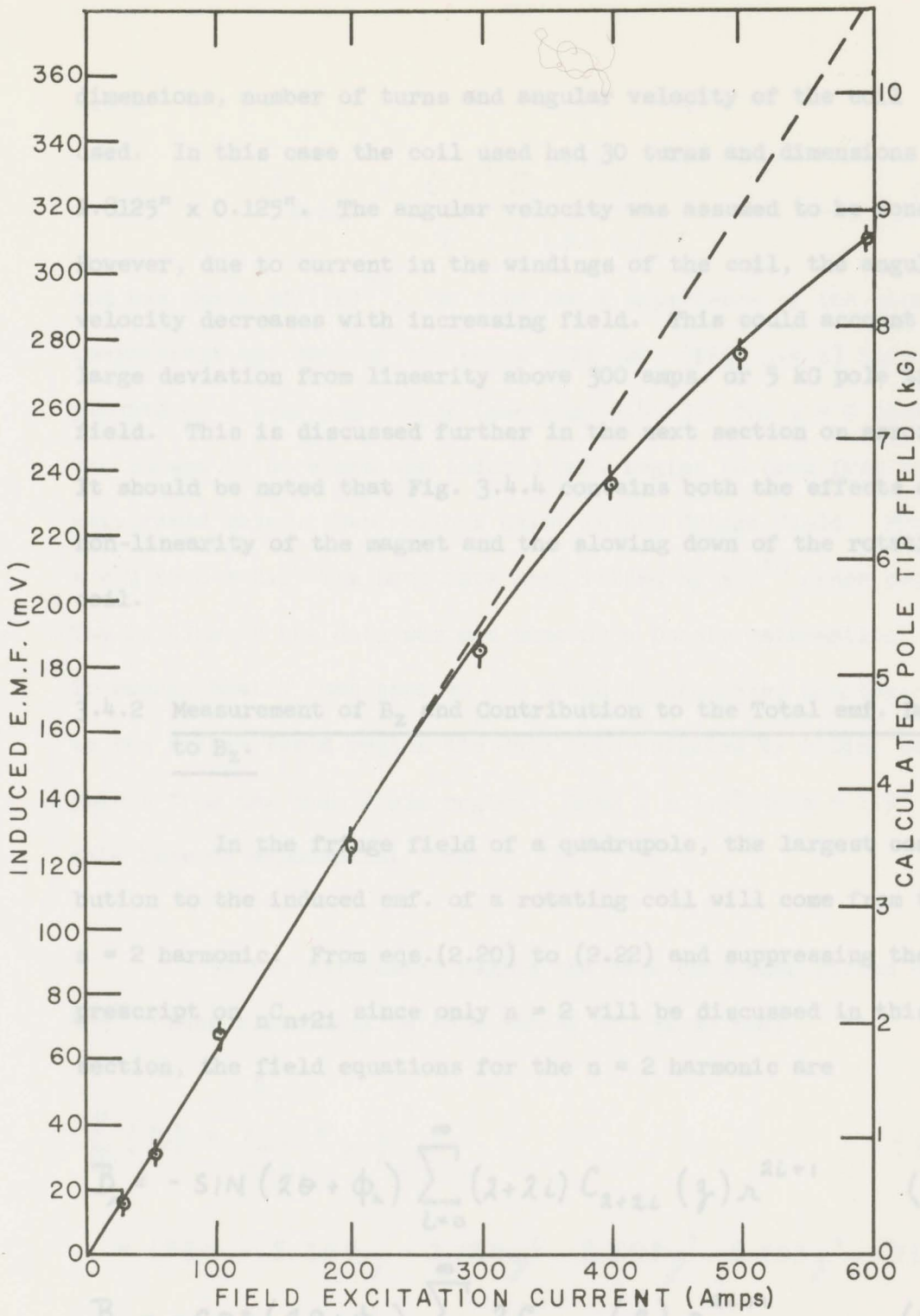

Fig. 3.4.4 The pole tip field vs. field excitation current as measured by the rotating coil. (The nonlinearity is due to iron saturation and decreasing rotational speed as the field increases.)

dimensions, number of turns and angular velocity of the coil used. In this case the coil used had 30 turns and dimensions 1.8125" x 0.125". The angular velocity was assumed to be constant. However, due to current in the windings of the coil, the angular velocity decreases with increasing field. This could account for the large deviation from linearity above 300 amps. or 5 kG pole tip field. This is discussed further in the next section on errors. It should be noted that Fig. 3.4.4 contains both the effects of non-linearity of the magnet and the slowing down of the rotating coil.

3.4.2 Measurement of B_z and Contribution to the Total emf. Due to B_z.

In the fringe field of a quadrupole, the largest contribution to the induced emf. of a rotating coil will come from the n = 2 harmonic. From eqs.(2.20) to (2.22) and suppressing the prescript on ${}_nC_{n+2i}$ since only n = 2 will be discussed in this section, the field equations for the n = 2 harmonic are

$$B_r = -\sin(2\theta+\phi_2)\sum_{i=0}^{\infty}(2+2i)\,C_{2+2i}(z)\,r^{2i+1} \qquad (3.15)$$

$$B_\theta = -\cos(2\theta+\phi_2)\sum_{i=0}^{\infty}2\,C_{2+2i}(z)\,r^{2i+1} \qquad (3.16)$$

$$B_z = -\sin(2\theta+\phi_2)\sum_{i=0}^{\infty}C'_{2+2i}(z)\,r^{2i+2} \qquad (3.17)$$

where

$$C_{2+2i} = \frac{(-1)^i C_2^{(2i)} 2!}{4^i i! (2+i)!} \qquad (3.18)$$

and has units kG/(in)^{2i}. To find the z dependence of the harmonic coefficient the data of the short coil emf. (Fig. 3.4.1) have been plotted on a semi-log. scale (see Fig. 3.4.5). The z = 0 position was chosen to be where the induced emf. begins to drop from the main field value. Two regions exist in the fringe field. From z = 0 to z = 1.5" the data have been fitted by a 5th order polynomial. The fitting of the data was not done on a purely mathematical basis. To ensure that B_z was zero at z = 0 and B_r decreased monotonically in the fringe field region the data were weighted by adding several points from the main field region. From z = 1.5" to z = 1.9" the data have an exponential form.

In the polynomial region the data have been fitted by a 5th order polynomial to an accuracy of .3% so that

$$f(z) = \sum_{p=0}^{5} e_p z^p \qquad (3.19)$$

$$= 157.4 - 3.204 z - 3.130 z^2 - 2.592 z^3 - 5.203 z^4 + 1.753 z^5$$

where z is measured in inches and e_p has units mV/(in)^p. Assuming the field also has a 5th order polynomial form in this region, the number of terms required from the recursion relation for C_{2+2i}

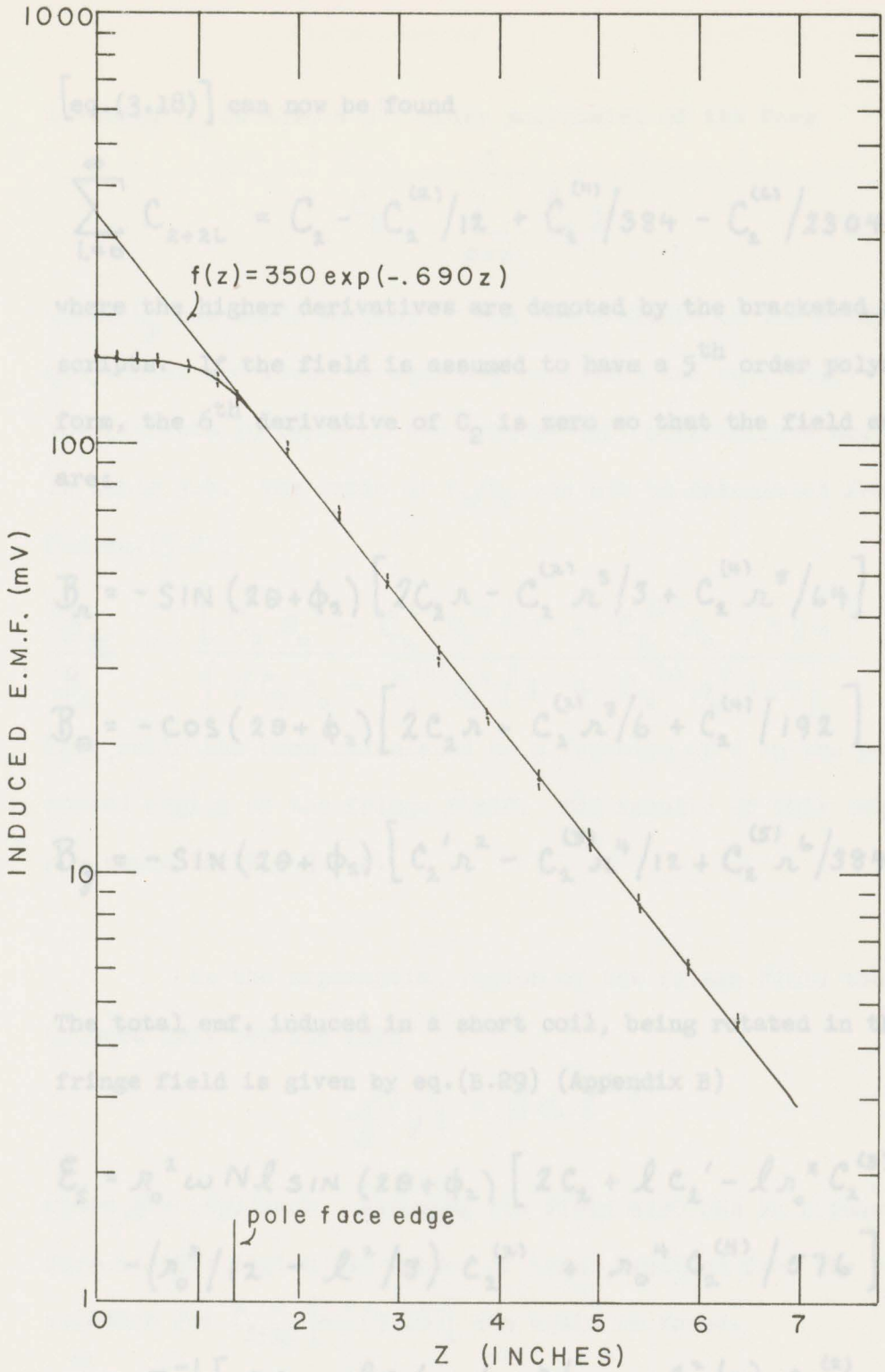

Fig. 3.4.5 The quadrupole harmonic of the induced emf. as a function of z as measured by the short coil.

[eq.(3.18)] can now be found

$$\sum_{i=0}^{\infty} C_{2+2i} = C_2 - C_2^{(2)}/12 + C_2^{(4)}/384 - C_2^{(6)}/23040 \qquad (3.20)$$

where the higher derivatives are denoted by the bracketed superscripts. If the field is assumed to have a 5^{th} order polynomial form, the 6^{th} derivative of C_2 is zero so that the field equations are:

$$B_r = -\sin(2\theta+\phi_2)\left[2C_2 r - C_2^{(2)} r^3/3 + C_2^{(4)} r^5/64\right] \qquad (3.21)$$

$$B_\theta = -\cos(2\theta+\phi_2)\left[2C_2 r - C_2^{(2)} r^3/6 + C_2^{(4)}/192\right] \qquad (3.22)$$

$$B_z = -\sin(2\theta+\phi_2)\left[C_2' r^2 - C_2^{(3)} r^4/12 + C_2^{(5)} r^6/384\right] \qquad (3.23)$$

The total emf. induced in a short coil, being rotated in the fringe field is given by eq.(B.29) (Appendix B)

$$\mathcal{E}_s = r_0^2 \omega N l \sin(2\theta+\phi_2)\left[2C_2 + l C_2' - l r_0^2 C_2^{(3)}/24 - (r_0^2/12 - l^2/3) C_2^{(2)} + r_0^4 C_2^{(4)}/576\right]$$

$$= E^{-1}\left[2C_2 + l C_2' - (r_0^2/12 - l^2/3) C_2^{(2)} - l r_0^2 C_2^{(3)}/24 + r_0^4 C_2^{(4)}/576\right] \qquad (3.24)$$

where E has units kG/(in)-(mV)

Assuming C_2 is also a 5^{th} order polynomial of the form

$$C_2 = \sum_{p=0}^{5} b_p z^p \qquad (3.25)$$

where b_p has units $kG/(in)^{p+1}$ the coefficients of the gradient polynomial are found by equating eq.(3.24) and eq.(3.19). These coefficients in terms of the induced emf. coefficients are listed in Table 3.4. The ratio of B_z/B_r can now be calculated from eq.(3.23) and eq.(3.21).

$$\frac{B_z}{B_r} = \frac{\left[C_2' r_o^2 - C_2^{(3)} r_o^4/12 + C_2^{(5)} r_o^6/384 \right]}{\left[2C_2 r_o - C_2^{(2)} r_o^3/3 + C_2^{(4)} r_o^5/64 \right]} \qquad (3.26)$$

This ratio has been calculated as a function of z in the polynomial region of the fringe field. The results of this calculation are shown in Fig. 3.4.6.

In the exponential region of the fringe field the induced emf. has the form

$$f(z) = A e^{-\beta z} \qquad (3.27)$$

where β = .690/inch. Assuming the field also has an exponential form in this region the number of terms required from the recursion relation for C_{2+2i} [eq.(3.18)] can again be found.

$$\sum_{i=0}^{\infty} C_{2+2i} = C_2 - C_2^{(2)}/12 + C_2^{(4)}/384 - C_2^{(6)}/23040 + \ldots$$

$$= C_2\left(1 - \beta^2/12 + \beta^4/384 - \beta^6/23040 + \ldots\right) \qquad (3.28)$$

TABLE 3.4

The Gradient Coefficients in Terms of the Induced emf. Coefficients

b_p		$r = 1.8125''$ $\ell = 0.125''$
b_0	$\{e_0/2 - \ell e_1/4 + (\ell^2/12 + r^2/24)e_2 + (\ell^3/8 - r^2\ell/16)e_3$ $+ (r^4/96 - r^2\ell^2/24 - 5\ell^4/12)e_4$ $+ (25r^2\ell^3/48 + 3\ell^5/8)e_5\}E$	77.87 E
b_1	$\{e_1/2 - \ell e_2/2 + (r^2/8 + \ell^2/4)e_3$ $+ (\ell^3/2 - r^2\ell/4)e_4$ $- (5r^2\ell^2/24 + 25\ell^4/12 - 5r^4/96)e_5\}E$	-.9861 E
b_2	$\{e_2/2 - 3\ell e_3/4 + (r^2/4 + \ell^2/2)e_4 + (5\ell^3/4 - 5r^2\ell/8)e_5\}E$	-6.081 E
b_3	$\{e_3/2 - \ell e_4 + (5r^2/12 + 5\ell^2/6)e_5\}E$	1.777 E
b_4	$\{e_4/2 - 5\ell e_5/4\}E$	-2.875 E
b_5	$\{e_5/2\}E$	.8765 E

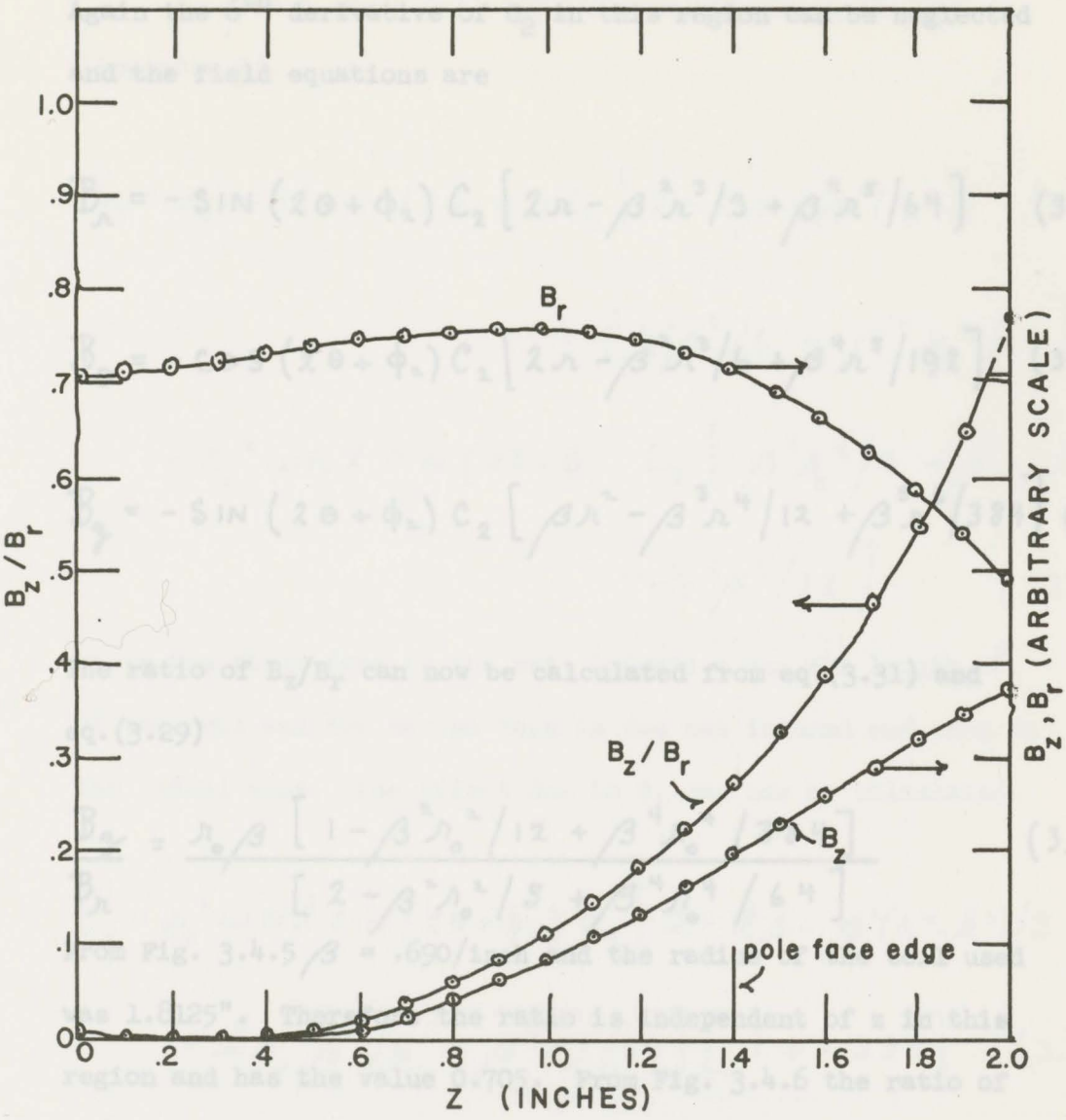

Fig. 3.4.6 B_z/B_r as a function of z in the polynomial and exponential regions of the fringe field

Again the 6th derivative of C_2 in this region can be neglected and the field equations are

$$B_r = -\sin(2\theta+\phi_2)\, C_2 \left[2r - \beta^2 r^3/3 + \beta^4 r^5/64\right] \quad (3.29)$$

$$B_\theta = -\cos(2\theta+\phi_2)\, C_2 \left[2r - \beta^2 r^3/6 + \beta^4 r^5/192\right] \quad (3.30)$$

$$B_z = -\sin(2\theta+\phi_2)\, C_2 \left[\beta r^2 - \beta^3 r^4/12 + \beta^5 r^6/384\right] \quad (3.31)$$

The ratio of B_z/B_r can now be calculated from eq.(3.31) and eq.(3.29)

$$\frac{B_z}{B_r} = \frac{r_0\beta\left[1 - \beta^2 r_0^2/12 + \beta^4 r_0^4/384\right]}{\left[2 - \beta^2 r_0^2/3 + \beta^4 r_0^4/64\right]} \quad (3.32)$$

From Fig. 3.4.5 β = .690/inch and the radius of the coil used was 1.8125". Therefore the ratio is independent of z in this region and has the value 0.705. From Fig. 3.4.6 the ratio of B_z/B_r in the polynomial region and exponential region has the same value approximately where the two regions meet in Fig. 3.4.5. Since the largest ratio of B_z/B_r occurs in the exponential region of the fringe field the effect of B_z on the induced emf. of the coil will be largest in this region. The amount of signal due to B_z in this region in the short and long coils used for measurement will now be calculated.

For a short coil the induced emf. is eq.(B.29) (Appendix B).

$$\mathcal{E}_s = r_0^2 \omega N l \sin(2\theta+\phi_2) C_2 \left[2 - l\beta - \beta^2(r_0^2-l^2)/3 + l r_0^2 \beta^3/6 + \beta^4 r_0^4/64 \right]$$

$$+ r_0^2 \omega N l \sin(2\theta+\phi_2) C_2 \left[\beta^2 r_0^4/4 - \beta^3 r_0^2 l/8 - r_0^4 \beta^4/72 \right] \qquad (3.33)$$

where the first term is the emf. induced along the length, l, of the coil and the second term is the net induced emf. due to the radial arms. The effect due to B_z can now be calculated.

$$\mathcal{E}_s = r_0^2 \omega N l \sin(2\theta+\phi_2) C_2 \left[2 - l\beta - \beta^2(r_0^2-l^2)/3 + l r_0^2 \beta^3/6 + \beta^4 r_0^4/64 \right] \left[1 + .234 \right] \qquad (3.34)$$

Therefore the amount of signal due to B_z in a short coil as a percentage of the total signal is

$$\frac{.234}{1.234} \times 100\% = 19.0\% \qquad (3.35)$$

For a long coil rotating in the fringe field the emf. in general is given by eq.(B.34) (Appendix B).

$$\mathcal{E}_L = r_0^2 \omega N \sin(2\theta + \phi_2) \cdot$$

$$\cdot \left\{ \frac{1}{\beta} \left(2 - \beta^2 r_0^2/3 + \beta_4 r_0^4/64\right)\left(C_2(z_2) - C_2(z_4)\right) \right.$$

$$+ \sum_{p=0}^{5} \frac{d_p}{p+1} \left(z_4^{p+1} - z_3^{p+1}\right) + 2A_2(z_3 - z_1)$$

$$\left. - \left[C_2' r_0^2/4 - C_2^{(3)} r_0^4/72 + C_2^{(5)} r_0^6/3072\right]_{z_1} \right\} \quad (3.36)$$

where the z positions z_1, z_2, z_3, and z_4 are shown in Fig. 3.4.7 and A_2 is the value of the gradient in the main field.

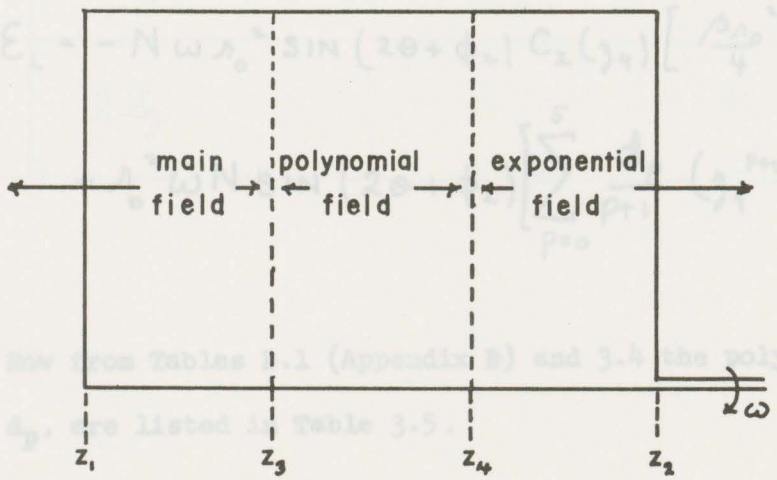

Fig. 3.4.7 The long coil in the fringe field.

The largest effect that B_z would have on the emf. is when B_z is largest. Since B_z/B_r is constant in the exponential region, B_z is largest where B_r is largest and this will occur where the exponential region starts at z = 1.5" (see Fig. 3.4.5). Therefore if the radial arm is at z_4, the induced emf. along the length will contain only the polynomial and constant terms.

$$\mathcal{E}_L = -N\omega r_o^2 \sin(2\theta+\phi_2)\, C_2(z_4)\left[\frac{\beta r_o^2}{4} - \frac{\beta^3 r_o^4}{72} + \frac{\beta^5 r_o^6}{3072}\right]$$
$$+ r_o^2 \omega N \sin(2\theta+\phi_2)\left[\sum_{p=0}^{5} \frac{d_p}{p+1}\left(z_4^{p+1} - z_3^{p+1}\right) + 2A_2(z_3 - z_1)\right] \quad (3.37)$$

From Fig. (3.4.7) z_3 is at z = 0 and z_4 = 1.5". Also the length of the long coil used was 2.625" so that $(z_1 - z_3)$ is 1.125". Therefore

$$\mathcal{E}_L = -N\omega r_o^2 \sin(2\theta+\phi_2)\, C_2(z_4)\left[\frac{\beta r_o^2}{4} - \frac{\beta^3 r_o^4}{72} + \frac{\beta^5 r_o^6}{3072}\right]$$
$$+ r_o^2 \omega N \sin(2\theta+\phi_2)\left[\sum_{p=0}^{5} \frac{d_p}{p+1}\left(z_4^{p+1}\right) + 2.25\, A_2\right] \quad (3.38)$$

Now from Tables B.1 (Appendix B) and 3.4 the polynomial coefficients, d_p, are listed in Table 3.5.

TABLE 3.5

The Field Coefficients in Terms of the Gradient Coefficients

d_p		$r = 1.8125''$
d_0	$2b_0 - 2b_2 r^2/3 + 3b_4 r^4/8$	157.4 E
d_1	$2b_1 - 2b_3 r^2 + 15b_5 r^4/8$	4.089 E
d_2	$2b_2 - 4b_4 r^2$	25.62 E
d_3	$2b_3 - 20b_5 r^2/3$	-15.64 E
d_4	$2b_4$	-5.75 E
d_5	$2b_5$	1.753 E

where

$$E = \left[r_0^2 \omega N l \sin (2\theta + \phi_2) \right]^{-1} \qquad (3.39)$$

$$= 2A_2 \Big/ (\text{QUADRUPOLE HARMONIC OF EMF. INDUCED IN THE SHOR COIL IN THE MAIN FIELD})$$

Therefore the polynomial has the value

$$\sum_{\rho=0}^{5} \frac{\alpha_\rho}{\rho+1} \gamma_4^{\rho+1} = 244.3\, E = 3.09\, A_2 \qquad (3.40)$$

The total emf. E_L can now be written as

$$\mathcal{E}_L = N \omega r_0^2 \sin (2\theta + \phi_2) \left[3.09 A_2 + 2.25 A_2 \right] \cdot$$

$$\cdot \left(1 - \frac{C_2(\gamma_4) \left[\beta r_0^2/4 - \beta^3 r_0^4/72 + \beta^5 r_0^6/3072 \right]}{\left[3.09 A_2 + 2.25 A_2 \right]} \right) \qquad (3.41)$$

From Fig. (3.4.5) $C_2(z_4) = .86 A_2$ (3.42)

Therefore

$$\mathcal{E}_L = N \omega r_0^2 \sin (2\theta + \phi_2) (5.34 A_2)(1 - .0836) \qquad (3.43)$$

Therefore of the total induced emf. in a long coil the amount due to B_z is a maximum of

$$\frac{.0836}{.9164} \times 100\% = 9.12\% \qquad (3.44)$$

If it is assumed that the n = 2 harmonic of the rotating coil is entirely due to the gradient of the field so that

$$\mathcal{E} = 2A_2 r_0^2 \omega N l \sin(2\theta + \phi_2) \qquad (3.45)$$

where A_2 is the gradient of the field, then B_z and additional terms in B_r represent an error in the assumption. In a short coil the induced emf. is from eq.(3.24)

$$\mathcal{E}_s = 2C_2 r_0^2 \omega N l \sin(2\theta + \phi_2)\left[1 + l C_2'/2C_2 + l^2 C_2^{(2)}/6C_2 - r_0^2 C_2^{(2)}/24C_2 - l r_0^2 C_2^{(3)}/48C_2 - r_0^4 C_2^{(4)}/1152 C_2\right] \qquad (3.46)$$

The largest error will occur in the exponential region where B_z/B_r is the largest so that eq.(3.46) becomes

$$\mathcal{E}_s = 2C_2 r_0^2 \omega N l \sin(2\theta + \phi_2)\left[1 - \beta l/2 + \beta^2 l^2/6 - \beta^2 r_0^2/24 + l r_0^2 \beta^3/48 - \beta^4 r_0^4/1152\right]$$

$$= 2C_2 r_0^2 \omega N l \sin(2\theta + \phi_2)\left[1 - .1021\right] \qquad (3.47)$$

Therefore the error as a percentage of the total signal is

$$\frac{.1021}{.8979} \times 100\% = 11.3\% \qquad (3.48)$$

3.5 Errors

The errors inherent in the equipment will now be analyzed. Systematic errors affect the calculations of effective length, the amount of B_z in the fringe field and the linearity of the field with excitation current. Not affected, however, are the integrated harmonic content calculations. The random errors affect all the measurements that were taken.

3.5.1 Systematic Errors

When winding the coils used for all the above calculations a systematic error exists due to the construction of the coils and the materials used. The coils are wound in plastic rectangular forms. The windings are held in position by .020" cuts. The effect of bends or kinks in the wire is minimized by using many turns, however due to the spreading of the windings at the corners and along the length an error exists in the measurement of the length and radius of the coil. In the radius measurement, an even distribution of wire within the cut is assumed. This assumption could produce a small error ($< 1\%$) in the measured average radius due to stacking in the cut along the inside edge. The effect of spreading at the corners on the length measurement is of the same order ($< 4\%$) but only for the short coil used and is much less ($< .1\%$) for the long coils.

The coil length is assumed to be parallel to the axis

of rotation. If it is not, the cross-product in eq.(3.2) is

$$\vec{\ell} \times \hat{\theta} = \begin{pmatrix} \hat{r} & \hat{\theta} & \hat{k} \\ \ell \sin\alpha & 0 & \ell\cos\alpha \\ 0 & 1 & 0 \end{pmatrix} = -\ell\cos\alpha\,\hat{r} + \ell\sin\alpha\,\hat{k} \qquad (3.49)$$

where α is the angle between the z direction and the length of the coil, ℓ. If $B_z = 0$, then the induced emf. is

$$\mathcal{E} = N \sum_{n=1}^{\infty} n\omega\ell C_n r_o^n \sin(n\theta + \phi_n)\cos\alpha \qquad (3.50)$$

Over the length of the long coil used the difference in radius is certainly less than .010". The resulting angle α is, then, less than 20 minutes of arc. Therefore, the error introduced in the induced emf. is less than .01%. The calculations affected by these possible errors are any involving the measurement of the dimensions of the coil, namely the r_o^n test, the misalignment test, the linearity of field with excitation current, and scaling of harmonic content with radius if required. An upper limit on the error introduced by coil construction is 1%.

The large deviation from linearity in the quadrupole above an applied excitation current of 300 amps is due in part to the current in the windings of the coil. This current is limited only by the 100 kΩ input impedence of the wave analyzer. In a dipole field the affect due to this current was strong enough to almost stop the rotation in a field of 6 kG. In a quadrupole the effect is not so severe and the reduction of rotational frequency has been

measured to be 4% at a pole tip field of 8 kG. Therefore, the linearity curve assuming a constant value for the rotational frequency has an error of 4% at 8 kG. However, the amount of current produced in the coil is also a function of field so that a calibration curve of ω vs. field excitation current would have to be plotted before a linearity curve could be drawn, increasing the possible errors in the calculation of the pole tip field.

When the coil is being stepped in and out of the field, the decrease in field that the coil sees will increase the rotational frequency, however, the effective length and harmonic content as a function of z were calculated from data taken in a field produced by an excitation current of 250 amps. From Fig. 3.4.5, the deviation from linearity is less than 2% or of the same order as the recorded experimental uncertainty in the induced emf. Therefore, the error introduced by current in the windings on the harmonics as a function of z plots (Figs. 3.4.1 and 3.4.2) can be included in the recorded uncertainties. The calculation of the effective length for a long quadrupole is not affected by this current. Referring to eq.(3.13), the quadrupole harmonic of the emf., e_2, is smaller in the main field but larger in the fringe field making $\sum e_2$ too small for a long magnet. For a very short magnet $\sum e_2$ would be too large. The value of e_2 per unit length in the main field is too small in either case. Therefor, for a long magnet such as 4Q19/8, the reduction in both terms

is almost equal and the error introduced is certainly within the calculated uncertainty due to measurement. For a very short quadrupole, the calculated effective length would be too long due to the current in the windings. Therefore the possible error introduced by current in the windings in the above calculations is 2%.

The effect that B_z has on the harmonic content and effective length calculations will now be discussed. When stepping the large coil through the fringe field by a distance equal to the length of the coil, the effect on the harmonic content calculations cancels out. This is because the two radial arm contributions to the emf. are of opposite sign so that when summing the emfs. for any harmonic from each z position the radial arm emf. contributions are cancelled in successive z positions. The harmonic content calculations are therefore unaffected by B_z.

When calculating the effective length from the n = 2 harmonic data the effect due to B_z again cancels out. But if the emf. is assumed to be due only to the gradient of the field C_2, the higher terms in B_r represent an error in this assumption. The error in the calculated value of the effective length due to this error is within experimental uncertainties since the error in the data affects less than 20% of the total emf. induced in the coil along the whole length of the magnet.

3.5.2 Random Errors

The random fluctuations in ω produce a small random error in the induced emf. According to eq.(3.3) the maximum percentage error caused by these small fluctuations is only 0.5%. This is only true for large harmonics however. The large uncertainties recorded from the wave analyzer meter when measuring the small higher harmonics of the induced emf. are caused by the filter response in the analyzer. The ripple over the centre of the bandpass response is about .03% of the largest harmonic (see Fig. 3.2.8). Therefore the small changes in ω cause the signal to drift slightly over the bandpass response of the filter causing a fluctuation of .03% of the largest harmonic regardless of the size of the harmonic being measured. This imposes a lower limit on the size of harmonics measurable with the Quan-Tech 304 wave analyzer. This lower limit is indicated in the measured results of 4Q19/8 in Table 3.3. The large uncertainties in the test results and in the calculated harmonic content are caused by the small fluctuations in ω ; the error being $\leq$ .03% of the largest harmonic.

The uncertainties due to changes in ω do not account for all the errors, especially in the r_o^n test, and misalignment test. The percentage errors indicated in Tables 3.1 and 3.2 do not include the uncertainties. Therefore, the stated percentage error must come from another source. The wave analyzer has a specified

accuracy of ±5% of full scale. With two scales available on the meter (0-10 and 0-3 mV) the possible inaccuracy for less than full-scale measurements is ±15%. Along with the systematic errors present in the test results the possible inaccuracy of the wave analyzer accounts for the percentage differences in Tables 3.1 and 3.2.

CHAPTER 4

THE HALL PLATE

4.1 Theory

The Hall plate is a galvanomagnetic device constructed of semiconductor material. To utilize the two effects present in a galvanomagnetic device, namely the Hall effect and change of resistance, in a magnetic field, the Hall plate is used as shown in Fig. 4.1.1.

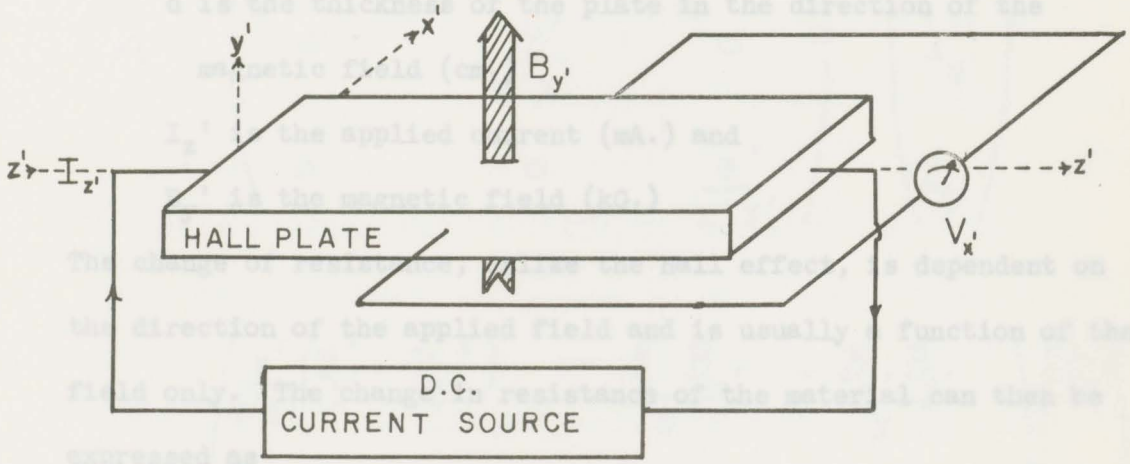

Fig. 4.1.1 The Hall Plate measuring system.

The Hall effect is the forcing of a current to one side of a conductor causing an induced voltage perpendicular to both the current and the applied field. The change in resistance occurs because the equipotential lines across the conductor are not parallel to the sides of the conductor in the presence of the applied field.

To first order in the magnetic field, the induced voltage, V_x' is proportional to B_y' and we have

$$V_{x'} = \frac{R}{d} I_{z'} B_{y'} \qquad (4.1)$$

where R is the Hall coefficient $\left(\Omega - cm./kG.\right)$

d is the thickness of the plate in the direction of the magnetic field (cm.)

I_z' is the applied current (mA.) and

B_y' is the magnetic field (kG.)

The change of resistance, unlike the Hall effect, is dependent on the direction of the applied field and is usually a function of the field only. The change in resistance of the material can then be expressed as

$$\Delta \rho = f\left(|B_{y'}|\right) \qquad (4.2)$$

To second order approximation the relationships for the electric field in terms of the magnetic induction are as follows (Weiss 1969).

$$\begin{pmatrix} V_{x'} \\ V_{y'} \\ V_{z'} \end{pmatrix} = \begin{pmatrix} 0 & -\frac{R}{y'} I_{z'} & \frac{R}{z'} I_{y'} \\ \frac{R}{x'} I_{z'} & 0 & -\frac{R}{z'} I_{x'} \\ \frac{R}{x'} I_{y'} & -\frac{R}{y'} I_{x'} & 0 \end{pmatrix} \begin{pmatrix} B_{x'} \\ B_{y'} \\ B_{z'} \end{pmatrix}$$

$$+ \rho_0 \begin{pmatrix} \frac{x'}{y'z'} & 0 & 0 \\ 0 & \frac{y'}{z'x'} & 0 \\ 0 & 0 & \frac{z'}{x'y'} \end{pmatrix} \begin{pmatrix} I_{x'} \\ I_{y'} \\ I_{z'} \end{pmatrix}$$

$$+ a\rho_0 \begin{pmatrix} \frac{x'}{y'z'}\left(B_{y'}^2 + B_{z'}^2\right) & -\frac{B_{x'} B_{y'}}{z'} & -\frac{B_{x'} B_{z'}}{x'} \\ -\frac{B_{y'} B_{x'}}{z'} & \frac{y'}{x'z'}\left(B_{x'}^2 + B_{z'}^2\right) & -\frac{B_{y'} B_{z'}}{x'} \\ -\frac{B_{z'} B_{x'}}{y'} & -\frac{B_{z'} B_{y'}}{x'} & \frac{z'}{x'y'}\left(B_{x'}^2 + B_{y'}^2\right) \end{pmatrix} \begin{pmatrix} I_{x'} \\ I_{y'} \\ I_{z'} \end{pmatrix} \quad (4.3)$$

where ρ_0 is the resistivity (Ω - cm.)

a is the magnetoresistive coefficient (kG^{-2})

and x', y', z' are the dimensions of the plate (cm).

When the plate is used in the magnetic field, the only electric field component measured is V_x' and the applied current is I_z'. Therefore the only voltage component of interest is V_x'. From eq.(4.3) we have

$$V_x' = -\frac{R}{y'} I_z' B_x' + \frac{R}{z'} I_y' B_z' + \rho_o \frac{x'}{y'z} I_x'$$

$$+ a\rho_o \frac{x'}{yz'} (B_y'^2 + B_z'^2) I_x' - \frac{a\rho_o}{z'} B_x' B_y' I_y'$$

$$- \frac{a\rho_o}{y'} B_x' B_y' I_z' \qquad (4.4)$$

In a homogeneous field where $B_x' = B_y' = 0$ the voltage to second order has the simpler form

$$V_x' = \frac{x'}{y'z'} \rho_o I_x' - \frac{R}{y'} I_z' B_y' + \frac{x'}{y'} a\rho_o I_x' B_y'^2 \qquad (4.5)$$

Three terms are left each representing the three effects present in the Hall Plate. The first is the pure resistance, the second is the Hall effect and the third, the magnetoresistive effect. The magnetoresistance coefficient, a, and the Hall coefficient, R, however are not constant but are functions of the applied magnetic field. In fact, for the precision required in the measurements taken in this paper (.02%) a 6^{th} order polynomial fit of Hall volts vs. magnetic field (B_y') is required (Gathright and Reeve 1972). Therefore, even if the Hall voltage is calibrated in a known homogeneous field the Hall coefficient and magnetoresistance coefficient values can only be approximated.

In an inhomogeneous field such as in a quadrupole eq.(4.4) must be used. This can be simplified, however if the currents in the x' and y' directions are neglected. The current in the y' direction is small since the plate is made very thin and $I_{x'}$ can be made small by measuring $V_{x'}$ with a high input impedence instrument such as a DVM. Therefore eq. (4.4) is reduced to two terms.

$$V_{x'} = -\frac{R}{y'} I_z B_{y'} - \frac{a\rho_0}{y'} B_{x'} B_z I_z \qquad (4.6)$$

To obtain the integrated harmonic content of the field, the Hall plate must be stepped around a complete circle in the aperture of the magnet as well as along the magnetic axis. The centre of this circle must lie on the magnetic axis of the quadrupole otherwise "false" harmonics will be generated in the Hall voltage. This effect is completely analogous to the misalignment of the rotating coil (Appendix A) and the mathematical treatment is the same. The Hall plate voltage for each data point is then changed to magnetic field values using the calibration. The field values are then analyzed by a Fourier analysis computer program. The harmonic order to which the data are fitted is limited by the number of data points taken around the circle. If the total number of data points is 2N+1 the maximum harmonic order available to fit the data is N.

The orientation of the Hall plate in the aperture of the magnet will determine what B_x' and B_y' are in terms of the field of the magnet. The Hall plate will always be placed in the field so that the z' axis will be parallel with the z axis of the magnet so that $B_z' = B_z$. In general the Hall plate will be oriented in the field so that it is rotated about its own axis with a fixed integral relationship to its angular position in the aperture of the magnet (Gathright and Reeve 1972) (see Fig. 4.1.2).

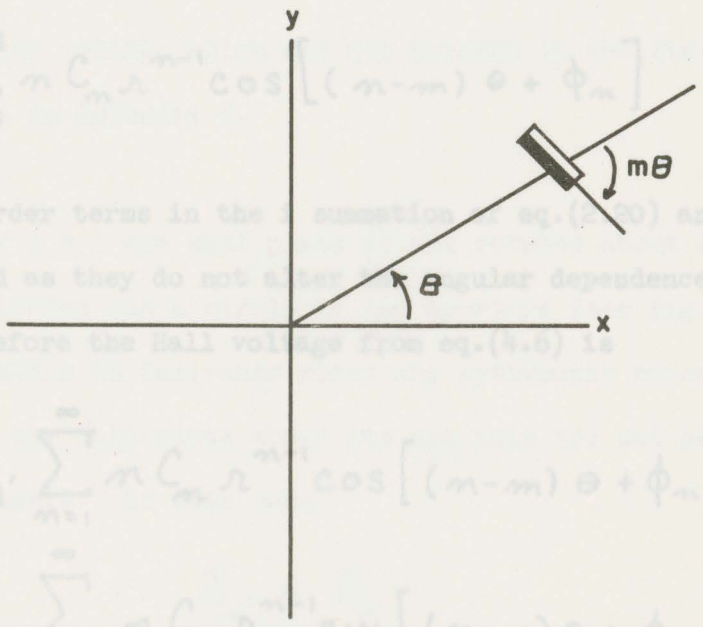

Fig. 4.1.2 Hall plate rotated about its own axis with a fixed integral relationship to its angular position

Therefore

$$B_{x'} = B_r \cos(m\theta) - B_\theta \sin(m\theta) \qquad (4.7)$$

$$B_{y'} = B_r \sin(m\theta) + B_\theta \cos(m\theta) \qquad (4.8)$$

where m is an integer.

Therefore in general using eq.(2.20) and eq.(2.22)

$$B_{x'} = -\sum_{n=1}^{\infty} n C_n r^{n-1} \sin\left[(n-m)\theta + \phi_n\right] \qquad (4.9)$$

$$B_{y'} = -\sum_{n=1}^{\infty} n C_n r^{n-1} \cos\left[(n-m)\theta + \phi_n\right] \qquad (4.10)$$

The higher order terms in the i summation of eq.(2.20) and eq.(2.22) were not used as they do not alter the angular dependence of the field. Therefore the Hall voltage from eq.(4.6) is

$$V_{x'} = \frac{R}{y'} I_{z'} \sum_{n=1}^{\infty} n C_n r^{n-1} \cos\left[(n-m)\theta + \phi_n\right]$$

$$+ \frac{a}{y'} \rho_0 \sum_{n=1}^{\infty} n C_n r^{n-1} \sin\left[(n-m)\theta + \phi_n\right] \cdot$$

$$\cdot \sum_{n=1}^{\infty} C_n' r^n \sin(n\theta + \phi_n) \qquad (4.11)$$

As examples of the different orientations possible with the Hall plate first let m = 0. In this case (see Fig.4.1.3)

$$\mathcal{B}_{x'} = \mathcal{B}_r \tag{4.12}$$

AND

$$\mathcal{B}_{y'} = \mathcal{B}_\theta \tag{4.13}$$

and we have

$$V_{x'} = \frac{R}{y'} I_z \mathcal{B}_\theta + \frac{a\rho_o}{y'} \mathcal{B}_r \mathcal{B}_z \tag{4.14}$$

In the second term cross-coupling can occur between B_r and B_z in the fringe field of the magnet. This will generate harmonics in the induced voltage which are not present in the field. This is discussed in Appendix C.

If m = 1 the Hall plate is not rotated about its own axis as it traces out a circle in the aperture (see Fig. 4.1.4). This orientation is desirable since any systematic errors due to rotating the Hall plate about its own axis are not present in the measurements. In this case

$$\mathcal{B}_{x'} = \mathcal{B}_x \tag{4.15}$$

AND

$$\mathcal{B}_{y'} = \mathcal{B}_y \tag{4.16}$$

and the Hall voltage is

$$V_{x'} = \frac{R I_z}{y'} \mathcal{B}_y + \frac{a\rho_o}{y'} I_z \mathcal{B}_x \mathcal{B}_z \tag{4.17}$$

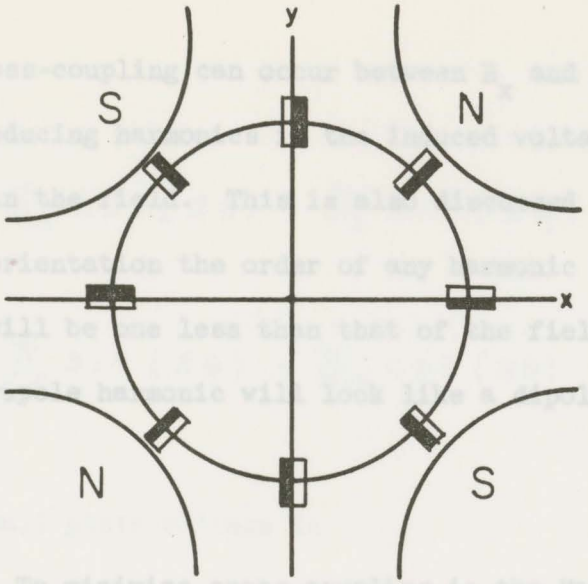

Fig. 4.1.3 The Hall plate orientation when m = 0

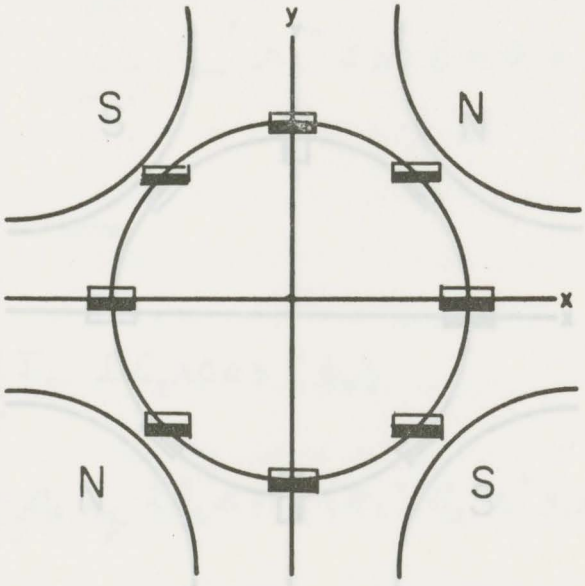

Fig. 4.1.4 The Hall plate orientation when m = 1

Again cross-coupling can occur between B_x and B_z in the fringe field producing harmonics in the induced voltage which are not present in the field. This is also discussed in Appendix C. In this orientation the order of any harmonic in the induced voltage will be one less than that of the field. Therefore the quadrupole harmonic will look like a dipole in the induced voltage.

To minimize cross-coupling in the Hall voltage an orientation can be chosen to minimize B_x'. The largest harmonic in the quadrupole field is n = 2 so that if m = 2 B_x' can be made to be zero for n = 2. In this case (see Fig. 4.1.5),

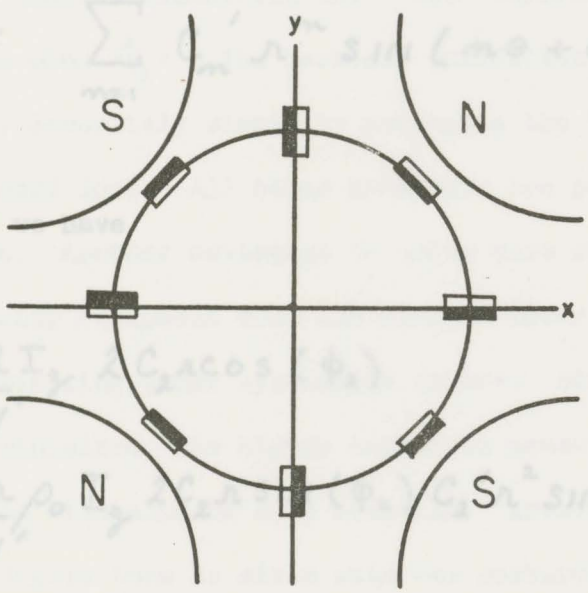

Fig. 4.1.5 The Hall plate orientation when m = 2

$$B_{x'} = B_r \cos(2\theta) - B_\theta \sin(2\theta) \tag{4.18}$$

$$B_{y'} = B_r \sin(2\theta) + B_\theta \cos(2\theta) \tag{4.19}$$

and the Hall plate voltage is

$$V_{x'} = \frac{R}{y'} I_z \sum_{n=1}^{\infty} n C_n r^{n-1} \cos\left[(n-2)\theta + \phi_n\right] + \frac{a}{y'} \rho_0 \sum_{n=1}^{\infty} n C_n r^{n-1} \sin\left[(n-2)\theta + \phi_n\right] \cdot \sum_{n=1}^{\infty} C_n' r^n \sin(n\theta + \phi_n) \tag{4.20}$$

For n = 2 we have

$$V_{x'} = \frac{R}{y'} I_z \, 2 C_2 r \cos(\phi_2) + \frac{a}{y'} \rho_0 I_z \, 2 C_2 r \sin(\phi_2) \, C_2' r^2 \sin(2\theta + \phi_2) \tag{4.21}$$

If ϕ_2 is chosen to be zero then the voltage is maximized and

$$V_{x'}\Big]_{MAX} = \frac{R}{y'} I_z \, 2 C_2 r \tag{4.22}$$

In this case the quadrupole harmonic (n = 2) of the field is a constant in the induced voltage. Therefore all harmonic orders in the voltage are two less than those of the field.

If in eq.(4.22), ϕ_2 is chosen to be 90° then the induced voltage is minimized and

$$V_{x'}\Big]_{MIN} = \frac{a}{y'}\rho_0 \, I_{z'} \, 2C_2 \, r \, B_z\Big]_{n=2} \qquad (4.23)$$

The ratio of $\frac{V_{x'}]_{MIN}}{V_{x'}]_{MAX}}$ for the n = 2 harmonic can then be used to calculate B_z

$$B_z\Big]_{n=2} = \frac{V_{x'}]_{MIN}}{V_{x'}]_{MAX}} \cdot \frac{R}{a\rho_0} \qquad (4.24)$$

Besides minimizing the cross-coupling errors in the Hall plate when $\phi_2 = 0$ the harmonic coefficient C_2 can be calculated very accurately simply by averaging the Hall plate voltage over a closed loop. All other harmonics are periodic and will cancel out. Another advantage to using this orientation is that the measuring equipment does not have to cover a wide range of values minimizing other systematic errors. Since the cross-coupling has been minimized, the higher harmonics measured in the m = +2 orientation will also be more reliable. However, in the m = +2 data the dipole term is mixed with the sextupole. From eq.(4.20)

$$V_{x'} \propto \sum n C_n r^{n-1} \cos\left[(n-2)\theta + \phi_n\right]$$

$$= C_1 \cos(\theta + \phi_1) + 2C_2 r \cos\phi_2$$

$$+ 3C_3 r^2 \cos(\theta + \phi_3) + 4C_4 r^2 \cos(2\theta + \phi_4)$$

$$+ \ldots . \qquad (4.25)$$

Therefore both the dipole and sextupole terms have the same harmonic order. These two terms can be separated by doing two surveys at different phase angles or radii.

To measure higher harmonics more accurately however, the m value for the orientation can be chosen to set any harmonic to a constant in the induced voltage.

To calculate the integrated harmonic content of the field, all of the field values for one angle are added along z. The harmonic analysis is then carried out as if all the field were at one z position. Since the B_z components of the field are of opposite sign (see Fig. 4.1.6) the effect of cross-coupling in the induced voltage for any m value will cancel out in the calculation of the integrated harmonic content.

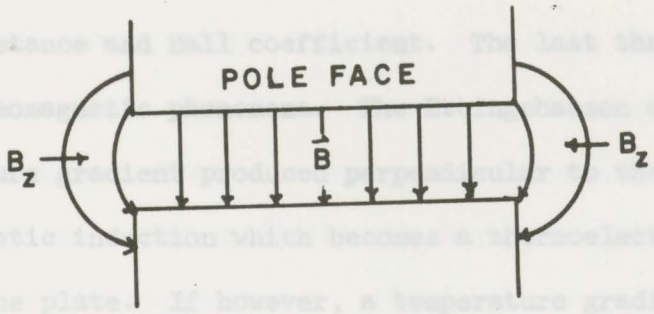

Fig. 4.1.6 The directions of B_z in the fringe fields of a magnet.

Therefore only the point analysis along z is affected by cross-coupling.

The Hall plate is constructed of semi-conductor material and therefore is affected by temperature changes. The temperature dependence of the Hall coefficient and resistance are also affected by the applied magnetic field. Therefore any change in temperature may look like a change in magnetic field.

The possible thermal and thermomagnetic effects which may occur in a Hall plate while in a magnetic field are as follows (Weiss 1969): the Seebeck effect, the Peltier effect, the Ettingshausen effect, the Ettingshausen-Nernst effect and

the Righi-Leduc effect. The Seebeck and Peltier effects arise due to heating in the longitudinal direction either by a temperature gradient or by the applied current. These would affect the resistance and Hall coefficient. The last three effects are thermomagnetic phenomena. The Ettingshausen effect is a temperature gradient produced perpendicular to the current density and magnetic induction which becomes a thermoelectric voltage across the plate. If however, a temperature gradient already exists perpendicular to the field, a voltage across the plate is again produced. This is called the Ettingshausen-Nernst effect. The Righi-Leduc effect is a temperature gradient produced perpendicular to both the field and another temperature gradient.

To minimize all these effects, either the Hall plate must be kept at a constant temperature or the change in performance of the plate with known magnetic fields must be calibrated with known changes in temperature. Also the current used to drive the Hall plate must be kept small enough so that self-heating does not occur. To monitor the temperature of the Hall plate a thermoelectric device is desirable since the temperature could then be recorded as a voltage or resistance.

Assuming the centre of the circle traced out is on the magnetic axis so that "false" harmonics will not be generated, the Hall voltage must then be corrected for possible temperature changes. The magnetic field values can then be found using the calibration.

The harmonic content of these data is then found by a Fourier analysis computer program HAQ (Williams and Reeve 1972), the actual Fourier analysis being accomplished by a FORTRAN library subroutine, FORIT (Appendix D). Since the plate is stepped through z, the harmonics as a function of z can be plotted by the computer. The phase angle of each harmonic is also available from FORIT and using eq.(3.11) the effective length for any harmonic can be calculated.

Using the calibration of Hall plate voltage vs. magnetic field, the magnetic field as a function of excitation current can be measured if the Hall plate is positioned to read a maximum signal in the aperture (i.e. m = 2) as close to the pole face as possible. No cross-coupling will occur if the Hall plate is well inside the magnet.

4.2 Equipment and Computer Software

The Hall plate (Seimens FS 33 field probe) was mounted inside a thermistor jacket with the intention of maintaining and monitoring the temperature of the Hall plate so that temperature corrections to the data would not have to be performed. At present, however, the thermistor material is used only to monitor the temperature with the data being temperature corrected afterwards. The Hall plate and its thermistor jacket are mounted on a stainless steel tubular arm which is mounted to the head of a lathe. The probe arm can be rotated about its own axis, the angle being set by a 180° vernier scaled protractor (accurate to 2' of arc) on the head of the lathe (see Fig. 4.2.1).

The probe arm itself is supported a distance of 19" from the head of the lathe. Also on the arm is a clamp for correcting any bends along the length of the probe.

The head of the lathe is equipped with a Versa-mill for x and y adjustments and the position along the axis of the magnet is monitored by an electro-mechanical counter. The x and y positions of the Hall plate is defined to $\pm$0.001" and the z position to 0.0125".

Because the misalignment of the magnetic axis and the z axis of measurement will produce "false" harmonics (Appendix A)

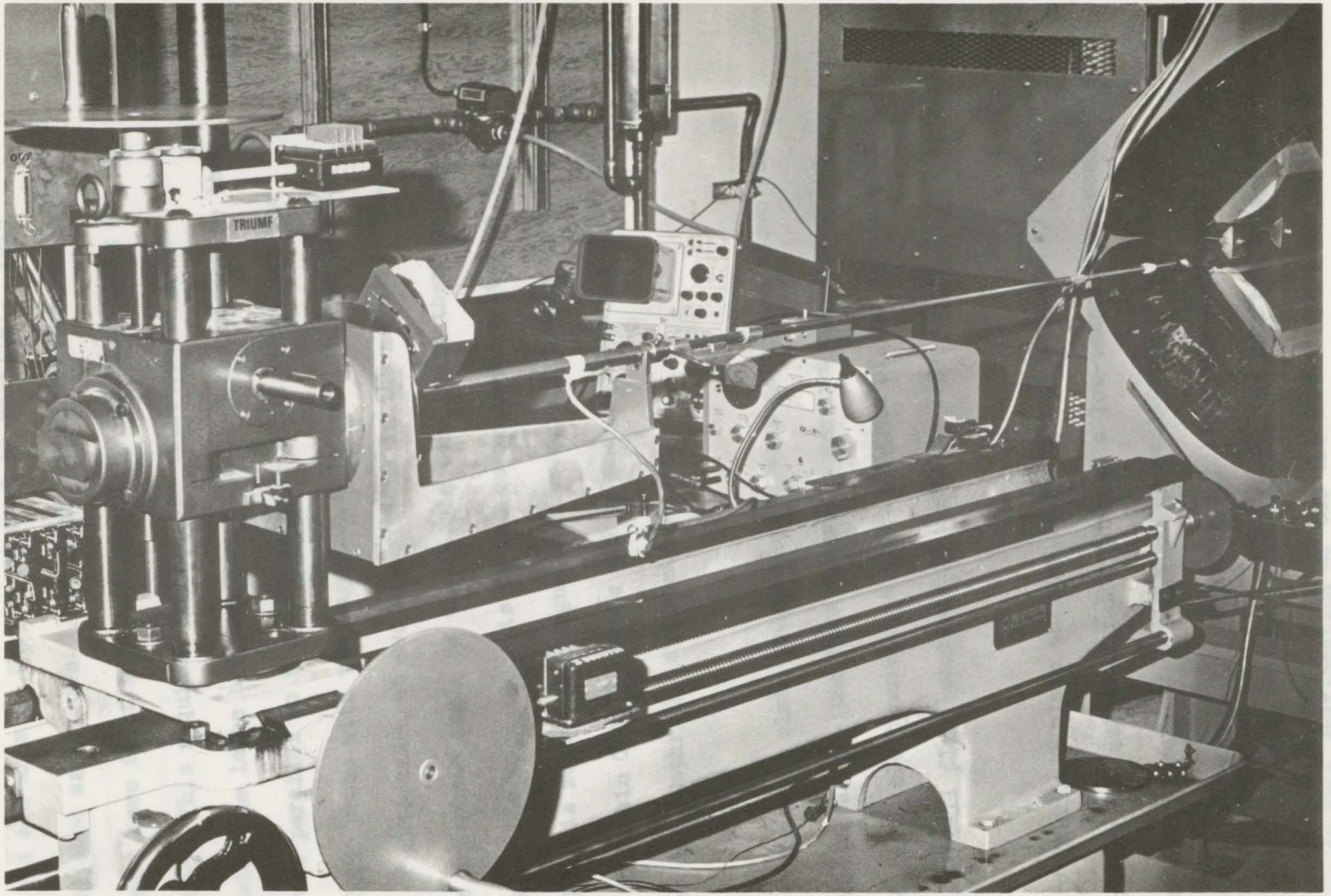

Fig. 4.2.1 The Hall plate is on the end of the probe shown here mounted on the head of the lathe.

the lathe bed and axis of the magnet must be parallel. This was accomplished as follows. The lathe bed and mechanical axis of the magnet were first made approximately parallel using a cathetometer. This required setting the cathetometer axis parallel with the lathe bed and then adjusting the magnet so that its axis was parallel to the cathetometer axis. To align the z axis of the probe with the magnetic axis required the Fourier analysis of data taken at two z positions in the magnet. The amplitude and phase angle of the dipole term could then be used to determine the magnetic axis in the co-ordinate system of the probe. By this method the magnet and measurement axes were aligned to within 0.007" at one end of the magnet and 0.026" at the other end (Gathright and Reeve 1972).

The Hall plate measurement system described above was interfaced to an on-line Data General Supernova computer using standard CAMAC electronics. A block diagram of the data acquisition system and Hall plate controls is shown in Fig. 4.2.2.

The Hall plate current of 50 mA was provided by a Fluke 382A Voltage Current calibrator through a low-temperature-coefficient resistor. This current could then be monitored as a voltage across the resistor. The thermistor voltage was provided by a Lambda LP412FM power supply. The current was limited by a series resistor so that self-heating of the thermistor did not occur. The

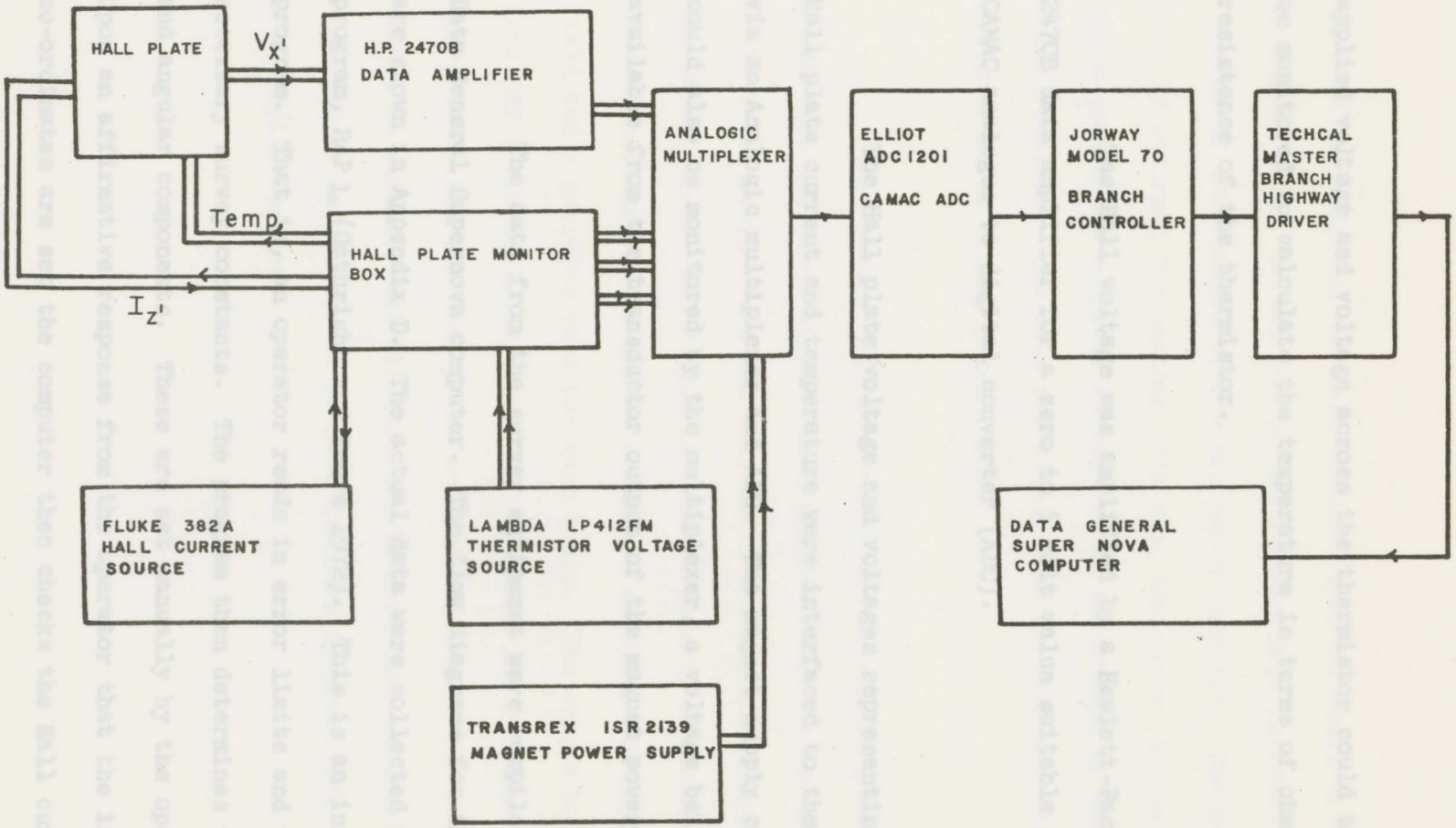

Fig. 4.2.2 A block diagram of the Hall plate survey equipment (Gathright and Reeve 1972)

applied voltage and voltage across the thermistor could then be monitored to calculate the temperature in terms of ohmic resistance of the thermistor.

The Hall voltage was amplified by a Hewlett-Packard 2470B data amplifier for a zero to 5 volt value suitable for the CAMAC analogue to digital converter (ADC).

The Hall plate voltage and voltages representing the Hall plate current and temperature were interfaced to the computer via an Analogic multiplexer and ADC. The magnet supply current could also be monitored by the multiplexer, a voltage being available from the transductor output of the magnet power supply.

The data from the survey equipment were compiled by a Data General Supernova computer. The flow diagrams for the programs are shown in Appendix D. The actual data were collected in the first program, RAP 1, (Gathright and Reeve 1972). This is an interactive program. That is, an operator reads in error limits and the necessary survey constants. The program then determines the spatial and angular components. These are set manually by the operator. Upon an affirmative response from the operator that the initial co-ordinates are set the computer then checks the Hall current, magnet current and temperature. Any drift beyond the prescribed error limits in these values is compiled. The lathe is then

started manually and the Hall voltages read at equal distances along the axis. At the end of one run any Hall current, magnet current or temperature errors are again compiled. The probe can then be returned for another data run, the number of runs through the magnet for a complete survey being determined by the harmonic order required. The data for each run along with any errors are punched on binary paper tape.

This binary tape is read by the second program RAP 2 (Gathright and Reeve 1972). This program corrects the Hall voltage for temperature and calculates the magnetic field using the calibration. The output of this program is a Mohawk format tape consisting of the survey constants used and the magnetic field and z position data for each angle. The errors compiled from RAP 1 are analyzed by a third program, ERR 2 (Gathright and Reeve 1972) and punched on the same Mohawk tape. The Mohawk format is used so that the data can be read onto magnetic tape suitable as input for the Fourier analysis program, HAQ, in an IBM 370/145 computer.

4.3 Calibration of the Hall Plate

Before the Hall plate could be calibrated in a known dipole field it was first calibrated for temperature and field. That is, the Hall plate was placed in a known magnetic field and the Hall voltage recorded as a function of temperature. Since the temperature dependence of the Hall voltage is also a function of magnetic field this was repeated for several known fields. For an accuracy of .1%, the magnetic field dependence of the temperature correction was not necessary if the thermistor resistance drift did not exceed $\pm 2k\Omega$ ($\pm 2°C$). The temperature correction used for the Hall voltage was found to be $0.13\%/k\Omega$ where the temperature is expressed in terms of thermistor resistance.

Once the temperature correction term was calculated the Hall plate could then be calibrated in a dipole field, with the temperature being recorded for each data point. This was done from -6 kG to +6 kG using a NMR gauss-meter. The dipole field was specified to be homogenous to 1 part in 10^4 over the central 0.5" with a gap of 0.75". The temperature corrected data were fitted to a 6^{th} order polynomial to an accuracy of .02% using the computer program POLFIT (Alexander and Reeve 1971).

4.4 Measurements of 4Q19/8

The harmonic analysis of the Hall plate data can be carried out at each z position. Therefore the harmonic content of the quadrupole as a function of z represents a point by point analysis of the data. The normalized harmonics of quadrupole 4Q19/8 as measured by the Hall plate are shown in Figures 4.4.1 to 4.4.9. The results are from two surveys, each representing a different orientation of the Hall plate. The m = +2 orientation represents the data obtained with the Hall plate positioned to always read the maximum field. The radius of the circle traced out by the Hall plate was 1.5". Because of the design of the probe arm it was not possible to do a survey at a radius of 1.8" or 90% of the 2.0" radius aperture. It is obvious from the figures that the m = 2 orientation has a measurement error associated with it. This is due to a bend in the probe arm and will be discussed in Sec. 4.5.

The integrated harmonic content of 4Q19/8 calculated from the m = 1 survey is listed in Table 41. This is at a radius of 1.8" and with a field excitation current of 250 amps. Since the survey results were measured at 1.5" these results have been scaled according to eq.(3.10). Note that in the integrated harmonic results of Table 4.1 the value for n = 4 does not reflect the size of that harmonic in Fig. 4.4.3. As stated previously, the cross-coupling will not affect the integrated harmonic

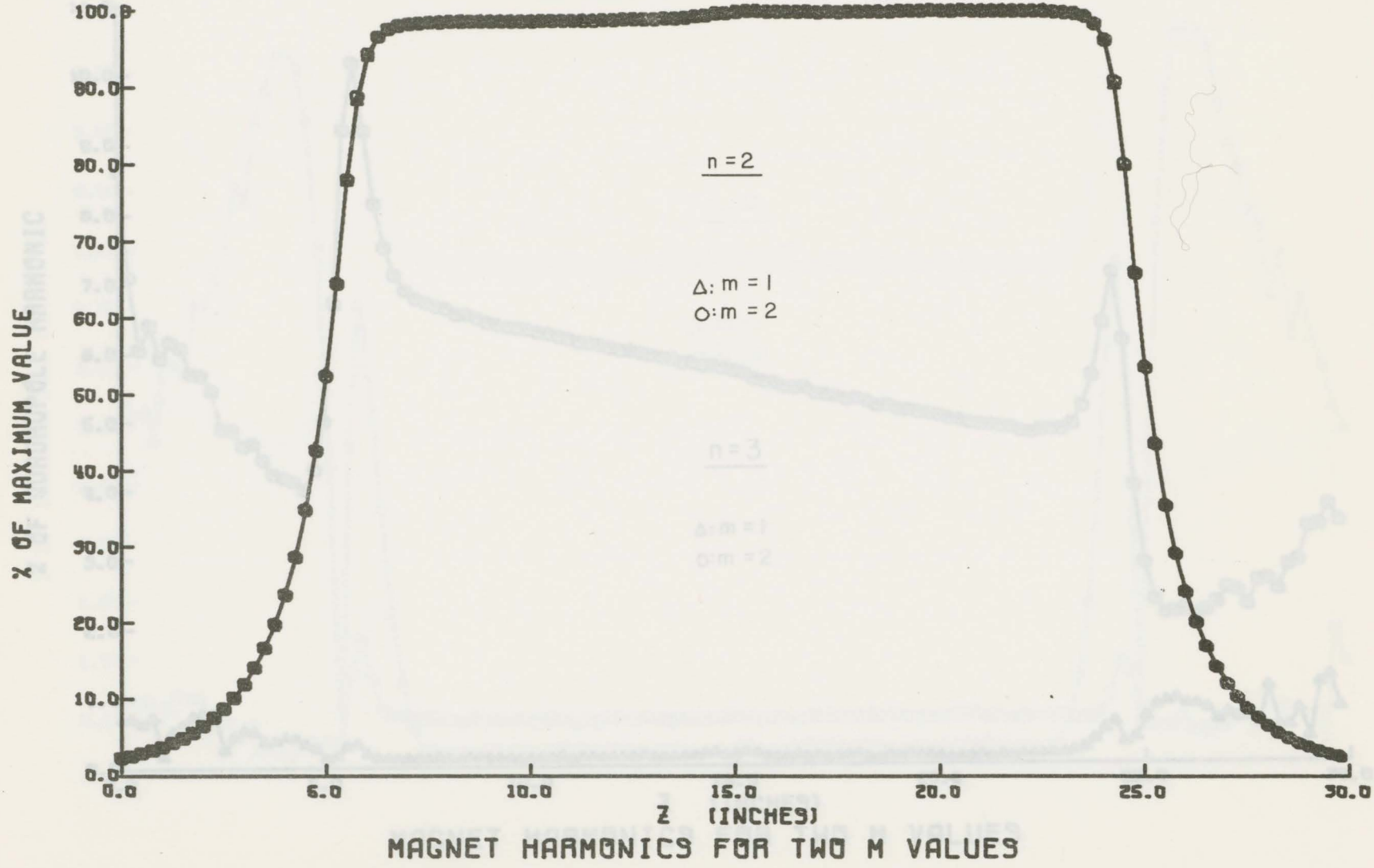

Fig. 4.4.1 Magnet harmonics as a function of z (n = 2)

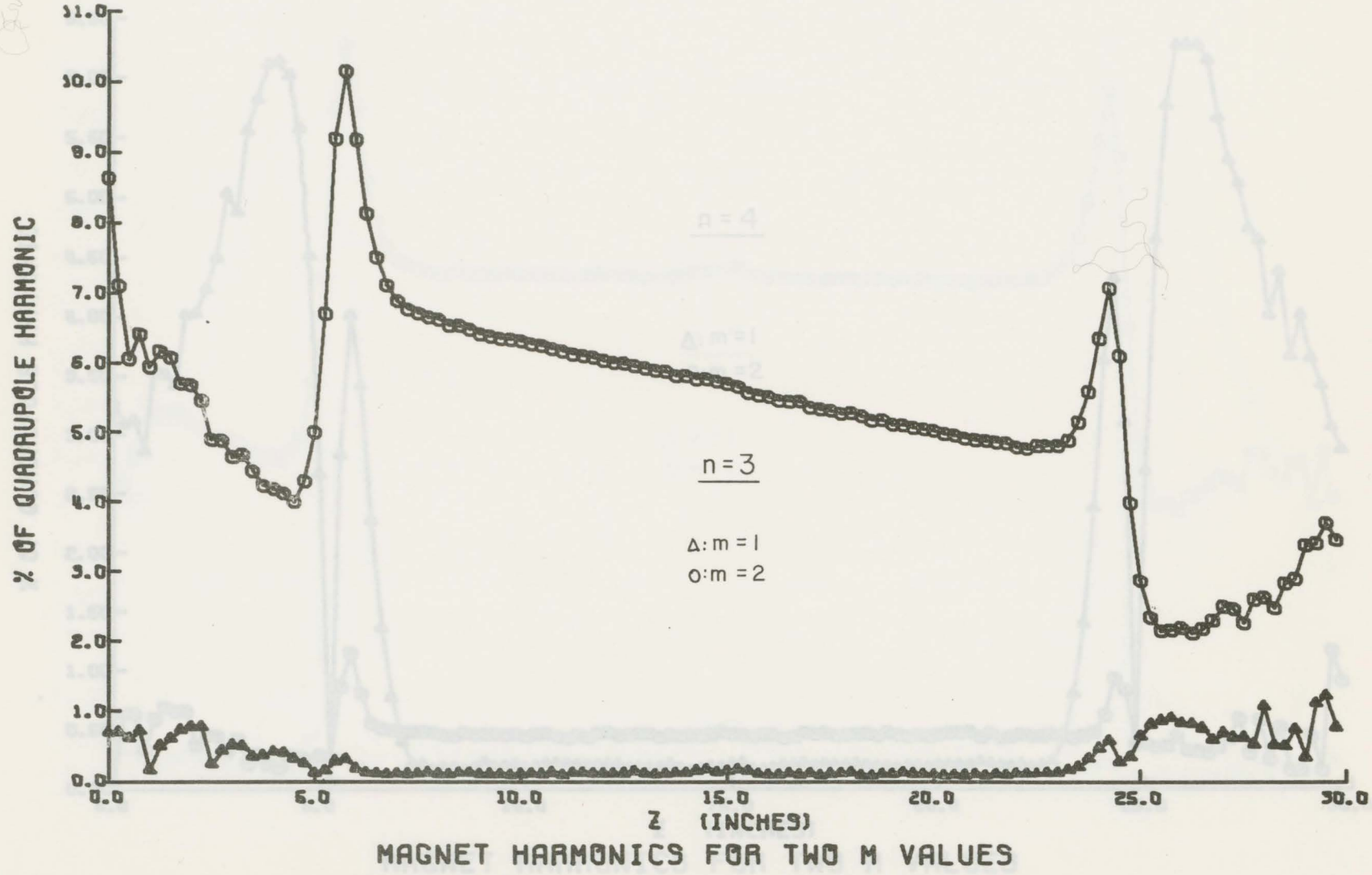

Fig. 4.4.2 Magnet harmonics as a function of z (n = 3)

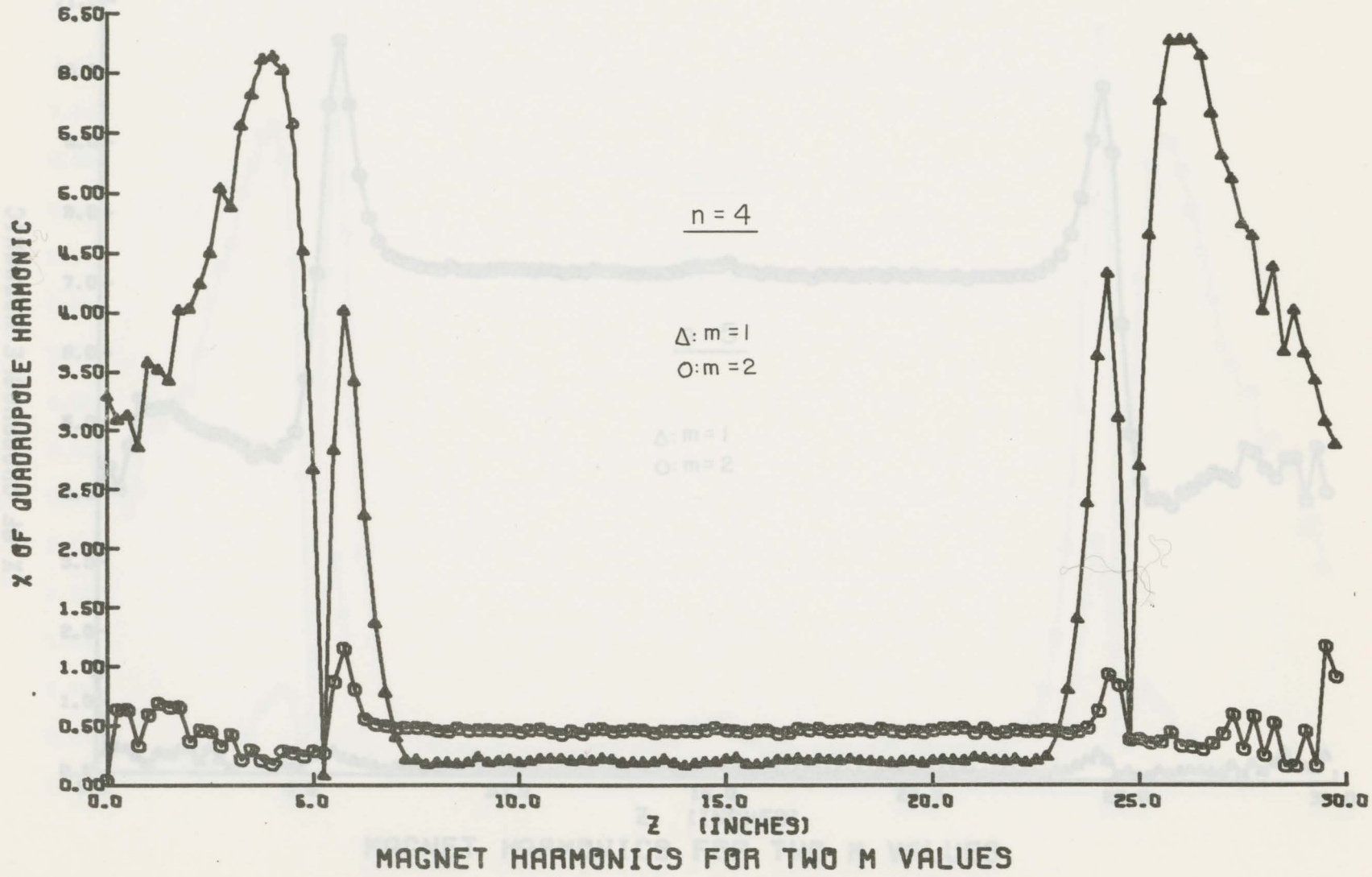

Fig. 4.4.3 Magnet harmonics as a function of z (n = 4)

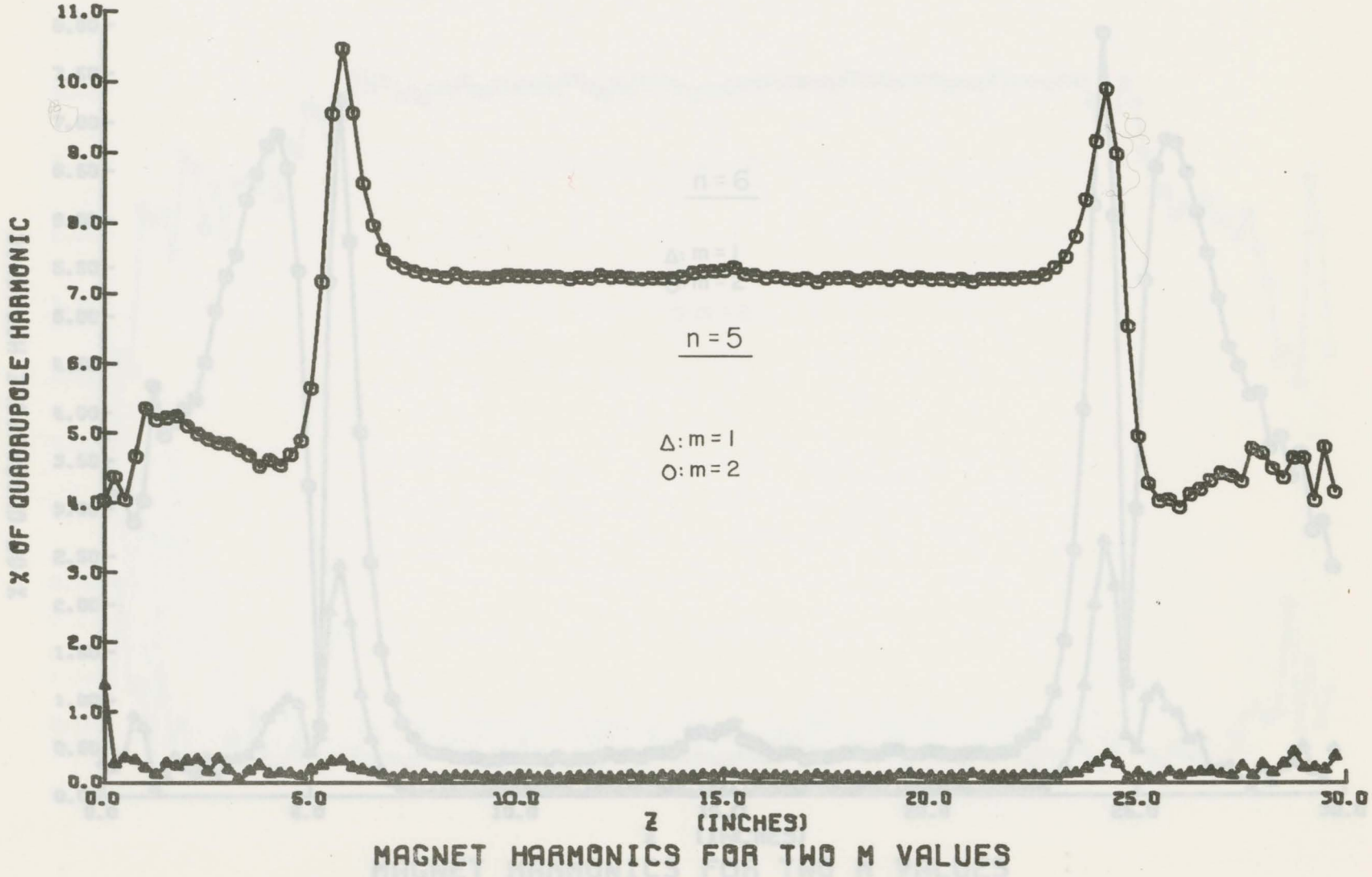

Fig. 4.4.4 Magnet harmonics as a function of z (n = 5)

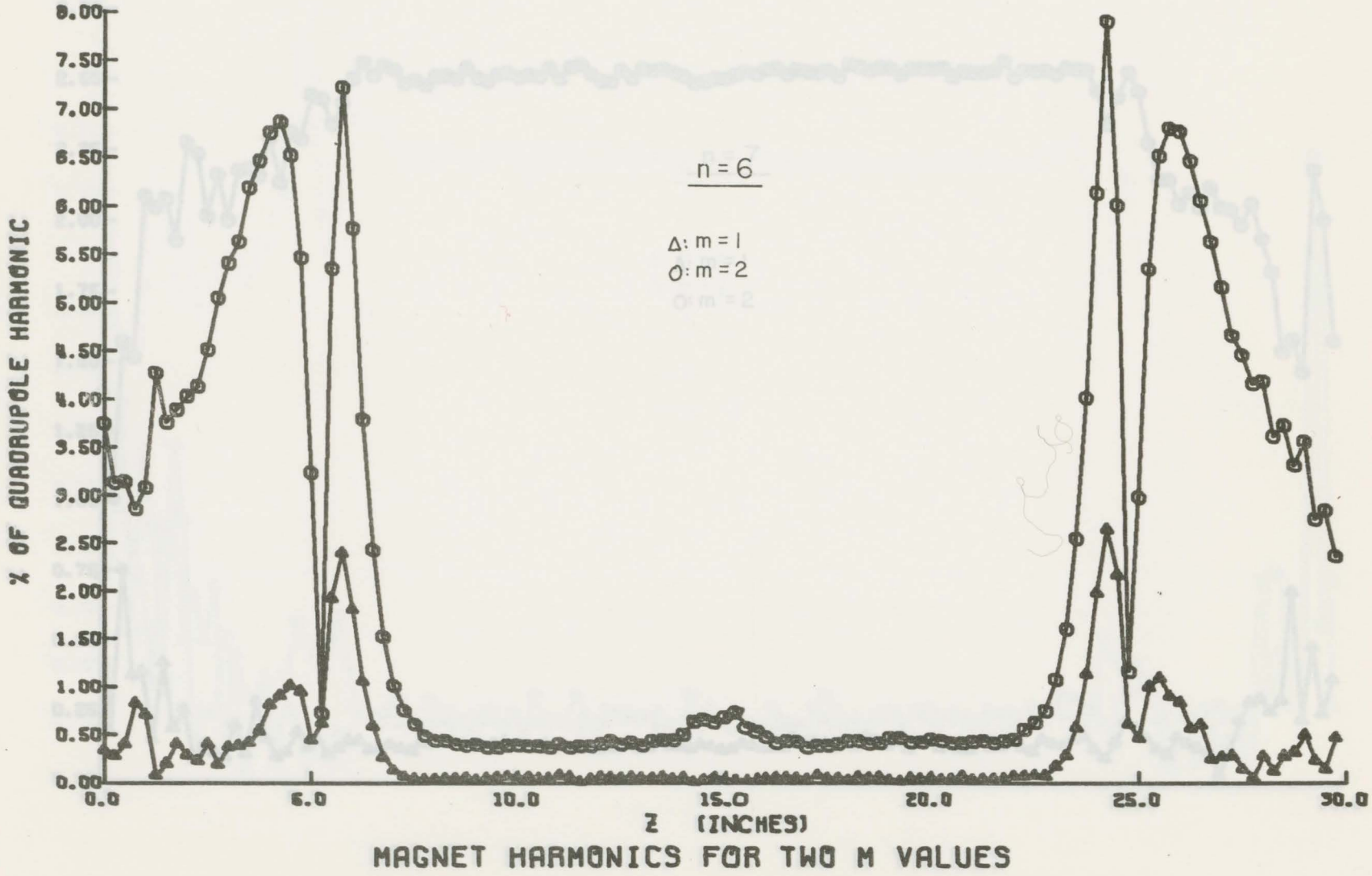

Fig. 4.4.5 Magnet harmonics as a function of z (n = 6)

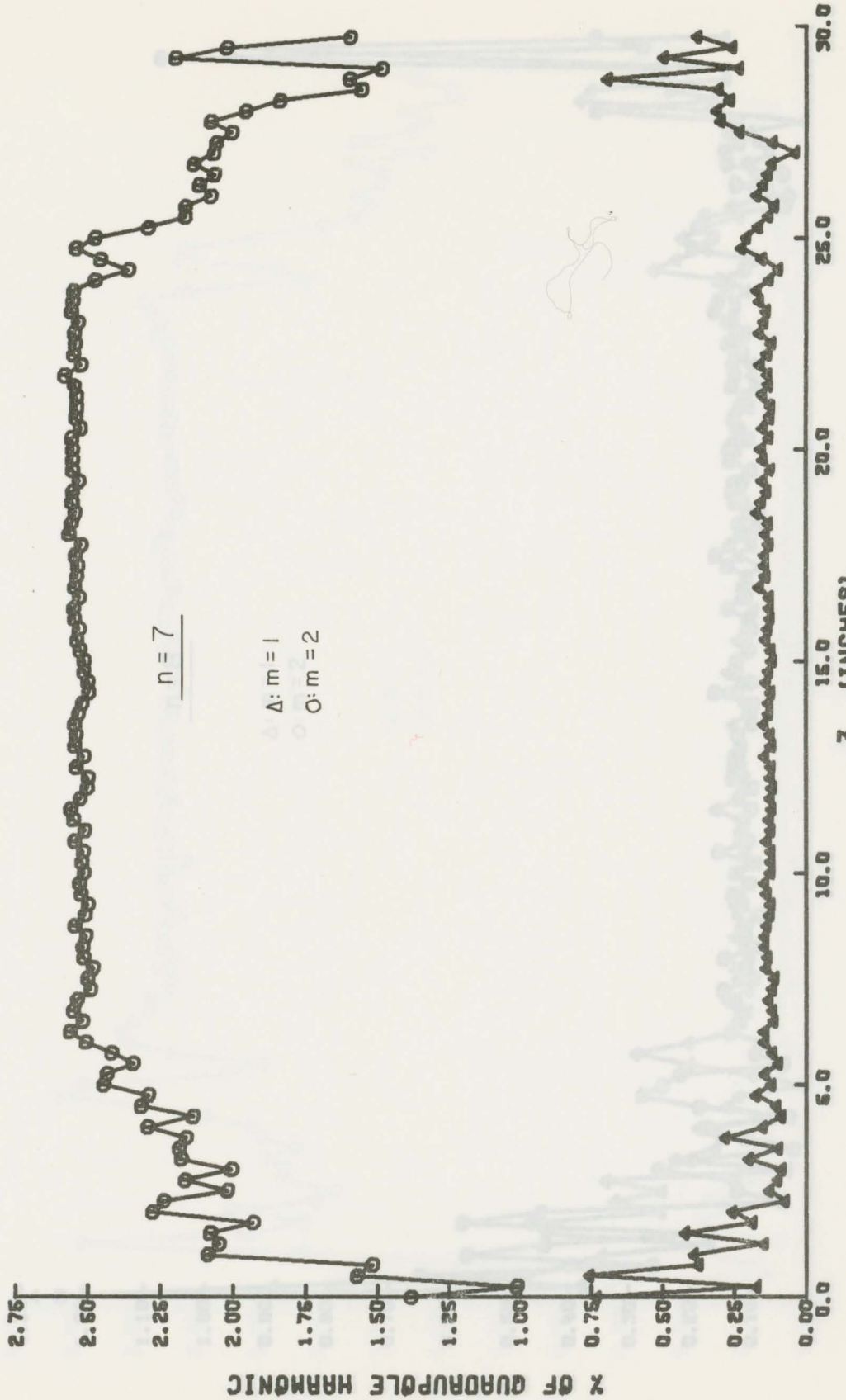

Fig. 4.4.6 Magnet harmonics as a function of z (n = 7)

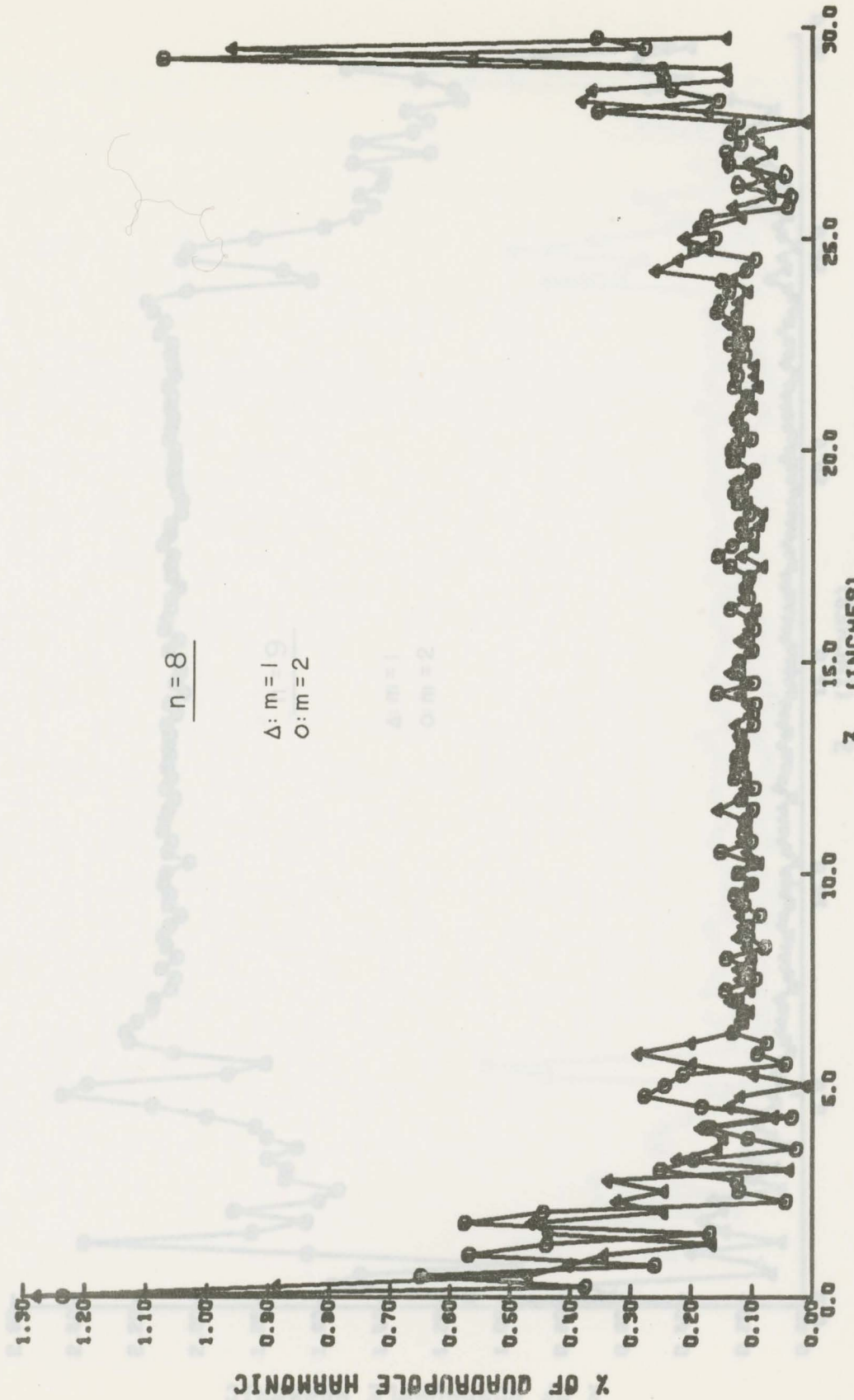

Fig. 4.4.7 Magnet harmonics as a function of z (n = 8)

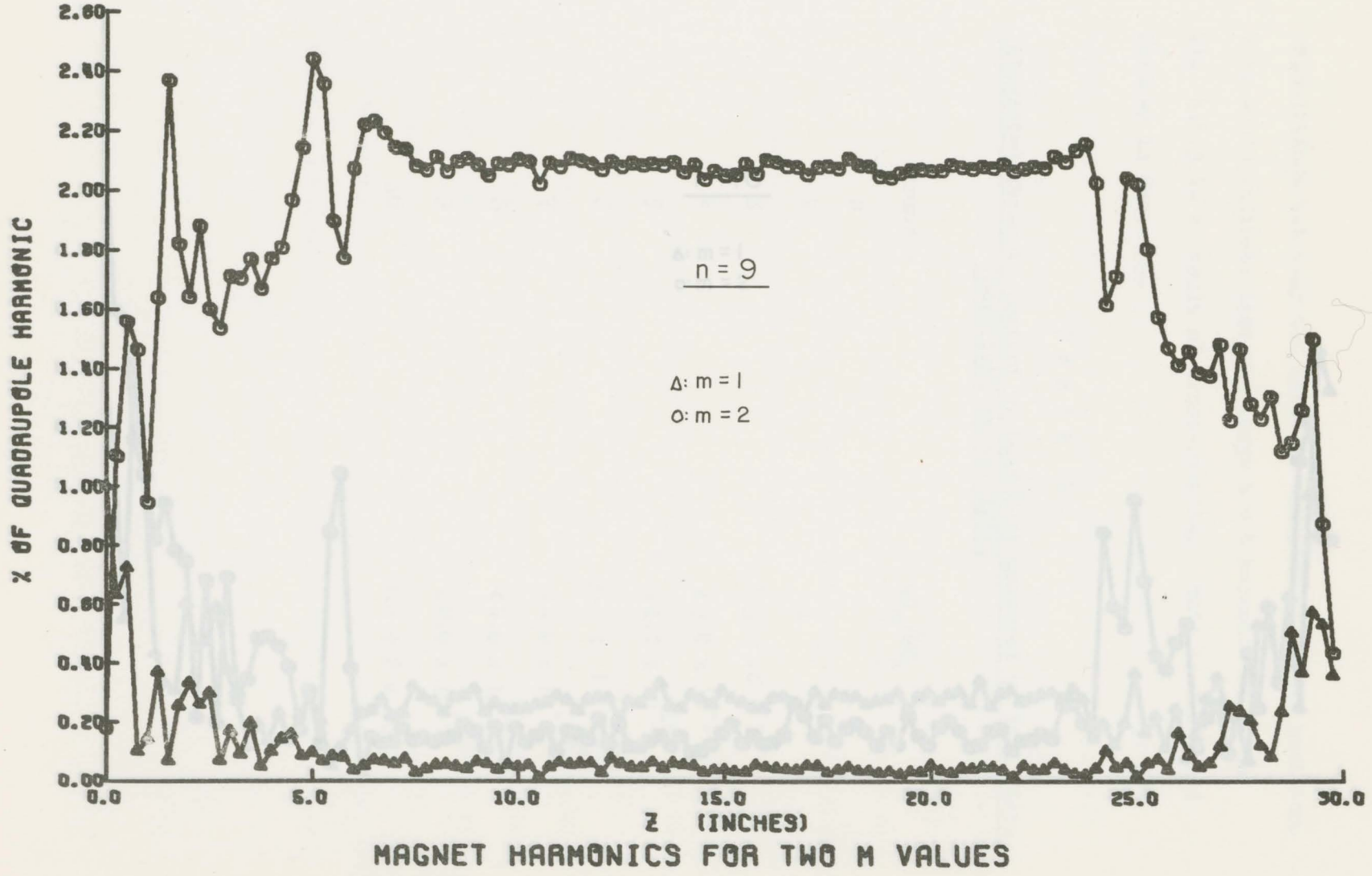

Fig. 4.4.8 Magnet harmonics as a function of z (n = 9)

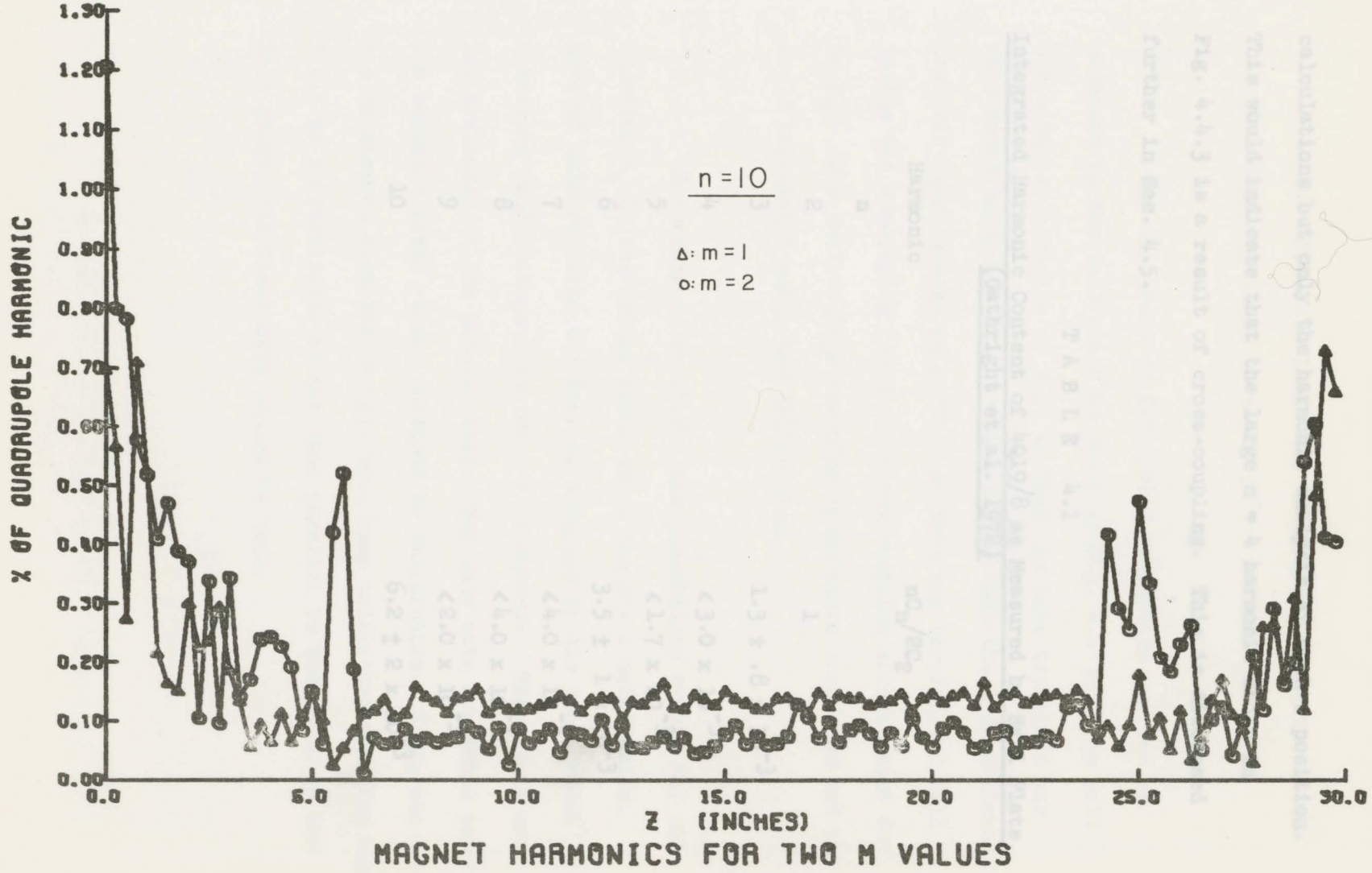

Fig. 4.4.9 Magnet harmonics as a function of z (n = 10)

calculations but only the harmonic analysis at each z position. This would indicate that the large n = 4 harmonic shown in Fig. 4.4.3 is a result of cross-coupling. This is discussed further in Sec. 4.5.

T A B L E 4.1

Integrated Harmonic Content of 4Q19/8 as Measured by Hall Plate (Gathright et al. 1972)

Harmonic n	$nC_n/2C_2$
2	1
3	$1.3 \pm .8 \times 10^{-3}$
4	$< 3.0 \times 10^{-3}$
5	$< 1.7 \times 10^{-3}$
6	$3.5 \pm 1 \times 10^{-3}$
7	$< 4.0 \times 10^{-3}$
8	$< 4.0 \times 10^{-3}$
9	$< 2.0 \times 10^{-3}$
10	$6.2 \pm 2 \times 10^{-3}$

The effective length of the magnet, using the n = 2 harmonic data was found to be 20.97".

The linearity of field with excitation current as measured by the Hall plate is shown in Fig. 4.4.10. The Hall plate was at a radius of 1.5" so that the pole tip field was calculated using eq.(2.12) which states that the 2-dimensional magnetic field scales as r^{n-1}. As this was carried out well inside the quadrupole field, no cross-coupling errors exist due to B_z . The Hall voltage was also temperature corrected and the field calculated using the calibration.

According to eq.(4.24) the possibility exists for calculating B_z in the fringe field using the m = 2 orientation. However this required the Fourier analysis of the temperature corrected Hall voltage from two m = +2 surveys. These data are not available at the present time. The only data available are the magnetic field values obtained by calibration. Since the m = +2 minimum orientation data have been calibrated assuming the field is perpendicular rather than parallel to the plane of the Hall plate, the field data cannot be used.

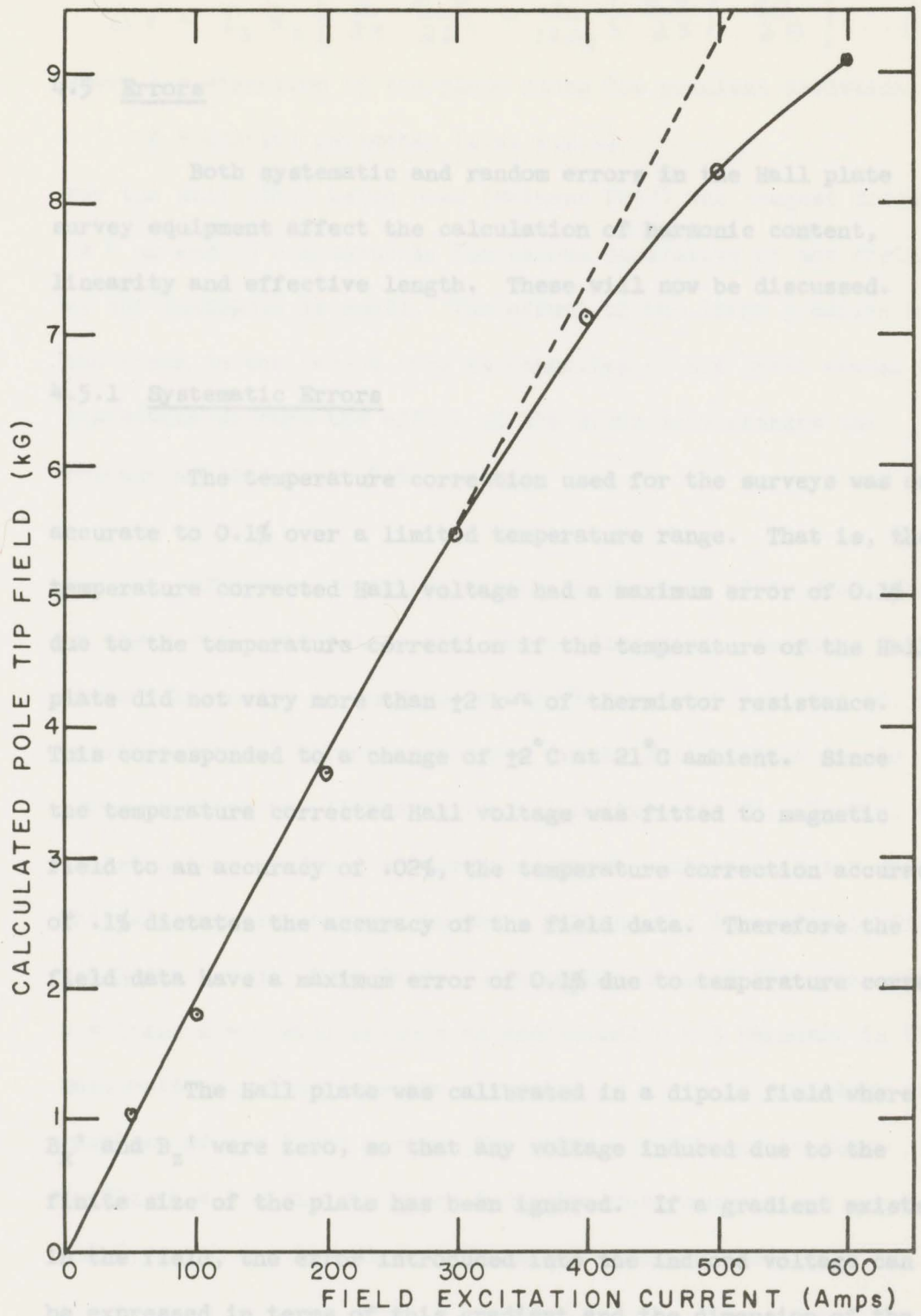

Fig. 4.4.10 The pole tip field vs. field excitation current as measured by the Hall plate. (Gathright et al. 1972).

4.5 Errors

Both systematic and random errors in the Hall plate survey equipment affect the calculation of harmonic content, linearity and effective length. These will now be discussed.

4.5.1 Systematic Errors

The temperature correction used for the surveys was only accurate to 0.1% over a limited temperature range. That is, the temperature corrected Hall voltage had a maximum error of 0.1% due to the temperature correction if the temperature of the Hall plate did not vary more than ± 2 kΩ of thermistor resistance. This corresponded to a change of $\pm 2^{\circ}$C at 21°C ambient. Since the temperature corrected Hall voltage was fitted to magnetic field to an accuracy of .02%, the temperature correction accuracy of .1% dictates the accuracy of the field data. Therefore the field data have a maximum error of 0.1% due to temperature correction.

The Hall plate was calibrated in a dipole field where B_x' and B_z' were zero, so that any voltage induced due to the finite size of the plate has been ignored. If a gradient exists in the field, the error introduced into the induced voltage can be expressed in terms of this gradient and the dimension of the plate along the gradient (Robins 1965). The change in voltage to second order in the plate dimension is

$$\Delta V \approx I_s R_s \left[\frac{L^2}{24} \frac{\partial^2 B}{\partial s^2} - \frac{L^2}{12 n_s} \left(\frac{\partial B}{\partial s} \right)^2 \frac{\partial n}{\partial B} \right] \qquad (4.26)$$

where L = dimension of the plate along the gradient direction

S = spatial parameter (i.e. x,y,z)

For the Hall plate being used (Seimens FC33) the longest dimension is 6 mm and in a quadrupole the second derivative of the field or the sextupole is small. The effect of the large gradient of the field in the second term is cancelled by the small change in resistance so that the effect of the probe size changes the voltage by less than .01%.

The cross-coupling errors in the Hall plate when used in the m = +1 orientation will now be discussed. Assuming the largest harmonics in quadrupole 4Q19/8 are n = 2,3,6, and 10, the possible "false" harmonics induced in the Hall voltage due to cross-coupling are listed in Table 4.2 (Appendix C). In Fig. 4.4.2 the structure of the n = 3 harmonic shows a minimum at z = 25 inches. This minimum also appears in the n = 4 and n = 6 results in Figs. 4.4.3 and 4.4.5. From Table 4.2 a combination of field harmonics n = 3 and n = 6 will produce an additional n = 3 harmonic in the Hall voltage. Therefore the structure of n = 3 is caused by cross-coupling of n = 3 and n = 6. The large n = 4 harmonic shown in Fig. 4.4.3 similarly comes from the cross-coupling of n = 2 and 6, n = 6 and 10 and from the n = 2 harmonic alone.

T A B L E 4.2

Harmonics Generated Due to Cross-Coupling

Field Harmonics	"False" Harmonics Due to Cross-Coupling
2 and 3	2m, 1,4,5,6
2 and 6	2m, 4,8,12
2 and 10	2m, 4,8,12,20
3 and 6	2m, 3,6,9,12
3 and 10	2m, 6,7,13,20
6 and 10	2m, 4,12,16,20

m refers to the orientation of the plate (see Fig. 4.1.2)

In comparing the n = 6 and n = 4 harmonics (Figs. 4.4.5 and 4.4.3) the relative size of the double peaks has been reversed. This is due to the contribution to the n = 4 harmonic from n = 2 alone. In this region the quadrupole harmonic of B_z is much larger than the n = 6 harmonic of B_z. Smaller effects of cross-coupling can be seen in n = 5 (Fig. 4.4.4) caused by n = 2 and 3 and n = 8 (Fig. 4.4.7) caused by n = 2 and 6. Absolute values of the cross-coupling errors cannot be calculated without B_z values for the higher harmonics and values for the magnetoresistive coefficient and Hall coefficient which in themselves are field dependent. When the field data are integrated over the length

of the magnet, the errors introduced into the n = 3,4,5 and 8 harmonics cancel out.

The large values of the odd harmonics in the m = +2 survey are from two related measurement errors. For m = +2 the plate must be rotated 360° about its own axis. It was only possible to rotate the plate 180° about its own axis. This meant that at some point during the survey the plate had to be flipped over. If the probe arm was bent, the two half circles traced out by the Hall plate would not have the same centre and a dipole assymmetry in the data would result causing the large odd order harmonics (see Fig. 4.5.1). (This is not the same as the misalignment of the centre of the circle and magnetic axis.) This error could account for the structure in n = 3,4, and 5 and the lack of structure in n = 7,8 or 9. Note that due to misalignment an n = 6 field harmonic would produce n = 5,4 and 3 in the induced voltage but not n = 7,8 or 9, and the peaks in the n = 3,4 and 5 results for m = +2 correspond exactly to the peak in the n = 6 harmonic. If the plate did not have to be flipped the bend in the probe arm would produce a quadrupole symmetry in the data (see Fig. 4.5.2) resulting in an n = 4 harmonic after analysis. Jung (1972) also found a weak octupole component caused by a sag in the probe arm if the plate is used in an m = +2 orientation.

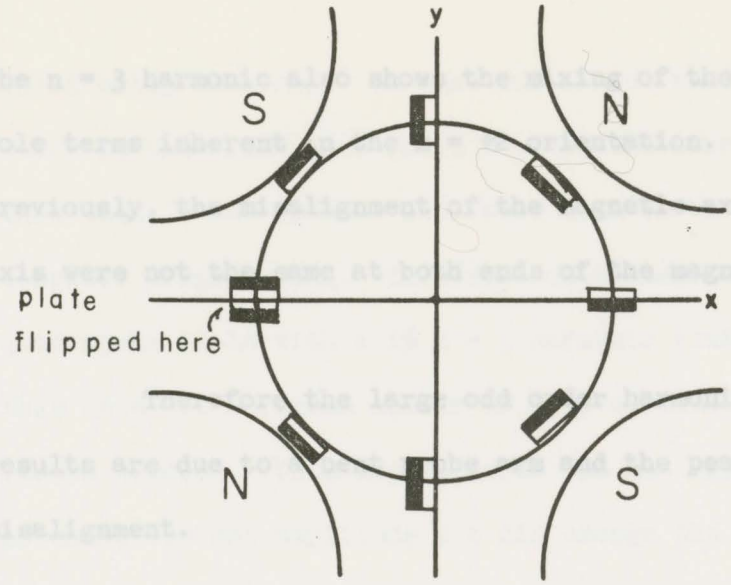

Fig. 4.5.1 The Hall plate orientation for m = 2 with a bent probe arm (Hall plate flipped).

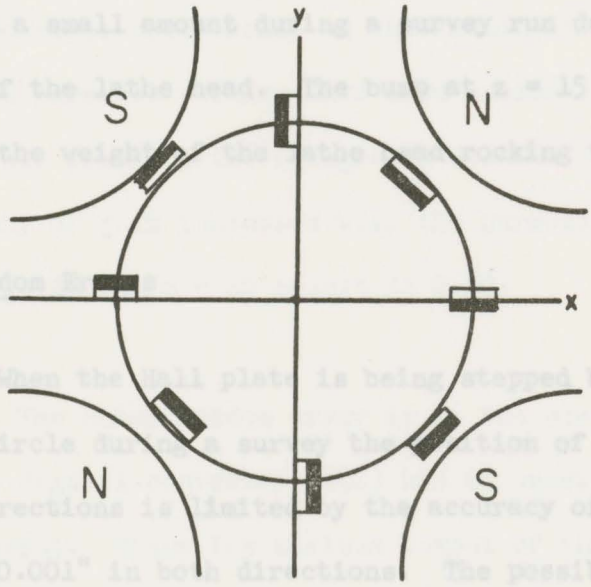

Fig. 4.5.2 The Hall plate orientation for m = 2 with a bent probe arm (Hall plate not flipped).

The n = 3 harmonic also shows the mixing of the dipole and sextupole terms inherent in the m = +2 orientation. As stated previously, the misalignment of the magnetic axis and measurements axis were not the same at both ends of the magnet.

Therefore the large odd order harmonics in the m = +2 results are due to a bent probe arm and the peaks are due to misalignment.

The small lump in the n = 2,3,5 and 6 harmonics at z = 15 inches (see Figs. 4.4.1, 4.4.2, 4.4.4, and 4.4.5) may be caused by the motion of the support apparatus. The supporting apparatus was not bolted to the floor so that it was possible for it to rock a small amount during a survey run depending on the position of the lathe head. The bump at z = 15 inches could be caused by the weight of the lathe head rocking the lathe bed.

4.5.2 Random Errors

When the Hall plate is being stepped by equal increments around a circle during a survey the position of the plate in the x and y directions is limited by the accuracy of the Versa-mill which is ±0.001" in both directions. The possible error in the radial position of the plate therefore is ±0.0014". At a radius of 1.5" this represents a possible error of ±0.1% in the radial position. This in turn could produce a 0.1% uncertainty in the

field being measured. To test the effect that a ±.1% random error in the field data would have on the harmonic analysis of that data, a set of test data were used in the Fourier analysis computer program, HAQ. This test data consisted of an ideal n = 2 quadrupole field with a 1% n = 3 harmonic content. Added to this data was a random number of ±.1% obtained from a table of random numbers. This random error did not affect the existing harmonic content amplitude but did change the phase angles of those harmonics by a few degrees. The random error of ±.1% appeared as small higher harmonics whose sum was 0.2% of the quadrupole harmonic. The largest "false" harmonic produced by this random error was .04%. Therefore the harmonic analysis was limited to .04% by the temperature correction used (±.1%) and the possible uncertainty in the radial direction. The integrated harmonic results have been scaled to 1.8" from 1.5". The possible error in the integrated results due to the radial uncertainty of ±.1% increases with the harmonic order. The uncertainty in the n = 10 result is 0.8%.

The other random error is in the electronics. The analog to digital converter (ADC) had an uncertainty of ±1 bit on the output. Since the maximum output of the ADC was 2^{12} (4096) bits the minimum uncertainty from the output of the ADC was ±.02% for a full scale input signal. Therefore, in the main field where the signal was large the possible error is only ±.02%. In

the fringe field where the induced voltage was small the possible error due to the uncertainty of the ADC could be several percent. This effect can be seen in all the harmonics for $z < 5$ inches and $z > 25$ inches in the Figs. 4.4.2 to 4.4.9.

CHAPTER 5

ANALYSIS OF THE TWO METHODS AND THE RESULTS OBTAINED

5.1 Harmonic Content

The present rotating coil equipment is capable of measuring the higher harmonic content at 90% of the bore radius in a quadrupole magnetic field to the following accuracy: for harmonics larger than .1% of the quadrupole field, the largest possible uncertainty is ±30% of the harmonic being measured; for harmonics less than .1% the uncertainty is ±.03% of the quadrupole harmonic with the smallest harmonic measurable being .03% of the quadrupole. This accuracy is limited by the wave analyzer. The measurement of harmonic content is not affected by B_z in the fringe field and no mixing of harmonic orders occurs in the induced emf. of the coil. Harmonics in the emf. not generated by the field are displaced from the field harmonics in frequency. The only "false" harmonics generated in the coil emf. are due to misalignment of the rotational and magnetic axes. This effect can be eliminated by dipole minimization.

The Hall plate survey equipment was capable of measuring higher harmonics to an accuracy of ±.04% of the quadrupole harmonic in the main field; the smallest harmonic measurable being .04% of the quadrupole. This lower limit was determined by the spatial accuracy and temperature correction. The measurement of harmonic

content as a function of z was strongly affected by cross-coupling in the fringe field and mixing of harmonic orders did occur in the induced voltage of the plate. This cross-coupling was minimized by selecting a particular Hall plate orientation in the field. However, this orientation produced "false" harmonics due to a bend in the probe arm. The integrated harmonic results were unaffected by cross-coupling because the field data were integrated before the Fourier analysis was carried out. Because of the design of the probe arm the Hall plate cannot be placed closer than half an inch to the pole face. In the quadrupole used for measurement the bore radius was 2" so that the largest radius available for surveys in that magnet was 1.5" which is only 75% of the bore radius. Therefore to compare the measured results with the specifications of the magnet, the results must be scaled. In the fringe field the uncertainty varied from ±.04% to ±.24% of the quadrupole field due to the possible uncertainty in the ADC.

The measured results of the harmonic content from the two methods will now be discussed. The form of the harmonics in the fringe field agree very well for n = 2,3 and 6. The only disagreement in the results is the strong n = 4 harmonic measured by the Hall plate in the m = 1 orientation. This result is due to cross-coupling. The values of the integrated harmonic content agree within measurement uncertainties for n = 6 and 10 but not for n = 3. Including the possible uncertainty in the wave analyzer

of 30% for the normalized harmonics above .1% of the quadrupole, the two n = 3 results do agree. Therefore, the integrated harmonic content for n = 3,6 and 10 as measured by the two methods, agree within experimental uncertainties.

5.2 Effective Length

The form of the quadrupole harmonic as measured by the two methods is identical within experimental limits. Because of this, the two calculated values of effective length for the quadrupole agree within experimental error.

5.3 Linearity of Magnetic Field with Field Excitation Current

The graph of the magnetic field vs. applied excitation current for the quadrupole as measured by the rotating coil contains both random and systematic errors. The calculated pole tip field could be in error by as much as ±5% due to the uncertainty in the wave analyzer readings and the measurements of the coil dimensions and rotational frequency. The dependence of ω on the magnetic field causes an additional error of 4% in the calculated pole tip field at 600 Amps and contributes to the non-linear characteristic of the graph above 300 Amps.

The only uncertainty in the Hall plate measurement is in the radial distance (±.1%) and the temperature correction (±.1%) so that the graph of magnetic field as a function of excitation current is accurate to ±.2%.

CHAPTER 6

SUGGESTED IMPROVEMENTS IN THE TWO METHODS

6.1 Rotating Coil

Possible improvements on the present rotating coil apparatus will now be considered. Because the equipment is to be used on several beam line multipole magnets, there should be incorporated in the apparatus a means of attaching it to the pole faces. This would then allow the rotational and mechanical axes of the multipole to be in the same reference co-ordinate system. The apparatus could then measure the difference between the magnetic and mechanical centres directly. This could involve an expandable cylinder with the actual rotating coil inside.

The bearings supporting the rotating coil shaft are made of plastic which necessitates frequent lubrication. A possible alternative is the use of stainless steel bearings. The friction drive mechanism also requires frequent lubrication due to the force required to hold the friction wheel in position. Also the rotational frequency variations are strongly dependent on the amount of force applied to the friction wheel. Redesigning of the drive wheel arrangement would be necessary to improve the performance.

Cobb (1970) suggested constructing coils which reduced the size of the quadrupole component of the induced emf. This would improve the sensitivity of the system to small harmonics. However the formula for the induced emf. of a specially constructed coil is more difficult since the relationship between the field harmonics and the induced emf. harmonics involves the measured dimensions of the coils. This would produce additional uncertainties in the calculated field harmonics from the errors of measurement. There is also the difficulty of the construction of the coils. There is an alternative method for reducing the quadrupole harmonic without affecting other harmonic terms. This involves filtering the induced emf. to attenuate the quadrupole harmonic before the signal enters the wave analyzer. An active twin "T" notch filter has been built for this purpose (see Fig. 6.1). The filter has a centre frequency at 31.0 Hz and a Q of 30 at the 3 db roll-off point with an attenuation of 20 db at centre frequency. The insertion loss is less than .5% above the centre frequency and less than 5% below the centre frequency. The filter has ample attenuation and good Q so that only the quadrupole frequency is attenuated. However, due to the frequency fluctuations of the rotating coil, the output from the filter is very unstable due to the high Q of the filter. To remove this problem, several filters of the same design but with slightly higher and lower centre frequencies could be constructed to make a bandwidth filter whose bandwidth at full attenuation would be greater than the fluctuation of the quadrupole frequency.

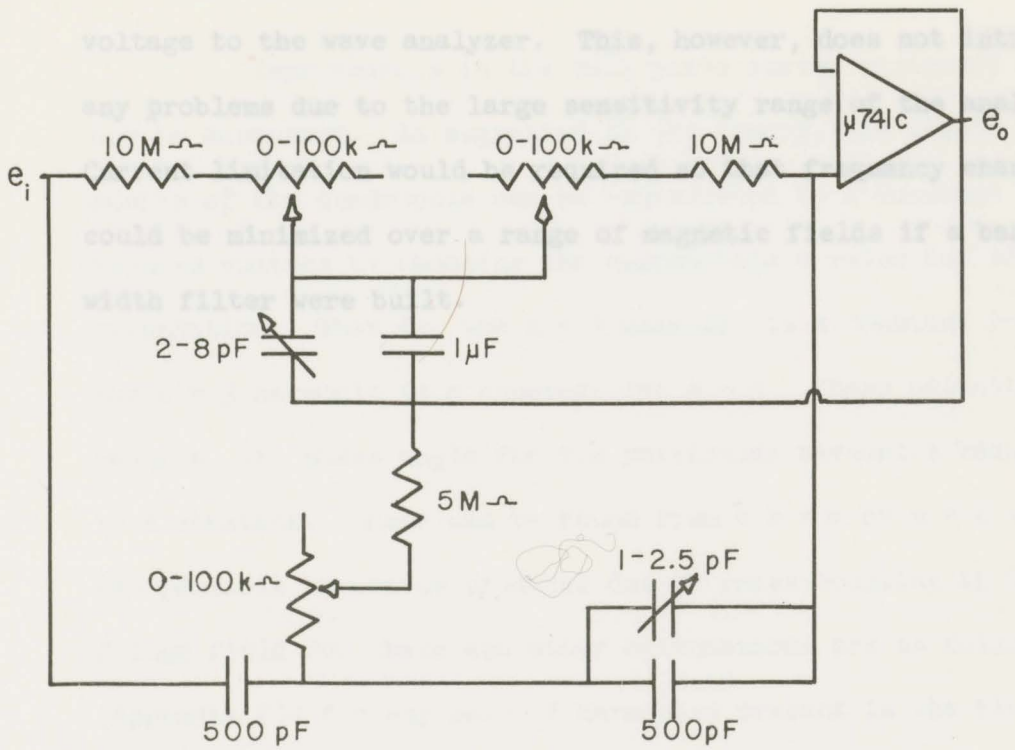

Fig. 6.1 Twin "T" Notch Filter.

A 20 db attenuation of the quadrupole harmonic would improve the lower limit of the harmonics measurable with this equipment by a factor of 10. The smallest harmonic measurable would then be .003% of the quadrupole harmonic.

The variation in rotational frequency in different magnetic fields due to the low input impedence of the wave analyzer could be improved by adding a resistor in series with the coil. The wave analyzer has an input impedence of 100 k$\sim$. To decrease the current in the coil series resistances of the order of 100 k$\sim$

would be required. This, of course, would decrease the input voltage to the wave analyzer. This, however, does not introduce any problems due to the large sensitivity range of the analyzer. Current limitation would be required so that frequency changes could be minimized over a range of magnetic fields if a band-width filter were built.

6.2 Hall Plate

Improvements in the Hall plate survey equipment will now be discussed. As suggested in the theory, the higher harmonics of the quadrupole can be represented by a constant in the induced voltage by choosing the appropriate m value for the orientation. That is, the n = 2 harmonic is a constant for m = 2; the n = 3 harmonic is a constant for m = 3. These orientations require the phase angle for the particular harmonics being set to a constant. These can be found from a m = 0 or m = 1 survey.

The possible harmonics produced due to cross-coupling in the fringe field for these and other orientations are as follows (Appendix C): for any pair of harmonics present in the field, say n = k and n = ℓ , the harmonics present in the induced voltage after analysis are n = 2m, k, ℓ , 2k, 2ℓ , $|k - \ell|$ and $k + \ell$; for the m = 2 orientation no additional constants representing the n = 2 harmonic are produced in the induced voltage due to cross-coupling. However, for m = 3 harmonics n = 3 and 6 in the fringe field can produce an additional constant representing the n = 3 harmonic. Similarly for an m = 4 orientation, the n = 2 harmonic of the field could produce an additional constant representing the n = 4 harmonic. The values of these cross-coupling errors are difficult to determine but should be small if the harmonics involved in the cross-coupling are small; the only appreciable cross-coupling error for any orientation being one involving the n = 2 harmonic. This cross-coupling will not

affect the integrated harmonic content calculations however.

In order to do these other orientations, the facility for rotating the Hall plate about its own axis by 360° is preferable to the present system where the plate is rotated by 180° and then flipped over. The large errors produced, by a bend in the probe arm, will always produce harmonics in the induced voltage. These harmonics will cancel out when determining the value of the constant over a closed loop.

Subsequent to the taking of the results reported in this work, the temperature correction of the Hall voltage has been changed to include the effects of magnetic field. The accuracy of this correction is ±.02% if the thermistor resistance does not drift more than ±1 kΩ. This corresponds to a temperature drift of ±1° C at an ambient of 21° C.

Also subsequent to the taking of the results reported in this work, the Hall plate voltage, instead of being read by the multiplexer and ADC which had a random error of ±1 bit, is now read by a Digital Voltmeter (DVM). The voltmeter is used on auto range and interfaced with the computer using the DVM digital recorder output. The random error from the electronics in the Hall plate voltage in all fields is now less than .05% due to the accuracy of the DVM.

CHAPTER 7

SUMMARY AND CONCLUSIONS

The magnetic field measurement of several beam-line multipole magnets for use at TRIUMF is required before they can be placed in the beam transport system. Since it would be more practical to carry out the measurements of each magnet at the TRIUMF site itself, a portable measuring system would be desirable.

The rotating coil system, although not as accurate as the Hall plate system, can determine whether or not the harmonic content and effective length of a multipole magnet are within the required specifications for that magnet. The system requires a minimal amount of equipment and could be redesigned as a portable system. Incorporated in this new design could be a means of determining the difference between the mechanical and magnetic centres. The harmonic content and effective length can be determined readily from the measured data without the aid of a computer. The linearity of the field as a function of applied current however, can not be measured accurately enough by the present rotating coil system to determine whether or not the magnet meets the required specifications.

The Hall plate system has a far better absolute accuracy than the rotating coil. However, it requires more equipment and

time to determine the harmonic content and effective length of a multipole magnet. It would also be difficult to make the system a portable one to measure several magnets. Since the Hall plate is an accurate field measuring device its use in measuring the magnetic field as a function of applied current is far superior than that of the rotating coil.

In conclusion, it is recommended that the rotating coil apparatus be redesigned as a portable measuring system to determine the harmonic content and effective length of multipole magnets. Incorporated in the design should be a means of determining the magnetic centre with respect to the mechanical centre of the magnet. It is also recommended that the Hall plate system be used to measure the linearity of the field and its absolute value as a function of applied current.

REFERENCES

Alexander, J.A. and Reeve, P.A. 1971. POLFIT, A curvilinear fitting program. TRIUMF Internal Report VPN-71-17.

Banford, A.P. 1966. The Transport of Charged Particle Beams. E. and F.M. Spon Ltd., London.

Bellendir, G.J. and Lari, R.J. 1965. Optimization of quadrupole magnets with circular pole tips. ANL Internal Report GJB/RJL-1.

Beth, R.A. 1966. Complex representation and computation of two-dimensional magnetic fields. J. Appl. Physics, 37 2568.

Cobb, J.K. and Cole, R. 1965. Spectroscopy of quadrupole magnets. In Proc. International Symposium on Magnet Technology, edited by H. Brechna and G.S. Gordon, pp 431-446, Stanford Linear Accelerator Centre, Stanford, California.

Cobb, J.K. and Muray, J.J. 1965. Magnetic field measurements and spectroscopy in multipole fields. SLAC Report No. 39 (Revised).

Cobb, R.W. 1970. The rotating coil method of measuring harmonic content of quadrupole magnets. TRIUMF Internal Report TRI-1-70-6.

Gathright, T.R. and Reeve, P.A. 1972. Magnetic field survey equipment. TRIUMF Internal Report VPN-72-16.

Gathright, T.R., Fyvie, R.D. and Reeve, P.A. 1972. Quadrupole 4019/8 measured performance. TRIUMF Internal Report VPN-72-14.

Germain, C. 1963. Bibliographical review of the methods of measuring magnetic fields. Nucl. Instr. and Meth., 21, 17.

Goertzel, G. 1958. An algorithm for the evaluation of finite trigonometric series. Amer. Math. Monthly, 65, 34.

Goertzel, G. 1960. Fourier Analysis. In Mathematical Methods for Digital Computors, edited by A. Ralston and H. Wilf, pp 258-262, John Wiley and Sons, New York.

Hildebrand, F.B. 1955. Numerical Analysis. McGraw-Hill Book Co., New York.

Jung, V. 1972a. Determination of multipole admixtures in quadrupole fields by incremental field measurement by means of a Hall probe. Nucl. Instr. and Meth., 98, 157.

Jung, V. 1972b. Distortions in the analysis of multipole components in quadrupole end fields caused by longitudinal field components and sag of the probe arm. Nucl. Instr. and Meth., 101, 225.

Kats, M.M. and Khasanov, F.M. 1970. Measurement of harmonic components of fields of standard magnetic quadrupole lenses. Instrum. and Exp. Tech., 2, 335.

Kobayashi, M. 1972. A study of pole shapes for quadrupole magnets having circular pole tips. Japan. J. Appl. Phys., 11, 47.

Kobayashi, M., Tanaka, J., Yamashita, S. and Baba, H. 1971. Field measuring system of drift tube quadrupole magnets. Institute for Nuclear Study Internal Report SJC-A-71-1.

Kobayashi, M. and Yamashita, S. 1972a. Precise measurements of peak fields of pulsed quadrupole magnets. Nucl. Instr. and Meth., 101, 187.

Kobayashi, M. and Yamashita, S. 1972b. Measurements of harmonic field contents of pulsed magnets using a stepping search coil. Nucl. Instr. and Meth., 103, 493.

Lamb, W.H. and Lari, J.R. 1965. Search coil measurements of the harmonic content of beam transport magnets. In Proc. International Symposium on Magnet Technology, edited by H. Brechna and G.S. Gordon, pp 487-496, Stanford Linear Accelerator Centre, Stanford, California.

Lee-Whiting, G.E. and Yamazaki, L. 1971. Semi-analytic calculations for circular quadrupoles. Nucl. Instr. and Meth., 94, 319.

Lobb, D.E. 1970. The effect on charges particle trajectories of higher multipolarity components in a magnetic quadrupole field. Nucl. Instr. and Meth., 86, 177.

Lobb, D.E. 1972. Methods for calculating the effects of errors which increase the beam spot size at the end of a beam transport system. Nucl. Instr. and Meth., 105, 129.

Quan-Tech. (undated). Instruction Manual for the Model 304 Wave and Noise Spectrum Analyzer.

Robins, J.K. 1965. Linearization of Hall probes by a new method, and an estimate of errors arising from spatial field variations. RHL Internal Report NIRL/M/81.

Steffen, K.G. 1965. High Energy Beam Optics. Interscience, New York.

Turck, B. 1971. Measurements in an inhomogeneous field with a rectangular Hall plate. Errors introduced by size effects on the perpendicular component. Nucl. Instr. and Meth., 95, 205.

Turck, B. 1972. Evaluation precise des 3 composantes d'un champ magnetique a partir des tensions prelevees sur 3 sondes de hall. Nucl. Instr. and Meth., 105, 97.

Turin, B. 1971. Sur l'utilisation des sondes de hall en champs inhomogenes. Nucl. Instr. and Meth., 91, 621.

Verma, J.K.D., Raju, V. and Aggarwal, M.D. 1972. Measurement of magnetic field, a bibliographical review. Nucl. Instr. and Meth., 104, 545.

Weiss, H. 1969. Structure and Application of Galvanomagnetic Devices. Pergamon Press Ltd., Oxford.

Williams, L.M. and Reeve, P.A. 1972. HAQ, A quadrupole field harmonic analysis. TRIUMF Internal Report TRI-72-17.

APPENDIX A

GENERATION OF "FALSE" HARMONICS DUE TO MISALIGNMENT

Beth (1966) has shown that a two-dimensional magnetic field in a source-free region can be expressed as an analytic function

$$\mathcal{B} = \mathcal{B}_y + i\,\mathcal{B}_x \qquad (A.1)$$

of the complex variable

$$Z = x + iy = re^{i\theta} \qquad (A.2)$$

This analytic function can be expressed in the complex Taylor series

$$\mathcal{B} = \sum_{n=1}^{\infty} a_n Z^{n-1} \qquad (A.3)$$

where a_n is a complex constant.

Consider a new x'y' co-ordinate system whose origin is displaced a distance, R, from the xy origin (see Fig. A.1).

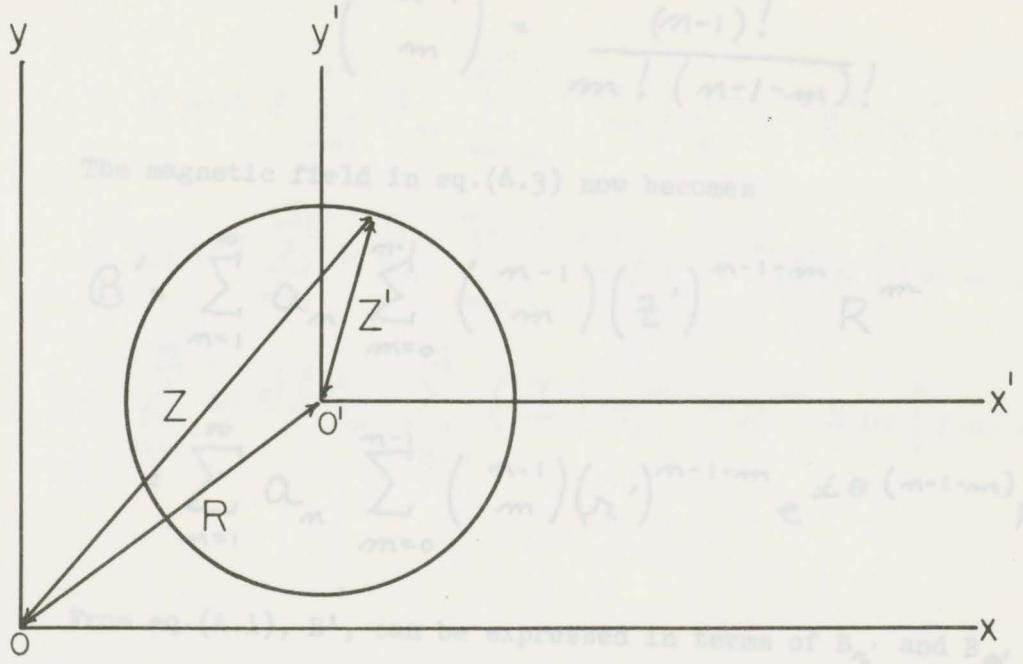

Fig. A.1 The rotational axis displaced from the magnetic axis by a distance R.

Let O' be the centre of rotation of the coil. In the complex plane

$$Z = Z' + R \tag{A.4}$$

where

$$Z' = r' e^{i\theta'} \tag{A.5}$$

Therefore

$$Z^{n-1} = (Z' + R)^{n-1} = \sum_{m=0}^{n-1} \binom{n-1}{m} (Z')^{n-1-m} R^m \tag{A.6}$$

where

$$\binom{n-1}{m} = \frac{(n-1)!}{m!\,(n-1-m)!} \qquad (A.7)$$

The magnetic field in eq.(A.3) now becomes

$$B' = \sum_{n=1}^{\infty} a_n \sum_{m=0}^{n-1} \binom{n-1}{m} (z')^{n-1-m} R^m$$

$$= \sum_{n=1}^{\infty} a_n \sum_{m=0}^{n-1} \binom{n-1}{m} (r')^{n-1-m} e^{i\theta(n-1-m)} R^m \qquad (A.8)$$

From eq.(A.1), B', can be expressed in terms of $B_{r'}$ and $B_{\theta'}$

$$B' = (B_{\theta'} + i B_{r'}) e^{-i\theta'} \qquad (A.9)$$

Therefore from eq.(A.8) and eq.(A.9), we have

$$B_{\theta'} = \sum_{n=1}^{\infty} a_n \sum_{m=1}^{n-1} \binom{n-1}{m} (r')^{n-m-1} \cos\left[(n-m)\theta'\right] R^m \qquad (A.10)$$

$$B_{r'} = \sum_{n=1}^{\infty} a_n \sum_{m=1}^{n-1} \binom{n-1}{m} (r')^{n-m-1} \sin\left[(n-m)\theta'\right] R^m \qquad (A.11)$$

In the x'y' co-ordinate system, r' is the radius of the coil, r_o, and θ' the angular position of the coil. Therefore, from eq.(3.3), ($a_n = nC_n$) the induced emf. in the coil is

$$\mathcal{E} = r_0 \omega N l B_n .$$

$$= r_0 \omega N l \sum_{n=1}^{\infty} a_n \sum_{m=0}^{n-1} \binom{n-1}{m} r_0^{n-1-m} R^m \sin\left[(n-m)\theta + \phi_n\right]$$

$$= \omega N l \sum_{n=1}^{\infty} n C_n \sum_{m=0}^{n-1} \binom{n-1}{m} r_0^{n-m} R^m \sin\left[(n-m)\theta + \phi_n\right]$$

$$= \sum_{n=1}^{\infty} \omega N l C_n \sum_{m=0}^{n-1} \binom{n}{m} r_0^{n-m} R^m \sin\left[(n-m)\theta + \phi_n\right] \quad (A.12)$$

The harmonics present in the field are unaffected by the misalignment. However, for every harmonic present in the magnetic field a second series of harmonics are produced in the induced emf. of the coil. These secondary harmonics will have lower orders than the magnetic field harmonic which produced them. That is, the quadrupole harmonic will generate a dipole only and will not produce a sextupole or octupole. The amplitudes of these secondary harmonics depend on the ratio of the distance R to the radius of the coil, r_0, and on the amplitude of the $n^{\underline{th}}$ harmonic. The expression obtained for the induced emf. is the same as the result obtained by Cobb (1970) for the same effect which he found by expansion in a Cartesian coordinate system.

As an example of the generation of secondary harmonics,

let n=2 so that eq.(A.12) contains two terms.

$$\mathcal{E} = 2\omega l C_2 \lambda_0^2 \sin(2\theta+\phi_2) + 2\omega l C_2 \lambda_0 R \sin(\theta+\phi_2) \qquad (A.13)$$

The first term is the same term that would be obtained if $r_0 = r$ for n=2 from eq.(3.5). That is, the quadrupole harmonic is unchanged. The second term is a generated dipole term whose amplitude depends on R. The above equation (A.13) may be written, then, as

$$\mathcal{E} = e_2 + e_1' \qquad (A.14)$$

where the prime denotes the secondary harmonic series. The amplitude of these secondary harmonic terms for other values of n are listed in Table A.1.

TABLE A.1

Theoretical Values of Harmonics Generated due to Misalignment

FIELD HARMONIC	"FALSE" HARMONIC	AMPLITUDE
2	1	$e_1' = \frac{R}{r_0} e_2$
3	2	$e_2' = 2\frac{R}{r_0} e_3$
	1	$e_1' = \left(\frac{R}{r_0}\right)^2 e_3$
6	5	$e_5' = 5\left(\frac{R}{r_0}\right) e_6$
	4	$e_4' = 10\left(\frac{R}{r_0}\right)^2 e_6$
	3	$e_3' = 10\left(\frac{R}{r_0}\right)^3 e_6$
10	9	$e_9' = 9\left(\frac{R}{r_0}\right) e_{10}$
	8	$e_8' = 36\left(\frac{R}{r_0}\right)^2 e_{10}$
	7	$e_7' = 84\left(\frac{R}{r_0}\right)^3 e_{10}$

APPENDIX B

CONTRIBUTION TO THE EMF. DUE TO B_z

B.1 General Theory

Consider the coil rotating in the fringe field of a magnet where B_z is not zero (see Fig. B.1).

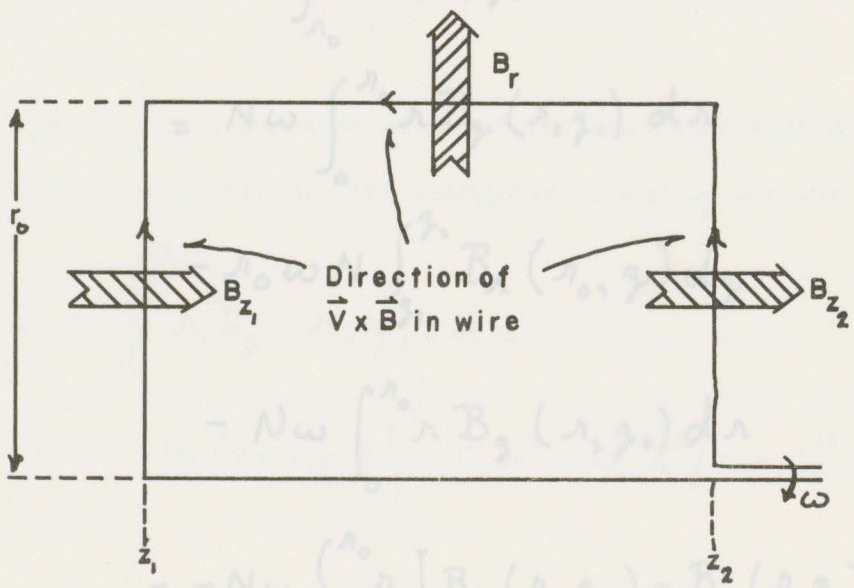

Fig. B.1 Coil rotating in the fringe field of a magnet where $z_1 < z_2$. Main field is to the left of the diagram.

Let the z positions of the two radial arms be z_1 and z_2 and let the radius of the coil be r_o. The total emf. in the coil will be

$$\mathcal{E} = N \int_0^{r_0} \vec{B}(r, z_1)\left(d\vec{r} \times r\omega\,\hat{\theta}\right)$$

$$- N \int_{z_1}^{z_2} \vec{B}(r_0, z)\left(d\vec{z} \times r_0\omega\,\hat{\theta}\right)$$

$$+ N \int_{r_0}^{0} \vec{B}(r, z_2)\left(d\vec{r} \times r\omega\,\hat{\theta}\right)$$

$$= N\omega \int_0^{r_0} r B_z(r, z_1)\, dr$$

$$- r_0\omega N \int_{z_1}^{z_2} B_r(r_0, z)\, dz$$

$$- N\omega \int_0^{r_0} r B_z(r, z_2)\, dr$$

$$= -N\omega \int_0^{r_0} r\left[B_z(r, z_2) - B_z(r, z_1)\right] dr$$

$$- r_0\omega N \int_{z_1}^{z_2} B_r(r_0, z)\, dz$$

$$= -N\omega\left[I_1 - I_3\right] - r_0\omega N I_2 \qquad (B.1)$$

These integrals will now be evaluated in the fringe field of the quadrupole field (n = 2). For the fringe field region we have in general for n = 2 from eq.(3.21) and eq.(3.23)

$$B_r = -\sin(2\theta+\phi_2)\left[2C_2 r - C_2^{(2)} r^3/3 + C_2^{(4)} r^5/64\right] \quad (B.2)$$

$$B_z = -\sin(2\theta+\phi_2)\left[C_2' r^2 - C_2^{(3)} r^4/12 + C_2^{(5)} r^6/384\right] \quad (B.3)$$

where C_2 is a function of z and the bracketed superscripts denote higher derivatives. The integrals I_1 and I_3 can now be evaluated

$$I_1 = \int_0^{r_0} r\, B_z(r, z_2)\, dr \quad (B.4)$$

$$= -\sin(2\theta+\phi_2)\int_0^{r_0}\left(C_2' r^3 - C_2^{(3)} r^5/12 + C_2^{(5)} r^7/384\right)\Big]_{z_2} dr$$

$$= -\sin(2\theta+\phi_2)\left[C_2' r_0^4/4 - C_2^{(3)} r_0^6/72 + C_2^{(5)} r_0^8/3072\right]_{z_2}$$

Similarly for I_3 we have

$$I_3 = -\sin(2\theta+\phi_2)\left[C_2' r_0^4/4 - C_2^{(3)} r_0^6/72 + C_2^{(5)} r_0^8/3072\right]_{z_2} \quad (B.5)$$

Therefore from eq.(B.4) and eq.(B.5) we have

$$I_1 - I_3 = -\sin(2\theta + \phi_2)\left\{ r_0^4/4\left[C_2'(z_2) - C_2'(z_1)\right] - r_0^6/72\left[C_2^{(3)}(z_2) - C_2^{(3)}(z_1)\right] + r_0^8/3072\left[C_2^{(5)}(z_2) - C_2^{(5)}(z_1)\right]\right\} \quad (B.6)$$

To evaluate the integral I_2, the z dependence of C_2 is required. Two regions exist in the fringe field; one in which the output signal has been fitted by a 5^{th} order polynomial in z and the other where the output signal is an exponential function of z. The position of $z = 0$ was chosen where the output signal began to drop below the main field value.

In the polynomial region we will assume

$$C_2 = \sum_{p=0}^{5} b_p z^p \quad (B.7)$$

where z has units of inches. From eq.(B.2) the radial magnetic field is

$$B_2 = -\sin(2\theta + \phi_2)\, r \sum_{p=0}^{5} d_p z^p \quad (B.8)$$

where the coefficients of the field, d_p, in terms of the coefficients of the gradient b_p are listed in Table B.1. Therefore, in the polynomial region the integral I_2 is

$$I_2 = \int_{z_1}^{z_2} B_r(r_0, z)\, dz$$

$$= -\sin(2\theta + \phi_2)\, r_0 \int_{z_1}^{z_2} \sum_{p=0}^{5} d_p z^p\, dz$$

$$= -\sin(2\theta + \phi_2)\, r_0 \sum_{p=0}^{5} \frac{d_p}{p+1}\left(z_2^{p+1} - z_1^{p+1}\right) \qquad (B.9)$$

In the exponential region we will assume the gradient has the form

$$C_2 = Be^{-\beta z} \qquad (B.10)$$

so that

$$B_r = -\sin(2\theta + \phi_2)\, Be^{-\beta z} r\left[2 - \beta^2 r^2/3 + \beta^4 r^4/64\right] \qquad (B.11)$$

Therefore in this region I_2 is

$$I_2 = \int_{z_1}^{z_2} B_r(r_0, z)\, dz$$

$$= -\sin(2\theta + \phi_2)\, r_0\left[2 - \frac{\beta^2 r_0^2}{3} + \frac{\beta^4 r_0^4}{64}\right] \int_{z_1}^{z_2} Be^{-\beta z}\, dz$$

TABLE B.1

The Field Coefficients in Terms of the Gradient Coefficient

d_p	$\sim$	B_r	B_θ	B_y
d_0	$b_0 - b_2 r^2/16 + b_4 r^4/16$	$2b_0 - 2b_2 r^2/3 + 3b_4 r^4/8$	$2b_0 - b_2 r^2/3 + 3b_4 r^4/32$	$b_1 r - b_3 r^3/2 + 5b_5 r^5/16$
d_1	$b_1 - b_3 r^2/2 + 5b_5 r^4/16$	$2b_1 - 2b_3 r^2 + 15b_5 r^4/8$	$2b_1 - b_3 r^2 + 5b_5 r^4/4$	$2b_2 r - 2b_4 r^3$
d_2	$b_2 - b_4 r^2$	$2b_2 - 4b_4 r^2$	$2b_2 - 2b_4 r^2$	$3b_3 r - 5b_5 r^3$
d_3	$b_3 - 5b_5 r^2/3$	$2b_3 - 20b_5 r^2/3$	$2b_3 - 10b_5 r^2/3$	$4b_4 r$
d_4	b_4	$2b_4$	$2b_4$	$5b_5 r$
d_5	b_5	$2b_5$	$2b_5$	—

$$= -\sin(2\theta+\phi_2)\frac{r_0}{\beta}\left[2-\frac{\beta^2 r_0^2}{3}+\frac{\beta^4 r_0^4}{64}\right]\left[Be^{-\beta z_2}-Be^{-\beta z_1}\right]$$

$$= -\sin(2\theta+\phi_2)\frac{r_0}{\beta}\left[2-\frac{\beta^2 r_0^2}{3}+\frac{\beta^4 r_0^4}{64}\right]\left[C_2(z_2)-C_2(z_1)\right] \qquad (B.12)$$

The induced emf. in a short and long coil will now be found from eq.(B.1)

B.2 Short Coil

The induced emf. is given by eq.(B.1)

$$\mathcal{E} = -N\omega\left[I_1-I_3\right]-r_0\omega N I_2 \qquad (B.13)$$

From eq.(B.6) we have for $(I_1 - I_3)$

$$I_1-I_3 = -\sin(2\theta+\phi_2)\left\{\frac{r_0^4}{4}\left[C_2'(z_2)-C_2'(z_1)\right]\right.$$

$$-\frac{r_0^6}{72}\left[C_2^{(3)}(z_2)-C_2^{(3)}(z_1)\right]$$

$$\left.+\frac{r_0^8}{3072}\left[C_2^{(5)}(z_2)-C_2^{(5)}(z_1)\right]\right. \qquad (B.14)$$

For the short coil where the length of the coil, ℓ, is 0.125" we can write

$$C_2(z_2)-C_2(z_1) \cong \left[\frac{\partial C_2}{\partial z}\ell+\frac{\partial^2 C_2}{\partial z^2}\frac{\ell^2}{2}+\frac{\partial^3 C_2}{\partial z^3}\frac{\ell^3}{6}\right]_{z_1} \qquad (B.15)$$

Therefore $I_1 - I_3$ has the form

$$I_1 - I_3 = -\sin(2\theta+\phi_2)\left\{\frac{r_o^2}{4}\left(C_2^{(2)}\ell + C_2^{(3)}\frac{\ell^2}{2} + C_2^{(4)}\frac{\ell^3}{6}\right)\right.$$

$$-\frac{r_o^6}{72}\left(C_2^{(4)}\ell + C_2^{(5)}\frac{\ell^2}{2} + C_2^{(6)}\frac{\ell^3}{6}\right)$$

$$\left.+\frac{r_o^8}{3072}\left(C_2^{(6)}\ell + C_2^{(7)}\frac{\ell^2}{2} + C_2^{(8)}\frac{\ell^3}{6}\right)\right\}_{z_1} \quad (B.16)$$

From eq.(3.20) we are neglecting the 6^{th} and higher order derivatives and we can neglect terms smaller than $\ell^2/10$ so that eq.(B.16) becomes

$$I_1 - I_3 = -\sin(2\theta+\phi_2)\left\{\frac{r_o^4\ell}{4}C_2^{(2)} + \frac{r_o^4\ell^2}{8}C_2^{(3)} - \frac{r_o^6\ell}{72}C_2^{(4)}\right\}_{z_1} \quad (B.17)$$

The integral I_2 will now be evaluated in both the polynomial and exponential regions for the short coil.

For the polynomial region I_2 is given by eq.(B.9)

$$I_2 = -\sin(2\theta+\phi_2)\, r_o \sum_{p=0}^{5} \frac{d_p}{p+1}\left(z_2^{p+1} - z_1^{p+1}\right) \quad (B.18)$$

For a short coil of length $\ell = 0.125"$ let

$$z_2 = z_1 + \ell \quad (B.19)$$

so that

$$z_2^{p+1} = (z_1 + l)^{p+1}$$

$$\simeq z_1^{p+1} + (p+1) z_1^{p} l + \frac{(p+1)p}{2} z_1^{p-1} l^2 + \frac{p(p+1)(p-1)}{6} z_1^{p-2} l^3 \qquad (B.20)$$

Therefore eq.(B.18) for I_2 becomes

$$I_2 = -\sin(2\theta + \phi_2)\, r_0 \sum_{p=0}^{5} a_p \left[l z_1^{p} + \frac{p l^2}{2} z_1^{p-1} + \frac{p(p-1)}{6} l^3 z_1^{p-2} \right]$$

$$= -\sin(2\theta + \phi_2)\, r_0 \left[l \sum_{p=0}^{5} a_p z_1^{p} + \frac{l^2}{2} \sum_{p=0}^{5} p\, a_p z_1^{p-1} + \frac{l^3}{6} \sum_{p=0}^{5} p(p-1)\, a_p z_1^{p-2} \right] \qquad (B.21)$$

From eq.(B.8) I_2 becomes

$$I_2 = -\sin(2\theta + \phi_2)\, r_0 l \left[B_{r_2} + \frac{l}{2} \frac{\partial B_{r_2}}{\partial z} + \frac{l^2}{6} \frac{\partial^2 B_{r_2}}{\partial z^2} \right]_{r_0, z_1} \qquad (B.22)$$

Replacing B_n, $\frac{\partial B_n}{\partial z}$ and $\frac{\partial^2 B_n}{\partial z^2}$ from eq.(B.2) we have

$$I_2 = -\sin(2\theta+\phi_2)\cdot \ell\left[2C_2 r_0 + \ell C_2' r_0 + \ell^2 C_2^{(2)} r_0/3 \right.$$

$$- C_2^{(2)} r_0^3/3 - \ell C_2^{(3)} r_0^3/6 - \ell^2 C_2^{(4)} r_0^3/18$$

$$\left. + C_2^{(4)} r_0^5/64 + \ell C_2^5 r_0^5/128 + \ell^2 C_2^{(6)} r_0^5/384 \right] \qquad (B.23)$$

Neglecting the 6^{th} order derivative and terms smaller than $\ell^2/10$ we have

$$I_2 = -\sin(2\theta+\phi_2) r_0 \ell \left[2C_2 - (r_0^2 - \ell^2) C_2^{(2)}/3 + \ell C_2' \right.$$

$$\left. - \ell r_0^2 C_2^{(3)}/6 + r_0^4 C_2^{(4)}/64 \right]_{z_1} \qquad (B.24)$$

In the exponential region I_2 is given by eq.(B.12).

$$I_2 = -\sin(2\theta+\phi_2) \frac{r_0}{\beta}\left[2 - \beta\frac{r_0^2}{3} + \beta^4\frac{r_0^4}{64}\right]\left[C_2(z_2) - C_2(z_1)\right] \qquad (B.25)$$

As in eq.(B.15)

$$C_2(z_2) - C_2(z_1) \simeq \left[\frac{\partial C_2}{\partial z}\ell + \frac{\partial^2 C_2}{\partial z^2}\frac{\ell^2}{2} + \frac{\partial^3 C_2}{\partial z^3}\frac{\ell^3}{6}\right]_{z_1}$$

$$= \left[-\beta C_2 \ell + \beta^2 \ell^2 C_2/2 - \beta^3 \ell^3 C_2/6\right]_{z_1} \qquad (B.26)$$

Therefore eq.(B.25) becomes

$$I_2 = -\sin(2\theta+\phi_2)\, C_2 r_0 l \left[2 - \frac{\beta^2 r_0^2}{3} + \frac{\beta^4 r_0^4}{64}\right] \left[1 - \frac{l\beta}{2} + \frac{l^2\beta^2}{6}\right] \qquad (B.27)$$

Again neglecting terms smaller than $l^2/10$ we have

$$I_2 = -\sin(2\theta+\phi_2)\, r_0 l \left[2C_2 + lC_2' - \frac{(r_0^2-l^2)}{3} C_2^{(2)} - \frac{l r_0^2}{6} C_2^{(3)} + \frac{r_0^4 C_2^{(4)}}{64}\right]_{g_1} \qquad (B.28)$$

Note that eq.(B.24) and eq.(B.28) are equivalent. Therefore in general the quadrupole harmonic of the emf. induced in the short coil in the fringe field region is

$$\begin{aligned}
\mathcal{E}_s &= -r_0 \omega N I_2 - N\omega (I_1 - I_3) \\
&= r_0^2 \omega N l \sin(2\theta+\phi_2) \left[2C_2 + lC_2' - \frac{(r_0^2-l^2)}{3} C_2^{(2)} \right. \\
&\quad \left. + \frac{r_0^2}{4} C_2^{(2)} + \frac{r_0^2 l}{8} C_2^{(3)} - \frac{r_0^4}{72} C_2^{(4)} - \frac{l r_0^2}{6} C_2^{(3)} + \frac{1}{64} r_0^4 C_2^{(4)}\right]_{g_1} \\
&= r_0^2 \omega N l \sin(2\theta+\phi_2) \left[2C_2 + lC_2' - \left(\frac{r_0^2}{12} - \frac{l^2}{3}\right) C_2^{(2)} \right. \\
&\quad \left. - \frac{l r_0^2}{24} C_2^{(3)} + \frac{r_0^4 C_2^{(4)}}{576}\right]_{g_1} \qquad (B.29)
\end{aligned}$$

B.3 Long Coil

For a long coil with only one arm in the fringe field the total emf. in the coil is

$$\mathcal{E}_L = N\omega \int_0^{r_0} r B_z(z_1, r)\, dr - r_0 \omega N \int_{z_1}^{z_2} B_r(r_0, z)\, dz$$

$$= N\omega I_1 - r_0 \omega N I_2 \qquad (B.30)$$

The integral I_1 is given by eq.(B.4)

$$I_1 = -\sin(2\theta + \phi_2)\left[C_2' r_0^4/4 - C_2^{(3)} r_0^6/72 + C_2^{(5)} r_0^8/3072 \right]_{z_1} \qquad (B.31)$$

The integral I_2 could contain 3 terms; one term for the exponential region of the fringe field, one for the polynomial region of the fringe field and one for the main field region (see Fig. B.2).

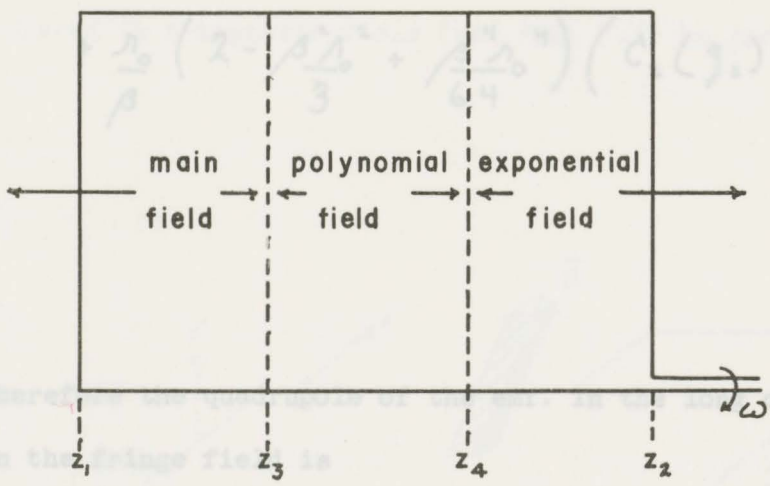

Fig. B.2 The long coil in the fringe field.

For the main field region, the field is independent of z. Let the gradient of the main field be a constant, A_2. The integral I_2 can then be written as

$$I_2 = B_r \Big]_{r_0} (z_3 - z_1) + \int_{z_3}^{z_4} B(r_0, z)\, dz + \int_{z_4}^{z_2} B(r_0, z)\, dz \qquad (B.32)$$

From eq.(B.9) and eq.(B.12), I_2 is

$$I_2 = -\sin(2\theta+\phi_2)\left[2A_2 r_0 (z_3-z_1) + r_0 \sum_{p=0}^{5} \frac{d_p}{p+1}\left(z_4^{p+1} - z_3^{p+1}\right) + \frac{r_0}{\beta}\left(2 - \frac{\beta^2 r_0^2}{3} + \frac{\beta^4 r_0^4}{64}\right)\left(C_2(z_2) - C_2(z_4)\right)\right] \quad (B.33)$$

Therefore the quadrupole of the emf. in the long coil rotating in the fringe field is

$$\mathcal{E}_L = r_0^2 \omega N \sin(2\theta+\phi_2)\left[2A_2(z_3-z_1) + \sum_{p=0}^{5} \frac{d_p}{p+1}\left(z_4^{p+1} - z_3^{p+1}\right) + \frac{1}{\beta}\left(2 - \frac{\beta^2 r_0^2}{3} + \frac{\beta^4 r_0^4}{64}\right)\left(C_2(z_2) - C_2(z_4)\right) - C_2'(z_1)\frac{r_0^2}{4} + C_2^{(3)}(z_1)\frac{r_0^4}{72} - \frac{C_2^{(5)} r_0^6}{3072}\right] \quad (B.34)$$

In practice it would be very difficult if not impossible to sort out the derivatives of the gradient, C_2, from a long coil measurement.

APPENDIX C

GENERATION OF "FALSE" HARMONICS DUE TO CROSS-COUPLING IN THE HALL PLATE

In general the induced voltage in the Hall plate when placed in a magnetic field (see Fig. C.1) is given

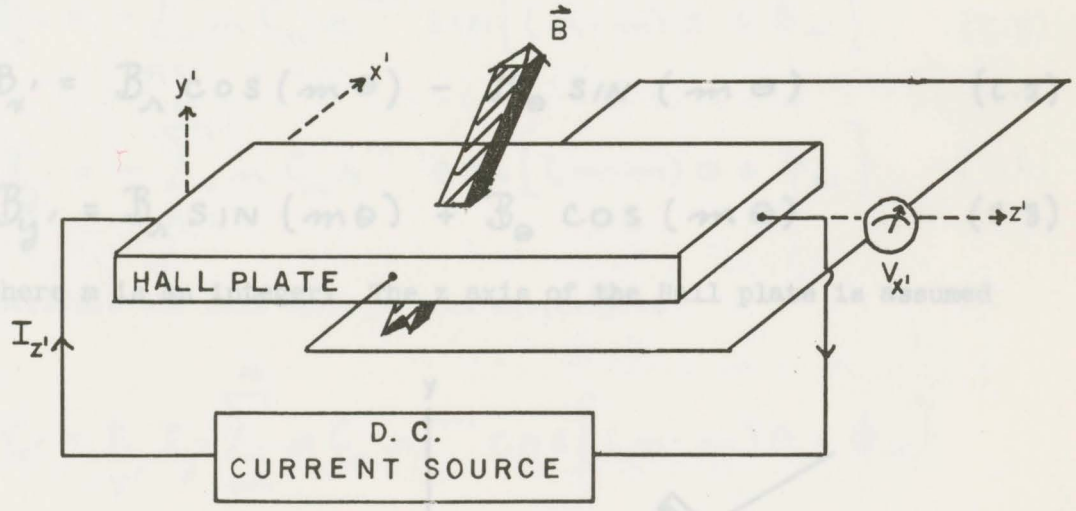

Fig. C.1 The Hall plate in a magnetic field B.

by eq.(4.6)

$$V_{x'} = +\frac{R}{y'} I_{z'} B_{y'} + \frac{a\rho_o}{y'} B_{x'} B_{y'} I_{z'} \qquad (C.1)$$

where R is the Hall coefficient (Ω-cm./kG)

a is the magnetoresistive coefficient (kG^{-2})

ρ_o is the resistivity (Ω-cm.)

and B_x', B_y', and B_z' are the components of the magnetic field $\vec{B}$ (kG).

If the Hall plate is orientated in the field so that it is rotated abouts its own axis (z') with a fixed integral relationship to its angular position in the aperture of the magnet (Gathright and Reeve 1972) (see Fig. C.2) the equations for B_x' and B_y' are

$$B_{x'} = B_r \cos(m\theta) - B_\theta \sin(m\theta) \qquad (C.2)$$

$$B_{y'} = B_r \sin(m\theta) + B_\theta \cos(m\theta) \qquad (C.3)$$

where m is an integer. The z axis of the Hall plate is assumed

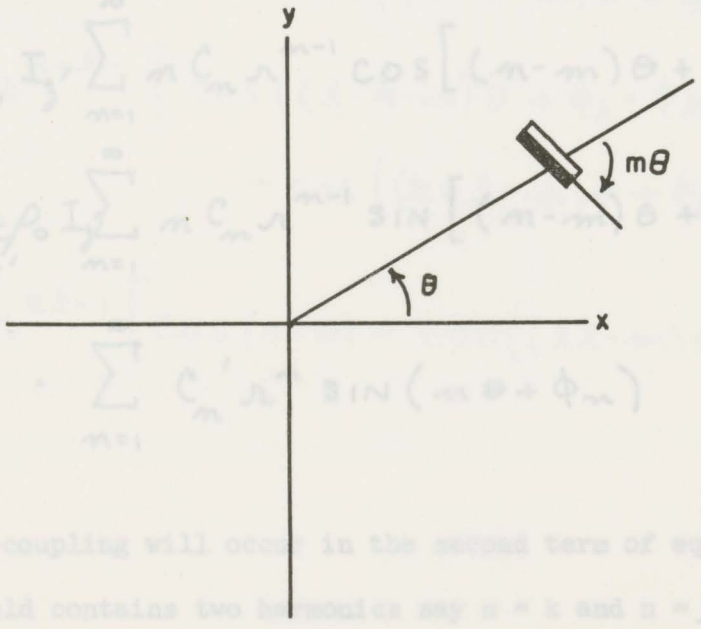

Fig. C.2 Hall plate rotated about its own axis with a fixed integral relationship to its angular position.

to be parallel with the z axis of the magnet so that from eq.(2.22)

$$B_{z'} = B_z = \sum_{n=1}^{\infty} C_n' r^n \sin(n\theta + \phi_n) \qquad (C.4)$$

Using eq.(2.20) and eq.(2.21) for the field components in a quadrupole, the field components B_x' and B_y' are

$$B_{x'} = -\sum_{n=1}^{\infty} n C_n r^{n-1} \sin\left[(n-m)\theta + \phi_n\right] \qquad (C.5)$$

$$B_{y'} = -\sum_{n=1}^{\infty} n C_n r^{n-1} \cos\left[(n-m)\theta + \phi_n\right] \qquad (C.6)$$

Therefore the Hall voltage from eq.(C.1) is

$$V_{x'} = \frac{R}{y'} I_{z'} \sum_{n=1}^{\infty} n C_n r^{n-1} \cos\left[(n-m)\theta + \phi_n\right]$$

$$+ \frac{a\rho_0}{y'} I_{z'} \sum_{n=1}^{\infty} n C_n r^{n-1} \sin\left[(n-m)\theta + \phi_n\right] \cdot$$

$$\cdot \sum_{n=1}^{\infty} C_n' r^n \sin(n\theta + \phi_n) \qquad (C.7)$$

The cross-coupling will occur in the second term of eq.(C.7). If the field contains two harmonics say n = k and n = ℓ the second term of eq.(C.7) is

$$\frac{a}{y'}\rho_0 I_{z'} \sum_{n=1}^{\infty} n C_n r^{n-1} \sin\left[(n-m)\theta + \phi_n\right] \sum_{n=1}^{\infty} C_n' r^n \sin(n\theta + \phi_n)$$

$$= \frac{a}{y'}\rho_0 I_{z'} \left\{ k C_k r^{k-1} \sin\left[(k-m)\theta + \phi_k\right] + l C_l r^{l-1} \sin\left[(l-m)\theta + \phi_l\right] \right\}$$

$$\cdot \left\{ C_k' r^k \sin(k\theta + \phi_k) + C_l' r^l \sin(l\theta + \phi_l) \right\}$$

$$= \frac{a}{y'}\rho_0 I_{z'} \left\{ k C_k C_k' r^{2k-1} \left[\cos(m\theta) - \cos\left((2k-m)\theta + 2\phi_k\right)\right] \right.$$

$$+ k C_k C_l' r^{k+l-1} \left[\cos\left((k-l-m)\theta + \phi_k - \phi_l\right) - \cos\left((k+l-m)\theta + \phi_k + \phi_l\right)\right]$$

$$+ l C_l C_k' r^{k+l-1} \left[\cos\left((l-k-m)\theta + \phi_l - \phi_k\right) - \cos\left((k+l-m)\theta + \phi_k + \phi_l\right)\right]$$

$$\left. + l C_l C_l' r^{2l-1} \left[\cos(m\theta) - \cos\left((2l-m)\theta + 2\phi_l\right)\right] \right\}$$

(C.8)

Therefore from eq.(C.8) the harmonic orders present in the induced voltage due to cross-coupling for any value of m are; m, 2k-m, $|k-\ell|$-m, $k+\ell$ -m, and 2ℓ-m. Therefore after analysis the "false" harmonics due to cross-coupling are n = 2m, 2k, 2ℓ, $|k-\ell|$, and $k+\ell$. In Table C.1 are listed the possible harmonics produced by cross-coupling in the Hall plate when used in the fringe field of a quadrupole with field harmonics n = 2,3,6 and 10 for any m value.

T A B L E C.1

Harmonics Generated due to Cross-Coupling

Field Harmonics	"False" Harmonics Due to Cross-Coupling
2 and 3	2m, 1,4,5,6
2 and 6	2m, 4*,8,12
2 and 10	2m, 4,8,12,20
3 and 6	2m, 3,6,9,12
3 and 10	2m, 6,7,13,20
6 and 10	2m, 4,12,16,20

* n = 4 is produced by both (6 - 2) and (2 x 2)

m denotes the orientation of the plate (see Fig. C.2)

APPENDIX D

SOFTWARE FOR THE HALL PLATE SURVEYS AND ANALYSIS

D.1 Supernova Programs

The three programs RAP 1, RAP 2 and ERR 2 (Gathright and Reeve 1972) used to collect the data and prepare it for the Fourier analysis program, HAQ (Williams and Reeve 1972) are listed here in flow chart form (see Figs. D.1, D.2, and D.3). The programs were written in "Basic" compiler language with machine language subroutines to read the CAMAC interfacing. Two additional subroutines were written to punch and read binary format paper tape. A third subroutine was written to punch paper tape in a format suitable for a Mohawk data converter. The converted data could then be placed on magnetic tape for IBM processing.

D.2 FORIT Subroutine

The analysis of the data in the IBM 370/145 computer is done by HAQ. The actual Fourier analysis of the data is performed by the FORTRAN library subroutine FORIT. This subroutine produces the Fourier coefficients of a tabulated function given the values of a function in a closed loop (0 to 2π) in steps of $2\pi/(2N + 1)$ where the desired order of the Fourier coefficients, M is less than or equal to N.

The problem of solving the equation

$$f_m = \frac{1}{2}a_0 + \sum_{p=1}^{N}\left[a_p \cos\left(\frac{2\pi m p}{2N+1}\right) + b_p \sin\left(\frac{2\pi m p}{2N+1}\right)\right] \qquad (D.1)$$

$$m = 0, 1, 2 \ldots . 2N$$

where f_m are the given numbers is treated by Hildebrand (1955). The solutions for a_ρ and b_ρ are

$$a_\rho = \frac{2}{2N+1} \sum_{m=0}^{2N} f_m \cos\left(\frac{2\pi m\rho}{2N+1}\right) \qquad (D.2)$$

$$b_\rho = \frac{2}{2N+1} \sum_{m=0}^{2N} f_m \sin\left(\frac{2\pi m\rho}{2N+1}\right) \qquad (D.3)$$

The efficient calculation of a_ρ and b_ρ is performed by a recursive technique described by Goertzel (1958, 1960). This algorithm requires trignometric function evaluations for only two numbers; namely

$$\cos\left(\frac{2\pi}{2N+1}\right) \qquad (D.4)$$

AND

$$\sin\left(\frac{2\pi}{2N+1}\right) \qquad (D.5)$$

The output of this subroutine are the coefficients a_m and b_m from which the Fourier coefficients C_m are

$$C_m = \sqrt{a_m^2 + b_m^2} \qquad (D.6)$$

and the phase angle ϕ_m is

$$\phi_m = \tan^{-1}\left(\frac{b_m}{a_m}\right) \qquad (D.7)$$

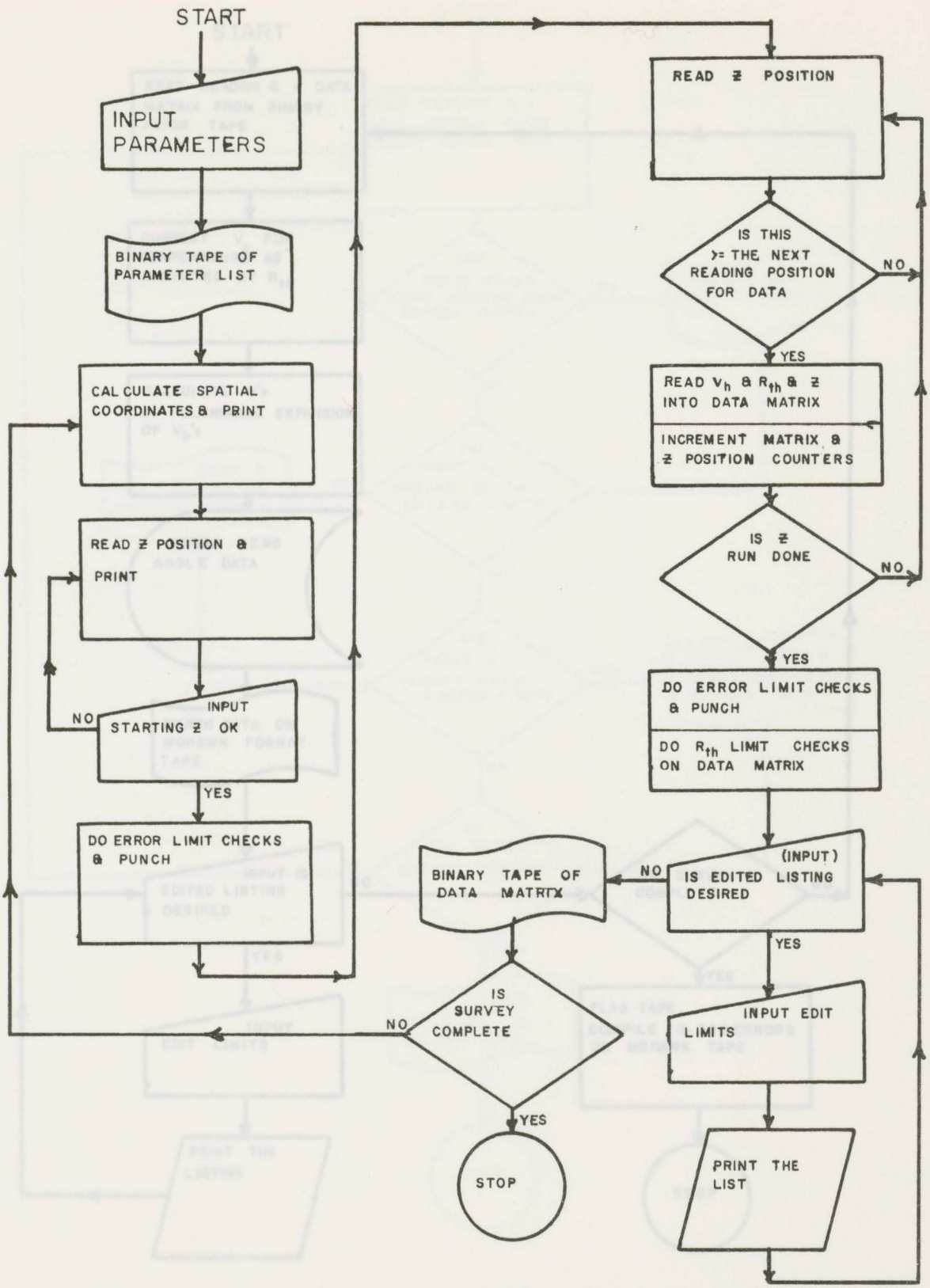

Fig. D.1 Flow diagram of RAP 1 (Gathright and Reeve 1972).

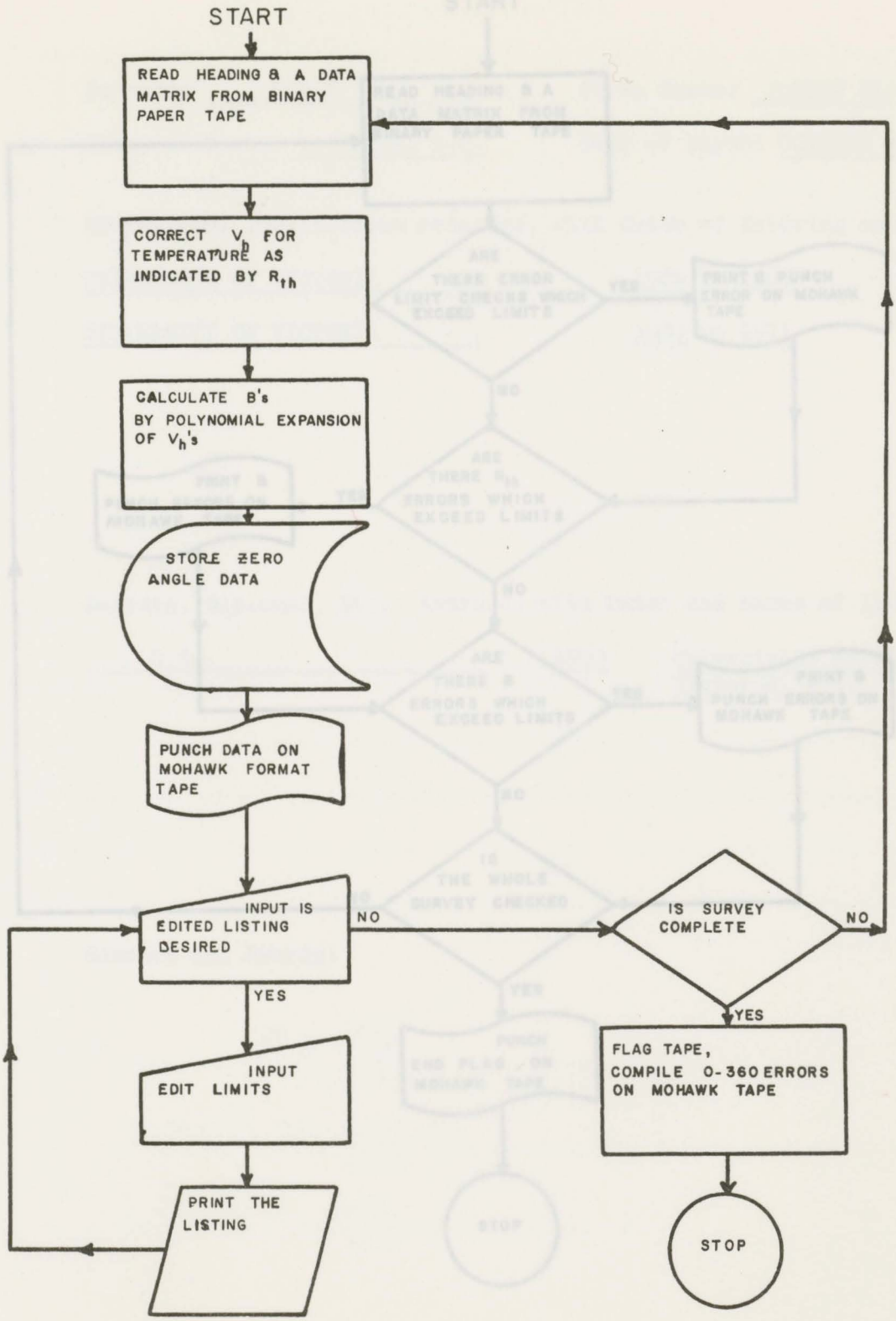

Fig. D.2 Flow diagram of RAP 2 (Gathright and Reeve 1972).

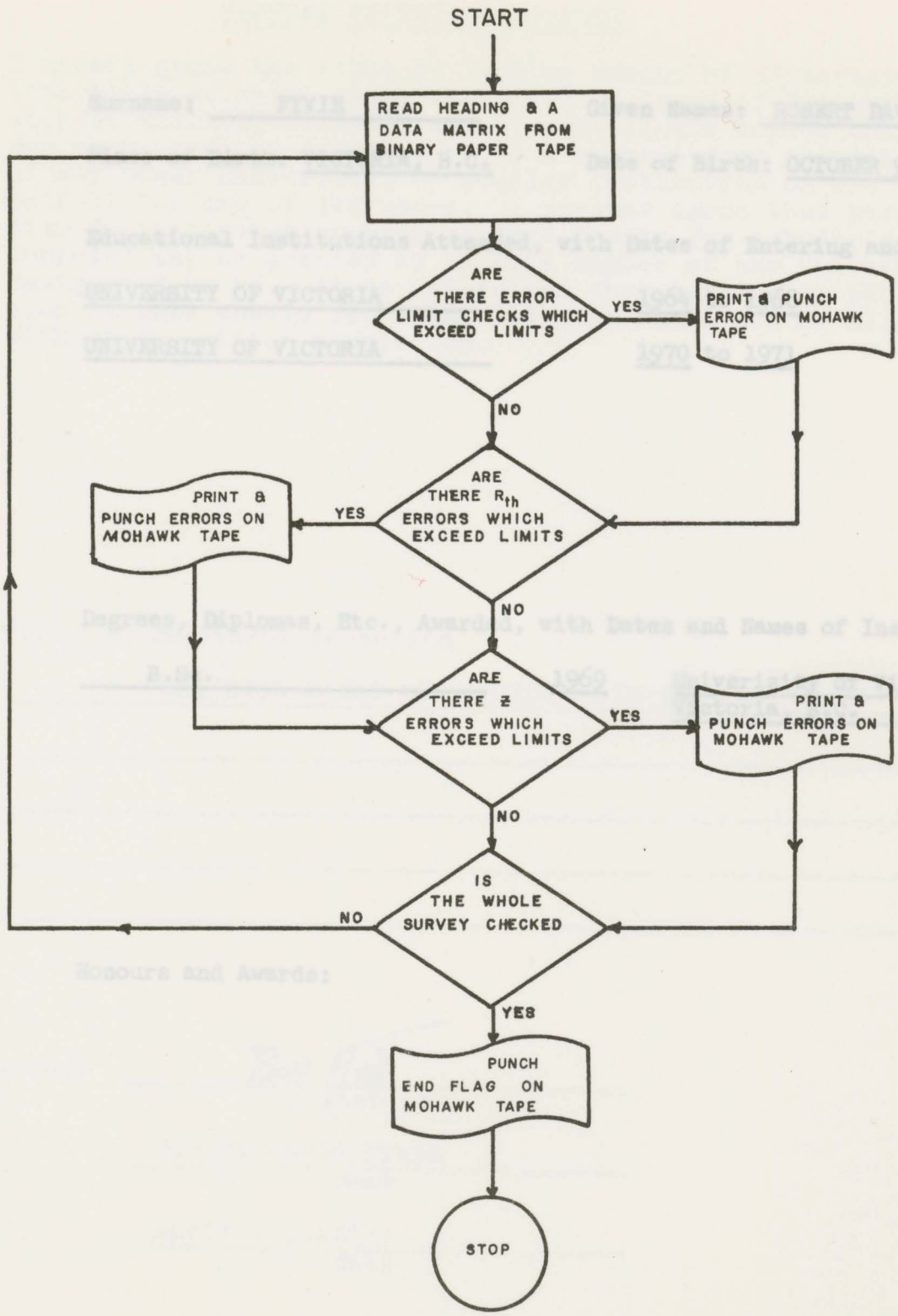

Fig. D.3 Flow diagram of ERR 2 (Gathright and Reeve 1972).

Surname: FYVIE Given Names: ROBERT DAVID

Place of Birth: VICTORIA, B.C. Date of Birth: OCTOBER 9, 1946

Educational Institutions Attended, with Dates of Entering and Leaving:

UNIVERSITY OF VICTORIA	1964 to 1968
UNIVERSITY OF VICTORIA	1970 to 1971

Degrees, Diplomas, Etc., Awarded, with Dates and Names of Institutions:

B.Sc.	1969	Univerisity of Victoria, Victoria, B.C.

Honours and Awards:

PARTIAL COPYRIGHT LICENSE

I hereby grant the right to lend my thesis or dissertation (the title of which is shown below) to users of the University of Victoria Library, and to make single copies only for such users or in response to a request from the library of any other university, or similar institution on its behalf or for one of its users. I further agree that permission for extensive copying of this thesis for scholarly purposes may be granted by me or a member of the University designated by me. It is understood that copying or publication of this thesis for financial gain shall not be allowed without my written permission.

Title of Thesis/Dissertation

MAGNETIC FIELD MEASUREMENTS IN QUADRUPOLE MAGNETS

Author [redacted]

signature

Robert David Fyvie

name

April 17, 1973.

date